LAPPEENRANTA-LAHTI UNIVERSITY OF TECHNOLOGY LUT

LUT School of Engineering Science

Master's Programme in Chemical Engineering for Water Treatment

Kalle Kakko

MEMBRANE FOULING IN HOLLOW FIBER MEMBRANE FILTRATION OF SURFACE WATER

1st Examiner: Prof. Mari Kallioinen

2nd Examiner: M.Sc. Panu Laurell

Supervisor: M.Sc. Tiina Virtanen

ABSTRACT

Lappeenranta-Lahti University of Technology LUT
LUT School of Engineering Science
Master's Programme in Chemical Engineering for Water Treatment

Kalle Kakko

Membrane fouling in hollow fiber membrane filtration of surface water

Master's thesis
2020
110 pages, 20 figures, 11 tables
Examiners: Mari Kallioinen, Panu Laurell

Keywords: membrane filtration, NOM, fouling, hollow fiber, cake formation

Membrane filtration is a promising process for production of drinking water. The main challenge for applying membrane filtration for this purpose is membrane fouling. For this work, literature concerning membrane filtration and membrane fouling has been reviewed focusing mainly on ultrafiltration (UF) and microfiltration (MF). The work also includes an experimental part, which analyses fouling that occurred in the pilot filtration plant operated by Helsinki Region Environmental Services Authority (HSY). The analysis techniques applied for this work include infrared spectroscopy, CHN (carbon-hydrogen-nitrogen) analysis, inductively coupled plasma mass spectrometry (ICP-MS), energy-dispersive X-ray spectroscopy (EDS), scanning electron microscopy (SEM), confocal laser scanning microscopy (CLSM), and Brunauer-Emmet-Teller (BET) analysis. The results show that the chemical cleaning used at the pilot plant was not effective at fully removing the formed cake layer from the modules, but rather pushed the cake layer towards the centre of the module. Cake layer formation was most likely the primary fouling mechanism. However, signs of pore blocking were also found on the membranes. The cake layer seems to have been mainly composed of humic substances, polysaccharides, and iron and aluminium flocs. Signs of fouling were also found from areas without visible cake layer, mainly by organic foulants and aluminium flocs.

.

TIIVISTELMÄ

Lappeenrannan-Lahden teknillinen yliopisto LUT
LUT School of Engineering Science
Master's Programme in Chemical Engineering for Water Treatment

Kalle Kakko

Membraanien likaantuminen pintavesien onttokuitumembraanisuodatuksessa

Diplomityö
2020
110 sivua, 20 kuvaa, 11 taulukko
Tarkastajat: Mari Kallioinen, Panu Laurell

Avainsanat: membraanisuodatus, likaantuminen, kakkukerros, onttokuitu

Membraanisuodatus on lupaava prosessi juomaveden tuottamiseksi. Suurin haaste membraanisuodatuksen käyttöönottamiseksi tässä tarkoituksessa on membraanien likaantuminen. Tämä työ sisältää kirjallisuuskatsauksen membraanisuodatuksesta ja likaantumisesta membraaniprosesseissa, mikä keskittyy ultra- ja mikrosuodatuksiin. Työ sisältää myös kokeellisen osion, jossa analysoidaan membraanien likaantumista, joka oli tapahtunut Helsingin seudun ympäristöpalvelujen (HSY) operoimalla pilottilaitoksella. Tätä työtä varten käytettyihin mittausmenetelmiin kuuluvat infrapunaspektroskopia, CHN (hiili-vety-typpi) analyysi, induktiivisesti kytketty plasma massaspektrometria (ICP-MS), pyyhkäisyelektronimikroskopia (SEM), konfokaalinen laseri pyyhkäisymikroskopia (CLSM), optinen mikroskopia ja Brunauer-Emmet-Teller (BET) analyysi. Myös pilottilaitokselta saatuja permeaattivuon ja paineen mittaustuloksia on analysoitu hyödyntäen likaantumisvastuksien mallintamista. Työn tulokset osoittavat, että pilottilaitoksella käytössä ollut kemiallinen pesu ei ollut tehokas kakkukerroksen poistamisesta moduuleista, vaan kakkukerrros on työntynyt pesujen aikana kohti moduulin keskustaa. Kakkukerroksen muodostuminen on luultavasti ollut membraanien pääasiallinen likaantumismuoto, mutta membraanien pinnalla on havaittu merkkejä myös huokosten tukkeutumisesta. Kakkukerros on muodostunut pääosin humusaineista, polysakkarideista ja metalliflokeista. Myös ne moduulien alueet, joissa ei ollut muodostunut kakkukerrosta, olivat likaantuneet. Tämä lika koostui lähinnä orgaanisista aineista ja alumiiniflokeista.

USED SYMBOLS

J	total volumetric velocity through the membrane (m s^{-1})
A	filtration area (m^2)
ρ	pore density, number of pores per area (m^{-2})
r	single pore radius (m)
μ	absolute viscosity of solution (Pa*s)
τ	tortuosity factor (-)
z	thickness of the filtration layer (-)
$\Delta p/\Delta z$	pressure gradient across the filtration layer (Pa m^{-1}).
k_D	diffusion coefficient (m^2 s^{-1})
δ	boundary layer thickness (m)
c_w	concentration at membrane surface (mol/l)
c_b	bulk concentration (mol/l)
t	filtration time (s)
V	filtration volume (l)
k	filtration coefficient (-)
m	the fouling coefficient of blocking filtration laws (-)
R_t	total filtration resistance (m^{-1})
R_m	membrane's resistance (m^{-1})
R_{cp}	resistance created of concentration polarization (m^{-1})
R_a	resistance created of polar adsorption (m^{-1})
R_b	resistance of pore blocking(m^{-1})
R_c	cake resistance (m^{-1})

R_r	resistance by reversible fouling (m^{-1})
R_{ir}	resistance by irreversible fouling (m^{-1})
r	distance from the center line of the module (cm)
d	distance from the closed-end of the module (cm)
q_i	initial volumetric flux after a cleaning (m^3/h)
Δp_i	initial transmembrane pressure corresponding to q_i (Pa)
q_o	initial volumetric flux after at the start of the pilot experiment (m^3/h)
Δp_o	transmembrane pressure corresponding to q_0 (Pa)
$C_{e,j}(i)$	ratio between the extracted amount of metal *i* and total amount of extracted metals in extraction *j* (g/g)
$C_c(j)$	ratio between the amount of metal *i* that was found in the cake layer and the total amount of metals (g/g)
$m_{e,j}(i)$	mass of extracted metal *i* in extraction *j* (g)
$m_{e,j}(tot.)$	sum of all metals extracted in extraction *j* (g)
$m_c(i)$	mass of metal *i* measured in the cake layer (g)
$m_c(tot.)$	total mass of all metals measured in the cake layer (g)

ABBREVIATIONS

AFM	atomic force microscope
ALG	aluminium sulfate
ATR-FTIR	attenuated total reflectance Fourier transform infrared spectroscopy
BET	Brunauer-Emmet-Teller from BET theory
BPA	bisphenol A
BSE	back-scattered electron
CA	cellulose acetate
CB	carbon black
CECs	chemicals of emerging concern
CFD	computational fluid dynamics
CHN	carbon-hydrogen-nitrogen
CLSM	confocal laser scanning microscopy
ConA	Concanavalin A
GAC	granular activated carbon
DBPs	disinfection by-products
DLVO	Dejaquin-Landau-Verway-Ovebeek from the DLVO theory
DOC	dissolved organic carbon
EDS	energy-dispersive X-ray spectroscopy
HPI	hydrophilic (fraction of NOM)
HPO	hydrophobic (fraction of NOM)
HSY	Helsinki Region Environmental Services Authority
ICP-MS	inductively coupled plasma mass spectrometry

MF	microfiltration
MWCO	molecular weight cut-off
NF	nanofiltration
NOM	natural organic matter
PAC	powdered activated carbon
PBS	phosphate buffered saline
PCA	principal component analysis
PE	polyethylene
PES	polyether sulfone
PP	polypropylene
PS	polysulfone
PVDF	polyvinylidene fluoride
RO	reverse osmosis
SEC	size-exclusion chromatography
SEM	scanning electron microscope
TC	total carbon
TMP	transmembrane pressure
TOC	total organic carbon
TPI	transphobic (fraction of NOM)
TSS	total suspended solids
UF	ultrafiltration
US	ultrasound
XDLVO	extended DLVO theory

ACKNOWLEDGEMENTS

First of I would like to thank HSY for providing an interesting topic and funding for this master's thesis. I'm also thankful to both the examiners, Mari Kallioinen and Panu Laurell, for making the completion of this work possible. Special thanks to Tiina Virtanen, who worked as a supervisor for this work, and provided lots of help with the laboratory work and helped immensely with the writing. I would also like to thank Mika Mänttäri for helping with formation of the topic and for providing ideas for the work.

Several other people also helped me with conducting the necessary laboratory work, all of whom I am thankful for. I am especially grateful for Liisa Puro, who provided expertise with several analysis methods, and Toni Väkiparta, who helped with conducting the SEM-EDS analysis.

TABLE OF CONTENTS

1. Introduction

Urbanization and increasing population densities around the world mean that the capacity for producing clean water must be increased and more polluted water sources may have to be utilized. Research for new flexible water purification processes is further driven by the fact, that the conventional coagulation-based process, which is currently the main process for purification of surface waters, has multiple drawbacks to it. The process is complex and typically includes several filtrations and oxidation treatments. It also consumes large amounts of chemicals and takes large areas of space, which is why it may be unsuitable for meeting the rising demand for clean water. New methods of rising interest designed for drinking water production include membrane filtration and others such as adsorption and ion-exchange. (Bhatnagar & Sillanpää, 2017; Bolto et al. 2002).

Applications for membranes are available for most types of water treatment. Several different membrane processes have also been researched and developed for drinking water production. These processes could decrease the chemical consumption currently needed for production of drinking water. One of the main drawbacks in membrane filtration is membrane fouling. Fouling decreases the treatment capacity and membranes' lifetime. Membrane fouling is a complex phenomenon, which makes it difficult to control due to the high number of factors affecting it. In order to control and model fouling efficiently, it must be studied carefully and foulants and fouling mechanisms affecting the process have to be identified. In the field of drinking water production, the methods for studying fouling are still rather underdevelopment and most studies focus on monitoring the development of permeate flux in small-scale laboratory or pilot experiments. New research with novel methodology is needed in order to identify factors affecting membrane fouling.

The experimental part of this work is based on fouling that has occurred during membrane filtration pilot plant experiments conducted by Helsinki Region Environmental Services Authority (HSY). The pilot plant used submerged hollow fiber ultrafiltration and was designed for testing the suitability of membrane filtration for drinking water production. The objective of the study was to identify different foulants and fouling mechanisms that affected the pilot filtration. Secondary objective was to assess how to fouling control at the pilot process could be improved.

2. Microfiltration (MF) and ultrafiltration (UF) used for drinking water production

Membrane filtration is a broad term covering multiple different processes. Most common application for membrane filtration is water treatment. The processes are based on membranes, which are films with selective permeability. Understanding the basic principles and operational parameters is vital before more complex events such as fouling can be understood. This section covers several important factors regarding membrane filtration including different types of membrane filtration, membrane material and configuration, pretreatments and chemicals used in the process and raw water quality.

MF and UF are both pressure-driven membrane filtrations, which means that the force used for driving water through the membrane is transmembrane pressure (TMP), which is created by an outside source, such as a pump. Other pressure-driven membrane filtrations include nanofiltration (NF) and reverse osmosis (RO). The pressure-driven filtrations can be classified based on the size of the compounds that they are capable of rejecting efficiently although there are other differences as well. The removal size ranges can be roughly estimated as (Vickers, 2016):

- MF: 1–0.1 µm or 100 000–500 000 Da
- UF: 0.1–0.01 µm or 1000–100 000 Da
- NF: 0.01–0.001µm or 100–1000 Da
- RO: <0.001 µm or <100 Da.

Compared to the other pressure-driven membrane filtration, MF and UF are quite similar in membrane and process designs. MF/UF are even commonly referred as low-pressure membrane filtrations. This is because, membranes with small cut-off size tend to require more pressure to force the process water through the membrane, thus MF/UF can operate effectively with smaller TMP than NF/RO. The pilot experiment run by HSY used UF, therefore this work also focuses on MF/UF.

MF and UF have been researched for well over 20 years for the production of drinking water. Membranes used for MF/UF contain pores, from which water can easily pass through the membrane but pollutants larger than the pores are sieved out. This mechanism is called size exclusion. (Vickers, 2016) While size exclusion is the most important separation mechanism in low-pressure membrane filtration, other mechanisms do exist as well, for example:

- Adsorption: For example, humic acids, which are highly abundance in raw water, can be adsorbed on the membrane surface (Sutzkover-Gutman et al. 2010).
- Electrostatic or charge repulsion: The zeta potential of a membrane affects its interactions with charged pollutants and can even repulse some away from the pores (Lee & Cho, 2004).
- Biological degradation: Because most membrane modules are not sterile, biological degradation caused by micro-organisms may occur inside them (Gao et al. 2011).

Size exclusion is primary affected by the pore size distribution of the membrane. Most commercial membranes have a molecular weight cut-off (MWCO) announced for them, which refers to the molecular weight at which 90 % of certain model compounds are rejected by the membrane and retained at feed side. Because there are multiple different types of interaction mechanisms with the pollutants and membrane surface, other membrane parameters such as roughness, surface charge and hydrophobicity are also important for the process.

2.1 Membrane modules and materials

The operational unit in membrane filtration is called a membrane module, which can contain several individual membranes. Filtration process can use several modules and the flow configuration between them can differ. For example, modules can be set-up in series or parallel to each other. There may also be a recirculation flow from the permeate flux back into the feed flux. Recirculation can be used to control the concentration of the feed, which allows for optimal conditions for the used membrane. Crossflow refers to the water flow parallel to the membrane surface. It is an important parameter for controlling fouling because the shear stress it induces reduces most types of fouling.

Most common membrane materials used in drinking water production are either polymeric or ceramic. Common polymeric porous membrane materials include polyvinylidene difluoride (PVDF), polypropylene (PP), polyethersulfone (PES) and polysulfone (PS). Membranes made from these materials are hydrophobic, light, thin and flexible. They also have high oxidant tolerance. Cellulose acetate (CA) is another well-researched polymeric membrane material. It is hydrophilic, which makes it more resistant to fouling by organic compounds than the hydrophobic polymeric membranes. The biggest drawback of CA membranes is their low

chlorine resistance, which makes unmodified CA membranes unviable for a lot of drinking water production processes due to common use of chlorine and other oxidants for disinfection. (Jacengelo & Noack, 2016)

Commercial polymeric membranes can be shaped in multiple different ways. Most common designs include flat-sheet, spiral wound, tubular and hollow fiber. In drinking water production, the hollow fiber module is the prevailing module design for both MF and UF applications. (Jacengelo & Noack, 2016) Hollow fiber modules will be the focus of this work, because that was the design used in the pilot plant run by HSY.

A hollow fiber membrane module consists of hundreds of hollow fiber membranes, which are bound together and encased. The inner diameter of the fibers ranges from 0.4–1.5 mm. The main advantage of hollow fiber membranes is high surface area to volume ratio due to their structure. Another advantage of the hollow fiber membranes is that the membranes can be efficiently cleaned by backwashing, because the small inner diameter of the fibers makes them unlikely to collapse under pressure. One disadvantage hollow fiber membranes have is that, due to the large number of fibers and the closed module, detection of fouling and other defects can be difficult, especially in an industrial setting. (Jacengelo & Noack, 2016)

Hollow fiber membranes have two common distinctive configurations for water flow: inside-out and outside-in. An outside-in module is less likely to be plugged by big particles. Also, because the surface area of hydraulic loading is larger, outside-in modules have less head loss and potentially larger fluxes. On the other hand, precise control over the hydrodynamic conditions is difficult and outside-in modules are more prone to dead-end zones and otherwise uneven flow patterns. (Jacengelo & Noack, 2016) Hollow fiber modules can be submerged in water in a large tank or they can be surrounded by smaller water-tight casing. The external case allows for better control of the hydrodynamic conditions around the fibers.

Ceramic membranes are functionally and structurally different from polymeric membranes. They are prepared by sintering from inorganic materials, such as aluminium oxide, titanium oxide, zirconium oxide or a carbon composite. (Jacengelo & Noack, 2016) In comparison to polymeric membranes, ceramic membranes are considered to have several advantages. Mainly, ceramic membranes are resistant to degradation from biological and chemical sources and they are also less prone to fouling and have better cleaning properties. This means that ceramic membranes can operate with higher foulant concentration. Ceramic membranes can also handle extreme temperatures and pH levels better than polymeric membranes. (Harman

et al. 2010). In a fouling experiment with simulated surface water conducted by Alresheedi et al. (2019), the backwashing efficiency (based on recovered flux) of a commercial ceramic membrane (nominal pore size: 0.01 µm) was over two times better than that of commercial polymeric membrane (nominal pore size: 0.01 µm). Because of the physical durability, ceramic membranes can handle higher fluxes than polymeric membranes, which further increases backwashing efficiency and can decrease the need for chemical cleaning (Harman et al. 2010). Currently the main disadvantage of ceramic membranes is that the modules are more expensive than polymeric ones (Harman et al. 2010). This is partly compensated by capability of the ceramic membranes to operate with higher pollutant concentrations due to having increased potential for fouling control, which increases overall potential process capacity (Bottino et al. 2001).

2.2 Raw water quality: characterisation of natural organic matter (NOM)

Optimization of any water treatment process is highly depended on the raw water quality. The water quality affects optimal dosing of chemicals, recirculation and the demand for cleaning. While proper pretreatment is important for improving filtration efficiency, adding excess amounts of coagulants or adsorbents can also have negative effects on the process, such as increased fouling. Excessive dosage amounts also cause unnecessary operational costs, so it is important to optimize the used dosages. For this optimization to be successful, analysis of the raw water quality is vital.

Natural water includes several organic and inorganic compounds. Largest solid particles, such as sand or parts of plants, are commonly sieved out before membrane treatment, but the feed water may still include bacteria, algae, inorganic compounds and other smaller organic compounds commonly referred as natural organic matter (NOM). NOM is a general term referring to a mixture of organic compounds present in fresh water. NOM has multiple sources. Part of it may origin from decaying plant-based organic matter like leaves, roots or algae. It may also include traces from dead animals and bacteria like cell fragments, macromolecules and acids. Another possible source is human waste like wastewater plant effluent. This part of NOM is sometimes referred as effluent organic matter (Speth & Reiss, 2016).

NOM is considered to be the most important factor for membrane fouling by natural waters due to its broad size range and abundance (Huang et al. 2007). Compounds present in NOM differ

largely in molecular size, charge and other properties, which makes pinpointing the factors and mechanisms behind NOM-induced fouling a difficult task (Matilainen et al. 2011). In order to be able to research the fouling properties of a large heterogenous mixture such as NOM, it's commonly categorized based on its properties such as origin, polarity, solubility and molecular weight. (Adusei-Gyamfi et al. 2019)

NOM consists of non-humics and humic substances. Non-humics refers to biopolymers and nutrients such as polysaccharides, proteins and amides, as well as other organic matter. Non-humic substances are the precursors of humic substances, which are formed through microbial decomposition of organic matter found in animals and plants. These substances are more stable than their precursors, which is why they are abundant in surface waters and ground. (Sutzkover-Gutman et al. 2010)

Humic substances can be classified roughly into three categories primarily based on their solubility to water: fulvic acids, humic acids and humins. Fulvic acids are soluble in water at all pH ranges. Humic acids precipitate at pH below 2 and they are generally more hydrophobic than fulvic acids. Humins are always insoluble in water and consist of fatty acids and bitumen. Humic and fulvic acids contain plenty of phenols and carboxyl groups. Humic substances contain approximately 40–60 % carbon, 30–50 % oxygen, 4–5 % hydrogen and 1–4 % of nitrogen and small amounts of sulfur and phosphorus. (Sutzkover-Gutman et al. 2010) Fulvic acids contain more hydrogen and less nitrogen relative to carbon content than humic acids. The average H/C and C/N ratios for non-commercial FA are around 1.1 and 93.1 based on research results gathered by Rodriguez & Nunez (2011). For non-commercial HA the same numbers were 0.9 and 32.5, respectively. Fulvic acids also tend to contain more carboxylic groups and less phenolic groups than humic acids. (Rodriguez & Nunez, 2011) It should be noted that the humic substance categories are not clean-cut and so differences between them are generalizations.

The molecular size and hydrophobicity of a particle are two of the most significant properties affecting membrane fouling. In research NOM is usually categorized into factors based on one of these properties. NOM can be divided into hydrophobic (HPO), transphobic (TPI) and hydrophilic fractions (HPI) using the XAD-4 and XAD-8 resin technique. (Matilainen et al. 2011) The chemical compositions of these fractions are presented in Table I.

Table I Hydrophobic fractions of NOM.

Fraction	**General description (Adapted from Speth & Reiss, 2016)**	**Examples (Adapted from Matilainen et al. 2011)**
Hydrophobic (HPO)	High-MW and low-density acids	Soil fulvic acids, carboxylic acids, humic acids
Transphobic (TPI)	Medium-MW and medium-density acids	Simple organic acids, sugar acids
Hydrophilic (HPI)	Biopolymers	Polysaccharides, alcohols, carbohydrates, amides, proteins

In literature, it is often stated that the HPO fraction constitutes about 50 % of total dissolved organic carbon (DOC) and the TPI and HPI fractions both include 25 % of total DOC. However, these fractions can vary a lot. For example, the HPO and HPI fractions of surface water samples analysed by Huang et al. (2007) varied between 39–60 % and 17–36 %, respectively.

Size-exclusion chromatography (SEC) is a popular method for dividing NOM into molar weight (MW) based fractions. Different techniques can be paired with SEC to improve the results. (Matilainen et al. 2011) In particular, high-performance SEC paired with online DOC and UV detectors (SEC-DOC/UV) has achieved popularity in published research. This method presents NOM in three distinctive peaks, which include compounds with different properties: (Huang et al. 2007)

- High-MW (>10 000 Da), low UV absorption: colloids and macromolecules
- Medium-MW (1000–10 000 Da), high UV absorption: humic substances
- Low-MW (>1000 Da): low-MW organic acids.

The NOM-based colloids are created when weak forces, such as Van der Walls forces, cause humic substances to form supramolecular structures. The form of these colloidal structures is controlled by their concentration and pH of the solution. These colloids can appear either as rigid colloidal particles or flexible linear polyelectrolytes. (Sutzkover-Gutman et al. 2010)

When fractions based on hydrophobicity and molecular weight are not specific enough, other methods may be used for characterisation of NOM. Techniques such as infrared or fluorescence spectroscopy can be used to differentiate between specific groups of non-humic and humic substances (Matilainen et al. 2011). These measurements can be combined with statistical multicomponent analysis, such as principal component analysis (PCA), to expand on the results. (Peiris et al. 2011)

2.3 Pretreatments used with membrane filtration

For drinking water production, low-pressure membrane filtration must often be coupled with other treatments to reach sufficient treatment results. Chlorination is commonly one of the used treatments. It is mainly used for disinfection and odour removal, but chlorination and other oxidation treatments can also be used for removal of metals, such as manganese (Kimura & Oki. 2017). Chlorination and other treatments with strong oxidation agents, create hazardous compounds known as disinfenction by-products (DBPs). It has been estimated that low-pressure membrane filtration removes less than 10 % of DBPs' precursors. Thus, if the feed water has been chlorinated prior to the membrane filtration, the removal efficiency of the filtration must be improved with pretreatments, or the DBPs have to be removed in posttreatment. (Vickers et al. 1995). Other common preatreatments with MF/UF are coagulation, adsorption and oxidation. Especially coagulation is used commonly due to DBPs and for treating fractions of NOM with small particle size. Coagulation can be used to reach higher removal rate for total organic carbon (TOC) and inorganic pollutants like metal ions (Jacengelo & Noack, 2016)

The most common coagulants used with membrane filtration for NOM removal are aluminium- or iron-based compounds such as aluminium sulfate (alum), aluminium chloride, ferric chloride and ferric sulfate. NOM removal efficiencies of iron and aluminium coagulants are fairly close (70 % to 67 % respectively) according to a review by Adusei-Gyamfi et al. (2019). Coagulation is based on the formation of flocs. When coagulants are added into NOM containing water, insoluble micro- or nanoparticles are formed around the coagulant metals. The formation of these small particles can be based on multiple different mechanisms simultaneously, which include entrapment, destabilisation, adsorption and complexation. (Jarvis et al. 2004). The dominant mechanism is affected by NOM characteristics, coagulant concentration and the

available ligands for complexation. (Adusei-Gyamfi et al. 2019) When the nano- or microparticles keep interacting with pollutants in water, they maintain growth in size and eventually full flocs are formed. (Jarvis et al. 2004) Floc formation is often accelerated by mixing, which takes place inside a flocculation tank or tube. Often coagulation processes aim specifically to form metal hydroxide-NOM complexes. Other metal-NOM complexes, such as Al-NOM or Fe-NOM, may dissoluble in water. Dissolved residue metals may lower the quality of the treated water and cause other harmful effects. The main method for ensuring that right kind of complexes are formed, is to ensure that the coagulant dosage is high enough. (Adusei-Gyamfi et al. 2019)

There are two common configurations for utilizing coagulation in membrane filtration processes: in-line coagulation and coagulation/sedimentation. In coagulation/sedimentation, most of the flocs—containing pollutants from the treated water—are separated in a sedimentation step before filtration, thus reducing the pollutant concentrations before filtration. In-line coagulation means that the coagulants are added into the process stream before filtration and the flocs are separated during membrane filtration (Gao et al. 2011). Compared to coagulation/sedimentation, in-line coagulation takes less steps to execute and has bigger impact on the membrane filtration. Flocs present during filtration are generally considered to have possible effects on removal efficiency and fouling by creating adsorptive protective layer on top of the membrane. However, in-line coagulation can also increase fouling in some cases (Ma et al. 2019). This happens mainly, when the flocculation is unsuccessful, and the formed flocs are small enough to enter membrane pores. Similarly to coagulation, adsorption dosage can also be used in-line or with a separate step for removal of the adsorbents. The benefits and disadvantages of in-line adsorption are similar to in-line coagulation; adsorbents may also form a protective cake layer on the membrane (Lohwacharin et al. 2010).

In Fig. 1, the unit operations in the conventional process and membrane filtration process are compared. The block diagram was modelled after a block diagram of the conventional water treatment process made by Lebeau et al. (1998). The block diagram for membrane filtration process is based on the pilot process by HSY although the in the actual pilot process this work is based on the final chlorination step was replaced by post-filtration. The conventional coagulation process commonly includes a combination of coagulation, flocculation, sedimentation, pre- and post-filtration and disinfection such as oxidation or chlorination. The plant in Paris utilized granular activated carbon (GAC) post-filtration. Sometimes other chemicals like lime and polymers can also be added. (Bottino et al. 2001) The process has high

space demand, especially due to the sedimentation step. Because membrane filtration has improved removal efficiency compared to coagulation/sedimentation, same or better water quality can be achieved with fewer process steps.

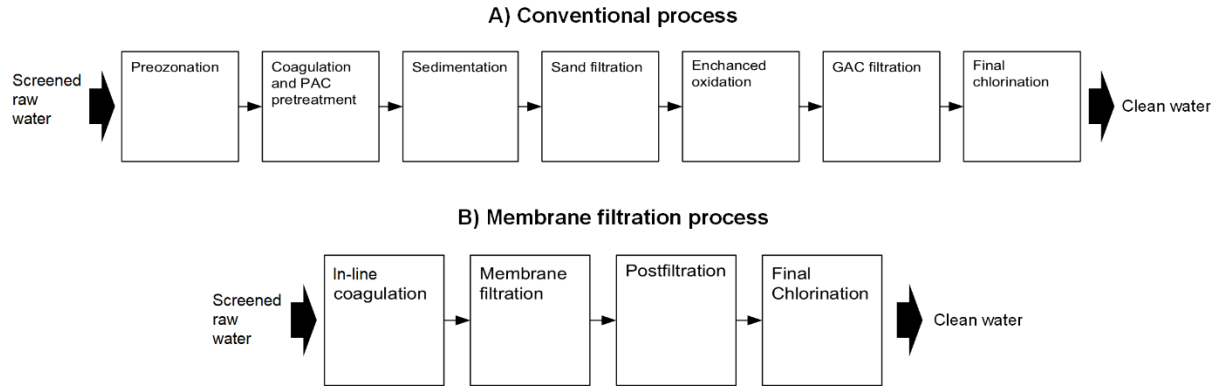

Figure 1 Unit operations in A) conventional water treatment plant in Paris (Adapted from Lebeau et al. 1998) compared to B) possible design for membrane filtration process (based on the pilot process by HSY)

2.4 Treatment results of MF/UF applications designed for drinking water production

In Table II, there are gathered treatments results related to drinking water production by low-pressure filtration. The sample studies chosen for Table II were selected to showcase different types of MF/UF processes and pretreatments. The first results presented were obtained by Nakatsuka et al. (1996) from a bench-scale filtration experiment run for 80 days. They used two membranes: one MF and one UF membrane. The tighter UF membrane was able to remove slightly more TOC and iron than the MF membrane. In addition to the listed results, close to all suspended solids (TSS) and bacteria were removed during the treatment by both membranes. The results by Lebaue et al. (1998) presented also in Table II are based on immersed hollow fiber MF/PAC process run in pilot-scale for over a year. They utilized in-line coagulation with polyaluminium chlorine and powdered activated carbon (PAC) slurry reactor integrated with the MF, but the treatment results are comparable to those obtained by Nakatsuka et al. (1996). Study by Fiksdal & Leiknes (2006) showcases difference in the virus removal efficiency of UF with and without coagulation. When aluminium sulfate (ALG) or

aluminium chloride were added, the removal rate increased close to 100 % as the log reduction value (LRV) reached over 7.2 with both coagulants. Table II also present a study by Lee & Cho (2003) comparing treatment results by a ceramic and polymetric membrane with similar MWCO. Although the treatment results by the membranes were similar, the ceramic membrane had much higher pure water permeability (9.4 to 6.8 L dm^{-2} kPa^{-1}), which may help to improve the process capacity.

Table II Treatments results by MF/UF application designed for drinking water production

Source	**Feed water**	**Membrane**	**Pretreament**	**Results**
Nakatsuka et al. (1996)	River water: Max. values Turbidity 67 NTU, TOC 12.8 mg/L, Total iron 540 ug/l	PES hollow fiber (MWCO: 30 000 Da)	Prefilter (200 µm mesh screen)	Turbidity 100 % TOC 46–83 %, Iron 92–96 %
		CA hollow fiber (MWCO: 200 000 Da)	Prefilter (200 µm mesh screen)	Turbidity 100 % TOC 47–74 %, Iron 88–94 %
Lebaue et al. (1998)	Raw water: TSS 16.9 mg/l TOC 3.4 mg/l DOC 3.2 mg/l Fe 450 ug/l	Hollow fiber MF/PAC (MWCO: 200 kDa)	Screening, In-line coagulation	TSS 99 % DOC 69 % Fe 96 %
Fiksdal and Leiknes (2006)	Simulated raw water spiked with MS2 virus ($10^{7.0}$–$10^{8.1}$ pfu/mL)	PP UF (MWCO: 30 kDa)	None	LRV 0.5
			3 mg ALG/ml	LRV>7.2
		PES MF (Pore diameter: 0.2 µm)	None	LRV 0
			3 mg/L ALG	LRV>7.2
Lee and Cho (2003)	Raw water: DOC 3.8 mg/l	Polyamide TFC (Thin-film composite, MWCO 8 kDa)	0.45 µm Nylon filter	DOC ca. 40–50 %
		TiO_2 Ceramic membrane (MWCO: 8 kDa)	0.45 µm Nylon filter	DOC ca. 40–50 %

2.5 Removal of emerging pollutants with MF/UF

While researching or developing a future process, it's reasonable to observe future threats and challenges in the field as well as prevailing conditions. Microplastics are today's hot topic in wastewater treatment. The health effects they have on humans are not completely understood yet, but some health hazards have been linked to them, mainly because microplastics can act as carriers for toxins (Ma et al. 2019). Low concentrations of microplastics have been detected in surface waters and are expected to keep rising, which is why it's important to ensure their removal from drinking water.

Microplastics float in water, which makes treating them through coagulation/sedimentation difficult. Because of their size, typically ranging from 5 mm to couple micrometres, UF/MF can be assumed to be an effective way to treat them. This assumption has been tested by Ma et al. (2019). In their experiment all polyethylene (PE) microplastics (0.5 mm < d < 5 mm) were removed from water with flat-sheet PVDF UF membrane (100 kDa) with or without coagulation. Currently, microplastic concentrations are low enough that they have significant effect on real-life membrane filtration processes, but they could potentially be a new source of foulants in the future.

Chemicals of emerging concern (CECs) are pollutants, which have been found to have increasing concentrations in surface waters. They raise concern due to the negative effects they could cause on wildlife and human health. CECs include a large variety of endocrine-disrupting compounds, pharmaceuticals and personal care products. Due to their small size (<1000 Da) they are less affected by size exclusion of MF and UF membranes, therefore other membrane process like NF and RO are more suitable for removing them. However, MF/UF membranes may still reject CECs through other means; Highly charged membranes have been found to repulse them through electrostatic repulsion (Kim et al. 2018). Some membranes can also absorb them, for example PS membrane has been shown to adsorb bisphenol A (BPA) as its main removal mechanism by Su-Hua et al. (2010). In their filtration experiment with PS membrane (MWCO: 20 kDa) 40.9 % of BPA was adsorbed on the membrane during initial filtration although the retention rate and adsorbed amount diminished with each additional filtration. This shows that for this kind of treatment to be effective, the bond between BPA and membrane has to be strengthened by modification of membranes or by optimizing conditions.

Coagulation or adsorbent dosage can improve the treatment results of MF/UF for removal of CECs. Sheng et al. (2016) combined membrane filtration with powdered activated carbon treatment to achieve 90 % average removal efficiency for 16 tested CECs while PAC and UF (MWCO 100 kDa) separately reached only 50 % and 29 % removal efficiency, respectively. Coagulation with aluminium chloride combined with UF improved the removal efficiency only slightly compared to treatment with only UF (to 33 % from 29 %).

3. Membrane fouling in MF/UF applications when treating surface waters

Membrane fouling is one of the biggest challenges in membrane technology. Membrane fouling has been given many different definitions, but essentially it means deposition and agglomeration of chemical compounds from the treated solution on the membrane surface or inside the membrane itself, which causes a change in the functionality of the membrane. Because membrane fouling is affected by multiple factors, a diagram summarizing contents of this section is presented in Fig. 2. The diagram does not present every factor relating to fouling nor does it show every connection between different categories but rather its purpose is to summarize factors and connections most relevant to this work.

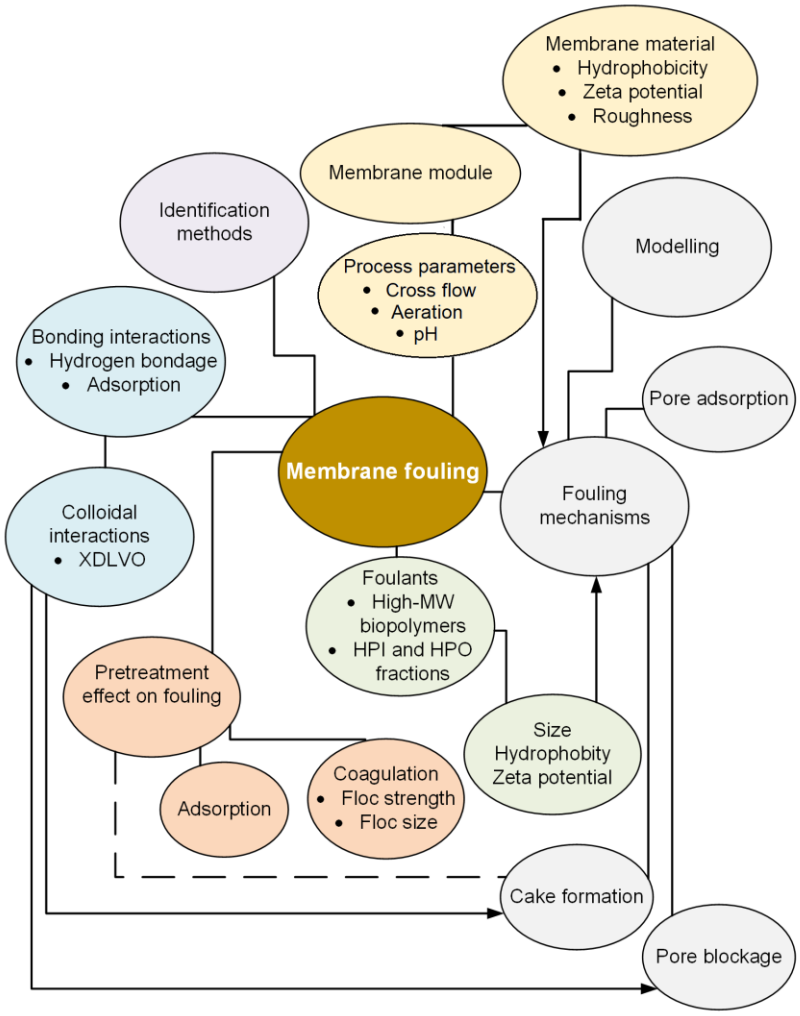

Figure 2 Diagram about the factors affecting fouling related to low-pressure filtration of surface waters.

Fouling can be categorized into physico-chemical fouling caused by particles in the water and biological fouling caused by biological activities. Most common form of biofouling is the formation of biofilm caused by microbes, commonly bacteria, in the filtrated water. Before the biofilm can be formed, the microbes must be able to attach to the membrane surface. This fouling type is more prevalent in NF and RO processes because the conditions are more suitable for the attachment of microbes and biological growth. Firstly, the typical fluxes are smaller, and secondly the regular cleaning and backwashing present in low-pressure filtration processes helps to disturb biological activities. (Chellam & Zandler, 2016)

Biofouling can be reduced in couple of different ways. The microbial attachment can be disturbed in its early stages by backwashing or crossflow (Chellam & Zandler, 2016). Another way would be to decrease the availability of nutrients in the water or increase the dose of inhibiting chemicals for example by chlorination. Membranes can also be modified to have inhibiting properties.

Biofouling is a more typical type of fouling for wastewater treatment than for drinking water production due to higher nutrient concentrations, slower filtration fluxes and high number of bacteria present. Because physico-chemical fouling is more typical for drinking water production processes, it will be the main focus of this section and will be referred simply as fouling.

3.1 Fouling mechanisms

Fouling can affect a membrane in multiple ways, but the most noticeable sign often is the decrease in permeate flux. Therefore, fouling modelling is usually focused on the permeate flux. The volumetric rate for permeate (*q,* $m^3\ s^{-1}$) can be defined as:

$$q = J * A \quad (1)$$

, where:

J is volumetric flux through the membrane ($m\ s^{-1}$)

A is filtration area (m^2).

By considering the membrane as a bundle of identical cylindrical pores, laminar flow through the membrane can be expressed using the Poiseuille's law as follow (Chellam & Zandler, 2016):

$$\mathrm{J} = \frac{\rho\,\pi \mathrm{D}^4}{128\mu\tau}\frac{\Delta \mathrm{p}}{\Delta \mathrm{z}} \qquad (2)$$

, where:

- ρ is pore density, number of pores per area (m^{-2})
- D is single pore diameter (m)
- μ is absolute viscosity of solution (Pa*s)
- τ is tortuosity factor
- z is the thickness of the filtration layer
- $\Delta p/\Delta z$ is pressure gradient across the filtration layer (Pa m^{-1}).

Initial flux (J_0) refers to the permeate flux at the start of the filtration. Due to fouling, the permeate flux decreases when the filtration continues. At any time, the ratio between the current flux and the initial flux can be calculated from equation (3), assuming that the transmembrane pressure, tortuosity of the pores and viscosity are constant, to be the following:

$$\frac{\mathrm{J}}{\mathrm{J}_0} = \frac{\rho}{\rho_0}\left(\frac{\mathrm{D}}{\mathrm{D}_0}\right)^4\left(\frac{\Delta \mathrm{z}}{\Delta \mathrm{z}_0}\right)^{-1} \qquad (3)$$

Each of the right side terms in equation (3) corresponds with a different type of membrane fouling. These fouling types and corresponding terms are: (Chellam & Zandler, 2016)

- Pore blocking, ρ/ρ_0
- Pore adsorption, $(r/r_0)^2$
- Cake formation, $(\Delta z/\Delta z_0)^{-1}$.

Pore blocking occurs when the filtrated particles are roughly equal in size with the membrane pores. In pore blocking, the particles either block the pore entrance on the membrane surface or first enter the pores and then block them internally. While pore blocking can occur on the membrane surface or internally, because pores of real membranes tend to widen in diameter

after the pore entrance, blocking is more likely to happen on the membrane surface. In either case, the permeate flux decreases because the number of effective pores on the membrane is reduced. When the filtrated particles or other compounds are substantively smaller than the pores, pore adsorption may occur. When the particles enter the pores, some may be adsorbed on to the pore walls. This leads to decreased effective pore size, which increases hydraulic loading. Cake formation i.e. surface coverage works in a similar way as in other filtration processes. Large particles, which can't enter inside the membrane, form a filtration cake or gel layer on top of the membrane. Cake layer adds resistance and it can be viewed to increase the effective filtration layer thickness. (Chellam & Zandler, 2016) The filtration cake can also act as an adsorption layer for smaller particles in the solution. (Zhao et al. 2000) The cake resistance created by cake formation is similar to the specific cake resistance used in non-membrane filtration models (Tien & Ramarao, 2011).

The resistance caused by cake layer to the filtration is related to the porosity of the cake layer similarly to cake filtrations. Cake layer with high porosity creates less resistance and doesn't decrease the permeate flux as much as cake layer with lower porosity. Cake porosity is related to the particle size of the particles forming it. This has been studied with coagulants and flocs but also with other particles. For example, when microplastics were filtrated through flat-sheet PVDF UF membrane (100 kDa) membrane in the study by Ma et al. (2019), the flux decrease was directly linked to the size range of microparticles that were filtrated. Larger particles (2 mm $<d<$ 5 mm) had higher flux at the end of filtration related to the initial flux (J/J_0=0.87) compared to smaller particles at otherwise same conditions (d<0.5 mm, J/J_0=0.83). In-line coagulation by aluminium chlorite was also shown to increase the flux decline, most likely because the average floc size formed by aluminium chlorite (<0.3 mm) was smaller than size of the microplastics. Thus, addition of the flocs in conjunction with the microplastics reduced the porosity of the formed cake layer in comparison to the cake layer formed from just the microplastics.

When discussing about fouling the terms reversible and irreversible fouling are often used. In practice the difference between the terms comes from how well the flux can be recovered to its initial value through a chosen cleaning method. If the flux can't be recovered, fouling is considered irreversible.

3.2 Concentration polarization and gel-polarization

Concentration polarization is a phenomenon, where the concentration of compound *i* is higher near the membrane's surface than in the bulk solution due to the restricted transport of *i* through the membrane. It is an important concept for understanding cake layer formation on membranes. Due to the created concentration gradient, the particles near the membrane surface are moved away from it by diffusion towards the bulk solution while the permeate flux transports particles to the membrane surface. According to film theory, this leads to a steady-state described by the following equation: (Chellam & Zandler, 2016)

$$J = -k_D/C \frac{dC}{dx} \quad (4)$$

, where:

k_D is diffusion coefficient ($m^2\ s^{-1}$).

If it is assumed that the concentration gradient is contained within a fixed thickness layer and that the permeate flux is independent on other factors, equation (4) can be integrated into:

$$J = \frac{k_D}{\delta} \ln\left(\frac{c_w}{c_b}\right) \quad (5)$$

, where:

δ is boundary layer thickness (m)

c_w is concentration at membrane surface (mol/l)

c_b is bulk concentration (mol/l).

Because of the assumptions made, equation (5) is not necessarily accurate in practice, but it can be used to demonstrate the dependency between permeate flux and the concentration at the membrane surface. When the permeate flux is increased, the surface concentration also increases in order to achieve steady-state conditions in the boundary layer. (Chellam & Zandler, 2016) Unlike in reverse osmosis (RO), concentration polarization does not directly affect the permeate flux, because the driving force of porous membrane filtration is not affected by the

osmotic pressure. However, concentration polarization increases fouling from all sources and decreases apparent rejection rates.

The concentration at the membrane surface cannot increase indefinitely with the permeate flux and at some point, it will reach its maximum value. This relates to the gel-polarization model. In gel-polarization model, a gel or cake layer is formed on the membrane surface and this layer acts as a limiting resistance to the permeate flow rate. In gel-polarization model, the concentration at the membrane surface is fixed at so called gel concentration. Because the concentration at membrane surface will no longer increase, gel layer thickness and porosity will change instead in response to changes in permeate flux. (Sablani et al. 2001)

Critical permeate flux and limiting permeate flux are terms often used in membrane literature, sometimes interchangeably. The definition differs with sources and models, but in general they are both used to describe a permeate flux, where membrane fouling is suddenly increased drastically. Limiting flux may also refer to the point, where concentration polarization reaches its maximum value (Chellam & Zandler, 2016). In conjunction with gel-polarization theory, critical flux is used to describe the point, where a cake i.e. gel layer is formed (Sablani et al. 2001).

3.3 Fouling modelling

Accurate modelling is important for simulating results and testing the effects of changes to different parameters. Accurate modelling can also be used to estimate important parameters or mechanisms that would be impossible to measure otherwise, such as the concentration polarization layer thickness. Because of the multiple simultaneous fouling mechanics and pollutants, modelling fouling in low-pressure membrane filtration is fairly complex. One approach is to apply the blocking filtration laws developed by Hermia (1982), which are all based on a single equation:

$$\frac{d^2t}{d^2V} = k\left(\frac{dt}{dV}\right)^m \quad (6)$$

, where:

t is filtration time (s)

V is filtration volume (L)

k is filtration coefficient

m is fouling coefficent, with possible values of 2, 1.5, 1 and 0.

The blocking filtration laws are sometimes used in research, because they are simple and in theory could be used to identify the type of fouling based on the flux decline (Jonsson et al. 1996). However, they have also been criticized heavily (Tien & Ramarao, 2011; Cheng et al. 2011). One of the main issues with the blocking filtration laws is that the primary fouling type may evolve during filtration and there may be more than one fouling mechanic active at any given time. To combat these shortcomings, new models have been developed by researchers, which have led to combining different laws and making coefficients depended on time or filtration volume. (Cheng et al. 2011)

The basic assumptions made in modelling have also been criticized. For example, the uniform coating used in the standard blocking filtration law has been deemed unrealistic. Tien & Ramarao (2011) have pointed out, that the different filtration laws are unnecessary as there are more complicated and better models for individual cases. For example, specific cake filtration models and gel-polarization models can be used for modelling cake formation.

An alternative way to model effect from different types of fouling is to use the modified form of Darcy's law, which can be written as (Tien & Ramarao, 2011):

$$\mathrm{J} = \frac{\Delta \mathrm{p}}{\mu \mathrm{R_t}} \tag{7}$$

, where the total fouling resistance R_t (m^{-1}) can be defined in several ways, for example as (Chellam & Zandler, 2016):

$$\mathrm{R_t} = \mathrm{R_m} + \mathrm{R_{cp}} + \mathrm{R_a} + \mathrm{R_b} + \mathrm{R_c} \tag{8}$$

, where:

R_m is membrane's resistance (m^{-1})

R_{cp} is resistance created of concentration polarization (m^{-1})

R_a is resistance created of polar adsorption (m^{-1})

R_b is resistance of pore blocking (m^{-1})

R_c is cake resistance (m^{-1}).

Each resistance term, apart from the membrane resistance, relates to a different type of fouling. The resistances can be determined through experimental data or with well-known mathematical equations like the Carmen–Kozeny equation for cake resistance. (Tien & Ramarao, 2011). Another way to define R_t is based on fouling reversibility for example Kimura & Oki (2017) defined it as:

$$R_t = R_m + R_r + R_{ir} \quad (9)$$

, where:

R_r is resistance by reversible fouling (m^{-1})

R_{ir} is resistance by irreversible fouling (m^{-1}).

This definition can be useful because it allows to track the irreversible fouling affecting the filtration and the resistances are easily defined by comparing the fluxes at the start of the filtration, at the end and after cleaning.

3.4 Colloidal interactions in membrane fouling

Colloidal particles are a major cause of fouling in surface water filtration. They are commonly associated especially with cake formation due to their large size (Peiris et al. 2011). There can be multiple different colloidal compounds present in surface water, but the colloidal particles present in NOM are the most important ones regarding fouling due to their abundance. Because the SEC-DOC/UV method does not differentiate between high-MW macromolecules and colloidal particles, they are often inspected in conjunction to each other in research. (Huang et al. 2007)

Fouling caused by colloidal particles is largely based on their interactions with other foulants and the membrane surface. Understanding of these interactions leads to better understanding of fouling and its causes. The Dejaquin-Landau-Verway-Ovebeek (DLVO) theory of colloidal stability states that there are two important interactions behind the attachment of colloidal particles: the van der Walls interactions and the electrical double-layer interaction. In DLVO theory, the colloidal stability is dependent on the sum of the attractive forces and repulsive

forces created by these two interactions. The van der Walls interactions create an attractive force between the colloidal particles and the membrane forces. This attractive force is impactful especially for larger particles. The force created by van der Walls interactions is also dependent on the separation distance between the colloidal particle and the surface, but it's independent of the solution medium. (Chellam & Zandler, 2016)

The electrical double-layer interactions affect especially large colloidal particles or particles with a surface charge. Charged particles attract smaller charged particles (such as ion), with the opposite charge. Ions surrounding the colloidal particle can create a compact layer called Stern layer at the colloidal particle's surface. The Stern layer is surrounded with a diffuse layer, which has a gradually decreasing electric potential when moving away from the particle. Slipping plane is a plane inside the diffuse layer which separates the fluid layer surrounding the particle from the mobile fluid phase. When two particles with electrical double-layers interact, force generated by the electrical double-layer interaction is depended on the particle size, separation distance between the surfaces, diffuse double layer thickness and the both surface potentials. (Chellam & Zandler, 2016) Zeta potential is commonly used parameter, which announces the electrical potential inside the slipping plane.

The DLVO theory does not cover all possible interactions between colloidal particles and membrane surface. Especially at very close ranges other forces start to have greater impact. Some non-DLVO forces include (Chellam & Zandler, 2016):

- Attraction between hydrophobic sites in water medium.
- Steric repulsion caused by polymers or other compounds attached to the colloidal particles.
- Hydration forces, which originate from a complex phenomenon related to binding enthalpy of water near solid surfaces (Parsegian et al. 2011).

In membrane filtration, the most important non-DLVO forces in lot of cases are acid-based interactions created by polar interactions. Acid-based interactions are included in the extended DLVO theory (XDLVO). The acid-base interactions can result in hydrogen bonding between the surfaces, which results in a strong attractive force. The acid-base interactions can also be repulsive by proxy (Brant and Childress 2002). The XDLVO theory explains only the chemical interactions between colloidal particles and surfaces. In membrane filtration, there is also a hydrodynamic drag force created by the permeate flow, which can be combined with the XDLVO forces. (Lee et al. 2007).

Fouling by colloidal particles can be decreased by increasing the repulsive forces between the particles and membrane surface. The electric-double layer interactions can reduce fouling if the particle's and membrane's surface are similarly charged and there are counterions present in the treated solution. In membrane filtration this removal mechanism called charge repulsion (Lee & Cho, 2004). The strength of the electric-double layer interaction can be estimated from the zeta potentials of the interacting surfaces. Most common membranes (like PVDF) and colloidal NOM have both negative zeta potentials, so neutralizing the zeta potential decreases the repulsive force created by the electric-double layer interactions (Kakihana et al. 2017, Ratnaweera et al. 1999). Zeta potential is affected by the pH of the solution, so a negative zeta potential can be partly neutralized by lowering pH. Zeta potential is also affected by ions present in the solution. Strong cations, such as Ca^{2+}, can cause neutralization of colloidal particles and increase fouling by them (Sutzkover-Gutman et al. 2010).

3.5 Fouling properties of compounds in NOM

Before fouling caused by NOM can be controlled and modelled, it is important to identify the roles that different fractions of NOM have in the overall fouling. Thus, there have been multiple studies attempting to identify the fouling characteristics of different foulants contained in NOM.

Kimura et al. (2004) found that the irreversible fouling, which had occurred on the used PES (MWCO: 750 kDa) membrane, was mostly caused by polysaccharide-like organic matter by comparing FTIR spectra of unused and used membranes. Similarly, Huang et al. (2007) found that high-MW foulants were a major cause of fouling in their study using four different hollow fiber membranes, which included two PVDF membranes (nominal pore sizes of 0.02 µm and 0.1 µm) and two PES membranes (MWCO of 150-200 kDa and 100 kDa). Sutzkover-Gutman et al. 2010 have published an extensive review of surface water fouling, focusing on humic substances, but the results were inconclusive due to varying conditions and methods of the reviewed studies.

Hydrophilic fraction (HPI) consisting of biopolymers, such as polysaccharides, has been linked to fouling in multiple other studies as well. Lee at al. (2004) found by comparing different raw waters that, the raw water sample with the highest HPI-fraction and highest hight-MW fraction caused the most fouling in three of the four tested membranes (Cellulose, 100 kDa; PVDF, 0.22 µm; mixed cellulose ester, 0.22 µm). The only exception was the hydrophobic UF

membrane (PES, MWCO: 100 kDa), with which the raw water ranked second in terms of fouling. Yamamura et al. (2014) found that the macromolecules in HPI fraction caused more irreversible fouling than the HPO fraction when filtrated with any of the four tested hollow fiber membranes. The used membranes included two MF membranes, which were made from PE and PVDF and had the same nominal pore size of 0.1 µm, and two UF membranes, which were made from PES and PAN both having MWCO of 100 kDa.

It should be noted that the fouling mechanisms and foulants may change as the filtration progresses. In a pilot microfiltration experiment using a PE hollow fiber membrane (nominal pore size: 0.1 µm) by Yamamura et al. (2008) filtrating river water from Chitose, the primary foulants were identified as iron carbohydrate and protein at the start of the experiment but the primary foulants had changed to smaller foulants, manganese and humic substances, after the plant had operated for 148 days. The pilot filtration used only a settlement basin for separating larger particles and no other pretreatments. The change in the primary foulants is explained by a decrease in effective pore size diameter due to pore adsorption and cake formation during the filtration.

Foulants interact with each other, which means that the fouling properties of a foulant may differ based on the presence of other foulants and compounds. Thus, foulants should not be examined independently but rather as a part of the overall feed composition. In a study by Peiris et al. (2011), which used a flat-sheet PES (MWCO: 60 kDa) membrane for filtrating Grand river water, it was found by combining fluorescence spectroscopy and PCA analysis, that colloidal and particulate matter were a cause of reversible fouling in their study while proteins and humic substances were associated with irreversible fouling. Interestingly the study also found that increased concentration of high-MW pollutants increased irreversible fouling caused by humic substances while decreasing fouling caused by proteins. Seems like under these conditions, the cake layer formed by high-MW pollutants was effective at capturing or rejecting fouling proteins but somehow increased the fouling caused by humic substances. Possible explanation is that, because the cake layer decreased the permeate velocity through the membrane, the humic substances travelled through the membrane more slowly making more time for accumulation. It should also be noted that a later study, which utilized similar methodology but hollow fiber membranes (PVDF UF) and different source of raw water (Lake Ontario), found no correlation between colloidal particles and irreversible fouling caused by other foulants (Peiris et al. 2013)

To conclude, polysaccharides contained in the HPI and high-MW fractions have been found to be the primary cause of irreversible fouling in multiple studies using both MF and UF membranes. However, humic substances may also cause irreversible fouling like in the study by Yamamura et al. (2008) after the effective pore size had diminished due to fouling. Peiris et al. (2011) also found that humic acids were a cause of irreversible fouling, perhaps because they used a UF membrane with low MWCO (60 kDa) compared to the other showcased studies in this section.

3.6 The effect of filtration parameters and membrane material on fouling

While the previous section examined fouling properties of different NOM-based foulants, it's important to note that fouling characteristics of any membrane filtration are always depended on the process itself. Fouling is not controlled only by the foulants but also affected by filtration parameters and the properties of the used membrane, among other things. Operational parameters, such as pH, can have significant and complex effects on NOM-induced fouling. At low pH, the negative electrical double layer of NOM is neutralized. This may reduce electrostatic repulsion between the membrane and pollutants, but also increase fouling caused by adsorption. (Braghetta et al. 1998) The aggregate size of NOM may also increase in low pH due to reduced repulsive forces and increased adsorption capacities. On the contrary, high pH may cause pore extensions in elastic membranes materials due to increased electrostatic repulsion (Kim et al. 2011). Despite the potentially complex effects pH can have on fouling, acidic conditions have been shown to increase NOM-induced fouling and rejection rates of membranes in several studies (Kim et al. 2011, Braghetta et al. 1998, Sutzkover-Gutman et al. 2010). Other important process parameters, which are not specific to just NOM-induced fouling, are hydrodynamic conditions, foulant loading, aeration and mixing conditions. Especially crossflow is an important parameter because it reduces cake formation. Crossflow should be balanced with the permeate flux to control the foulant accumulation rates on the membrane surface (Crozes et al. 1997).

The presence of metals in the filtration feed also influences NOM-induced fouling. Most NOM compounds have negative charges, so large colloidal particles in NOM containing solutions have negative zeta potentials in most cases (Ratnaweera et al. 1999) Because the colloidal particles have mostly negative zeta potential, strongly charged ions, especially Ca^{2+}, can

neutralize high-MW colloidal NOM, which may increase fouling as charge repulsion is diminished. Some metals (such as iron, calcium and aluminium) may also form complexes with NOM and increase its particle size, which has an effect on its fouling properties. (Adusei-Gyamfi et al. 2019). The presence of different metal ions (Ca^{2+}, Fe^{3+}, Mg^{2+}, Na^{+}) have all been shown to increase fouling and rejection rates by humic acid when filtrated through a PES hollow fiber membrane (MWCO: 300 kDa) (Hao et al. 2011).

The used membrane is very influential on the fouling that occurs during filtration. The properties of the membrane may even have significant influence on the prevailing fouling mechanisms. As hinted towards in the previous section, the cut-off size of the utilized membrane is obviously important as the prevailing fouling mechanism is depended on whether the foulant can enter inside the pores or not. However, the average pore size is not the only factor, and in some cases the membrane material itself can have even larger effect on fouling. In addition to pore size, fouling is affected by such membrane properties as hydrophobicity, surface charge and roughness (Jacangelo & Noack, 2016).

Hydrophobic membranes are often considered to be more prone to fouling but this is not always the case as shown in a study conducted by Zhang et al. (2015). The subject of this study was colloid interactions with membranes in submerged bioreactors. The results suggested that the hydrophobicity of the membrane was irrelevant under the chosen conditions and membrane roughness and zeta potential were more influential to fouling properties.

Membrane material itself can have significant effect on fouling. Yamamura et al. (2014) found that during NOM filtration the used PVDF membrane fouled more rapidly than a PE membrane, although the membranes had the same nominal pore size of 0.1 µm. This was suggested to be caused by potential hydrogen bonding between hydroxyl groups in HPI-fraction and fluorine. Wang et al. (2011) had similar results while experimenting on the fouling properties of different membranes, which all had the same pore size of 0.22 µm, with different polymeric coagulants. In these experiments the PVDF membrane was more prone to fouling than other membrane materials (PES and PS). Lee at al. (2004) also found that a PVDF MF (nominal pore size: 0.22 µm) membrane fouled more than a PES UF (MWCO: 100 kDa) membrane or either of the hydrophilic membranes (mixed cellulose ester, nominal pore size: 0.22 µm; regenerated cellulose, MWCO: 100 kDa) tested in the study. However, the PVDF membrane was also the roughest membrane and by far the most hydrophobic one, so the increased fouling could have been caused by other factors than hydrogen bonding.

3.8 The effect of pretreatments on fouling

Pretreatments typically aim to reduce fouling, but the precise effects can be hard to estimate beforehand and effect is depended on the type of pretreatment being used. Pretreatments that successfully lower certain foulant concentrations before the membrane filtration (without breaking them into smaller by-products) can be expected to have positive effects on fouling in most cases because the foulant loading is reduced. These types of treatments include different sorts of filtrations, coagulation/sedimentation and adsorption followed by adsorbent removal. However, removing all of the aggregates formed during the used pretreatment is often impossible, and thus residue aggregates may still affect filtration in some manner. (Gao et al. 2011) There are also pretreatments, which function by breaking pollutants into smaller by-products, such as oxidation pretreatments. These types of treatments can have varied effects on the filtration. However, their effects are not covered in this work.

Pretreatments that induce extra particles into the membrane module, such as in-line coagulation or adsorption, can have varied effect on fouling. In-line coagulation increases the average aggregate size in the feed water, which may increase cake formation but also rejection rates (Hao et al. 2011). If the in-line pretreatment is successful, the cake layer can function as an adsorbent layer, which may prevent irreversible fouling (Gao et al. 2011). It may also reduce flux decline caused by cake formation by increasing the porosity of the formed cake layer. However, in-line coagulation and adsorption can also have negative effects on irreversible fouling, mainly when the aggregates formed by the coagulants/adsorbents are small enough to enter inside the membrane.

Flocs formed by coagulants are insoluble and large compared to other pollutants in the water, which makes them very likely to cause cake formation. The cake layer causes flux decline by default but in can also have positive effects as explained. Howe & Clark. (2006) have published a study considering the effects of in-line coagulation on membrane fouling when treating NOM containing surface water. The results showed that while underdosing, alum (5 mg/L) increased fouling but with high enough dosage (50 mg/L) the fouling was reduced for all three tested membranes (CA, MWCO: 100 kDa; PES, MWCO: 20 kDa; PP, nominal pore size: 0.2 µm). As mentioned in section 2.4, coagulant dosage is one of main parameters controlling flocculation. The study also compared three types of coagulants, (aluminium sulfate, ferric sulfate and

polyaluminum chloride) in terms of fouling reduction potential and NOM removal. None of the coagulants performed better than others constantly but each coagulant could be more effective than the others with specific raw water and conditions. Kimura & Oki (2017) had similar results to Howe & Clark (2006) concerning coagulant dosage. In their experiment coagulation/sedimentation with 20 mg/L of polyaluminium chloride (PaCl) constantly outperformed coagulation with 10 mg/L of PaCl under the same conditions. Adjusting the pH to 6 from 7 also improved the performance of the coagulation. This is most likely caused by minimizing residue by partly neutralizing the zeta potential of the flocs, an effect which is covered in the next section (Sharp et al. 2006).

In another part of the study by Howe & Clark (2006), in-line coagulation and coagulation followed by separating the flocs were compared. For the UF membranes (made of CA and PES) the final flux after filtration stayed similar (67 %) with both methods but for the MF membrane (PP) the final flux after filtration was much lower when in-line coagulation was used (26 % compared to 50 %). The most likely explanation for this is that because the MF membrane had larger pores than the other membranes, thus the flocs formed by in-line coagulation were able to enter and clog them.

Kimura et al. (2008) studied the effects of in-line coagulation (using polyaluminum chloride) on membrane filtration with hollow fiber MF membranes (PE, nominal pore size: 0.1 µm) in both bench-scale and pilot-scale experiments. They found that coagulation under acidic conditions generally increased irreversible fouling. Under acidic conditions, more aluminium particles in the smallest size group (d < 0.025 µm) were detected in the coagulated water. Those small particles may have been the cause for the increased irreversible fouling. Compared to neutral conditions, alkaline conditions (8 pH) also caused increase in irreversible fouling, but more noticeable was the increase in aluminium detected in the permeate. Increased amounts of aluminium were detected in the permeate in acidic filtration conditions as well, but the amounts were generally lower than in alkaline conditions. This was explained by the formation of aluminium-based anions under alkaline conditions. Aluminium is also known form soluble Al-NOM complexes under suboptimal flocculation conditions (Adusei-Gyamfi et al. 2019) In either case, the formed aluminium compounds were small enough to pass through the membrane.

The effect of dosage was also compared during the filtration experiments of Kimura et al. (2008). The results indicated that excess dosage of coagulants can have negative effects on fouling especially under non-optimal pH conditions, which is somewhat at a disagreement with

the overall results of the study conducted by Howe & Clark (2006). Interestingly, increasing coagulant dosage would have clear negative effects on irreversible fouling when filtrating commercial humic acid, but in turn when filtrating river water NOM, the high dosage didn't cause clear increase in irreversible fouling. When filtrating river water NOM opposed to the commercial humic acid, the effect of coagulation compared to no-coagulation was almost always positive. The extraction experiments on fouled membranes conducted by Kimura et al. (2008) confirmed that under non-optimal conditions the coagulant metals can enter and stay inside the membranes causing irreversible fouling. After the filtration at pH 5, 30 mg/m^2 of aluminium and 6-7 mg/m^2 of TOC were extracted from the fouled membrane with HCl (pH 2). When the filtration had happened at 7 pH with same dosage (5 mg Al/L), only > 2 mg/m^2 of aluminium and < 1 mg/m^2 TOC were extracted from the fouled membrane. In order to ensure successful in-line coagulation, it's critical that the flocs formed by coagulations don't break into nano- or microparticles small enough to enter the membrane pores. Based on the study, acidic conditions would increase this type of breakage. On the contrary, alkaline conditions caused formation of soluble aluminium particles, which did not cause similar amounts of irreversible fouling, but had negative effect on the treated water quality.

The use of adsorbents, such as PAC or carbon black (CB), is another common pretreatment method. Adsorbents behave similarly to coagulants during filtration meaning that they form a cake layer on top of the membrane, which may reduce other fouling by adsorbing foulants from the water. (Lohwacharin et al. 2010) The overall effect on fouling is depended on the cake resistance and the fouling properties of the adsorbates.

Lohwacharin et al. (2010) compared the fouling properties of in-line CB and PAC adsorption treatments when treating NOM containing river water. The results were compared to UF with cellulose membrane (MWCO: 100 kDa) without pretreatment. Because CB had much larger average particle size than PAC (24.4 to 0.84 nm), CB formed a more porous cake than the PAC or just river water (cake pore volumes were 0.454, 0.081 and 0.042 cm^3/g for CB, PAC and river water respectively). Both adsorbents reduced flux decline: after 4 cycles of filtration and backflushing, the flux of the UF system dropped 77 % while the fluxes of the UF/PAC and UF/CB systems dropped 70 % and 65 %, respectively. In other words, the results show inverse correlation between the cake porosity and flux decline due to cake formation. However, PAC improved the NOM removal rates more compared to CB (DOC removal at final batch was 40-50 % for UF/PAC and about 25-30 % for both UF/CB and UF), most likely due to forming tighter cake layer and having increased surface area (993 m^2/g to 144 m^2/g). Between the two

adsorbents, CB was better at reducing irreversible fouling having full flux recovery after the cycles (about 97 % for both PAC/UF and UF). Based on alginate adsorption test, CB was more efficient at adsorbing macromolecules than PAC, which might have been the main cause of fouling during these experiments and explain why CB more effective at reducing irreversible fouling. These results support the idea that cake layer formed from adsorbate material can reduce irreversible fouling by absorbing foulants that cause it.

As seen from a previous section a fair amount of studies have tried to discover the dominant fouling fraction of NOM. However, most of the studies don't consider in-line coagulation in their experiments. Even free NOM colloids can affect fouling properties of other compounds according to Peiris et al. (2011), so it reasonably to assume that in-line coagulation could change the dominant fouling fraction completely as the fouling properties of flocs are considerably different from fouling properties of free NOM compounds. Unfortunately, not a lot of studies have been published about the composition of the NOM residue after floc formation or the effect NOM composition has on the fouling properties of flocs. Studies by Howe & Clark (2006) and Kimura & Oki (2017) both found correlation between high DOC removal during coagulation and decreased fouling (determined from permeate flux). How effective the coagulation is at removal of DOC might in term be depended partly on DOC composition. Hypothesis for this could be that while HPO-fraction causes hydrophobic sites in the flocs, which reinforces them through creating attractive forces, HPI-fraction might cause more repulsive forces and decreases floc strength leaving more residue. The results of Howe & Clark (2006) seem to support this suggestion, as the HPO-fraction in the DOC content of the treated raw water was correlated with DOC removal efficiency. However, more research would be needed in order to reach stronger conclusions.

3.9 The effect of flocculation conditions of in-line coagulation on fouling

As shown in previous section, floc size affects fouling the cake layer porosity and resistance. Flocculation conditions affect the properties of the formed flocs, which makes flocculation conditions important for controlling fouling especially when using in-line coagulation. Flocs are colloidal particles and thus are affected by the interactions covered in XDLVO-theory, like other colloids. The strength of flocs is mainly increased by van der Waals forces and polymer bridging in the floc. NOM affects the structure of the formed flocs by creating steric repulsions and

hydrophobic sites. Steric repulsions increase the separation distances inside the flocs making them looser and weakening their structure, while hydrophobic sites may create additional attractive forces inside the flocs. (Sharp et al. 2006)

The three main ways to control floc size are dosage, flocculation time (while mixing is active) and pH, which affects the zeta potential of the formed flocs. In general, particle size increases during flocculation until a steady state is reached (Sharp et al 2006). The final value of the steady state is affected by the ratio between coagulant dosage and foulant concentrations as well as zeta potential, which controls the strength/breakage of the flocs. Mixing increases the rate at which this steady state may be achieved but can also cause breakage among the flocs. Floc size and fractal dimensions are critical parameters affecting fouling. Lower fractal dimension is commonly associated with looser floc structure. Low fractal dimension and high floc size can indicate that the cake layer formed by flocs will be more porous and have less resistance, which may have a positive effect on permeate flux. (Dong et al. 2014)

NOM-based flocs have naturally negative zero potential in most pH ranges. Minimizing the zeta potential has been shown to reduce residue after floc formation and to strengthen the formed flocs, making them more resistant to breaking under shear (Sharp et al. 2006). This may be caused by decreasing the repulsive electrostatic forces inside the flocs. Sharp et al. (2006) found that for ferric sulfate flocs the optimal zeta potential range for was between—10 and +3 mV. The optimal range was largely independent of NOM concentration or coagulant dosage. While low zeta potential minimized residue, the median size of the formed flocs also decreased. For example, median floc size for ferric sulfate was 795 µm in –18 .1 mV (pH 6) and 594 µm in +3.5 mV (pH 4.5). Floc size correlated with greater floc breakage under mixing making them less stable (presented in the study as logarimic slope between floc size and RPM, –0.58 and –0.52 for flocs with zeta potentials of –18 .1 mV and +3.5 mV, respectively). This shows that while increasing the floc size can seem beneficial, it can also have negative effect on their durability.

Even though Sharp et al. (2006) managed to improve some floc properties by neutralizing zeta potential, it's important to note that this also decreased the average floc size. In the context of in-line coagulation for membrane filtration, lowering the floc size might have more negative effects than positive ones, especially when using MF membranes, which increases the change that the flocs may enter inside the membrane. In the already showcased study by Kimura et al. (2008) lowering flocculation pH caused an increase in irreversible fouling.

As stated earlier, flocs with neutral zeta potential are considered to have multiple improved properties, but because most membranes surfaces have negative zeta potential, strong negative charge on the flocs could reduce cake formation and make hydraulic cleaning easier. For example, PVDF membranes have negative zeta potentials at the pH values used for filtration (> 3) (Kakihana et al. 2017). Fouling of organic polymer coagulants with different type of charges have been compared in a study by Wang et al. 2011. The study compared fouling of three different membranes (PVDF, PES, PS) with same nominal pore size of 0.22 µm with different polymeric coagulants. The cationic polymer (pDAD-MAC, 400–500 kDa) caused more fouling in the more negatively charged membranes (PVDF and PES, zeta potentials at 7 pH approximately –32.5 and –25 mV) than the non-ionic (PAM, 5000–6000 kDa) or anionic (PACA, 520 kDa) coagulants. For the membrane with closest to neutral zeta potential (PS, zeta potential at 7 pH approximately -15 mV) the fouling was very similar with all coagulants unlike for the charged membranes. It appears neutralizing flocs might lead to negative effect on fouling as is the case with neutralizing NOM.

Average or median floc size isn't the only factor controlling cake porosity. At least couple studies have linked the increased size of the nanoparticles formed during flocculation with higher cake porosity. Yu et al. (2013a) conducted a study comparing iron and aluminium coagulants (aluminum sulfate and iron chloride) with the use simulated surface water. The experiment used PVDF hollow fiber membrane (0.01 µm) with constant permeate flux (20 LMH), which was controlled by TMP. The iron-based coagulant had constantly lower zeta potential at the tested pH range (6.5–7.9) but larger floc size (ca. 650 µm to 400 µm after 7 min flocculation) and lower fractal dimension (2.73 to 2.82). However, it also formed smaller nano-scale particles than the aluminium-based coagulant. Largest size group of nano particles at range of 15–50 nm at 5 nm intervals was 25 nm for the iron-based and 35 nm for aluminium-based coagulant. The porosity of the cake layer formed by iron chloride was likely smaller than the one formed by aluminium sulfate based on SEM images. Because of this, as the filtration was kept going the iron-based coagulant caused sharper increase in TMP than the aluminium-based coagulant. Smaller floc size can correlate with greater floc strength, which could be one reason why the aluminium coagulant formed larger nano-scale particles. (Jarvis et al. 2004).

In-situ coagulation could be a way to improve floc properties. Yu et al. (2013b) managed to improve the properties of iron-based flocs by producing the flocs *in-situ* from $FeSO_4$ and $KMnO_4$. The produced flocs were compared to the flocs created by normal dosage of coagulants ($Fe_2(SO_4)_3$). The initially formed nanosized aggregates were slightly larger for in-

situ coagulation. The cake layer formed by in-situ flocs after same filtration time was thinner (ca. 10 µm to 20 µm) and had higher porosity (based on SEM images). During pilot filtration experiment, simulated surface water was filtrated through a PVDF hollow fiber membrane (nominal pore size: 0.03 µm). The TMP reached 50 kPa in 8 days without coagulation. When the raw water was coagulated with the normal dosage of iron coagulant, the TMP reached that same pressure in 16 days. With in-situ coagulation after 16 days, the TMP had only reached 30 kPa. The study showed again a link between size of nano-sized particles and improved cake properties.

To conclude, studies presented in this section show that floc size is depended on the floc's zeta potential. Flocs with close to neutral zeta potential are also linked with less residue during flocculation and may be less likely to break under shear stress. While zeta potential can be controlled by pH, predicting the final properties of the cake layer is difficult as it's also depended on the nano-sized particles formed during flocculation. Acidic conditions, used for reducing zeta potential of the flocs, could also increase the degree of fouling caused by the flocs as well as residue NOM.

3.10 Fouling characteristics specific to submerged outside-in hollow fiber filtration

As stated earlier, the pilot experiment that this work is based on used hollow fiber membrane modules. The design for hollow fiber modules is complex and fairly unique, thus the fouling occurring in these modules can be expected to have different characteristics from other module types. One of the key parameters defining fouling in hollow fiber modules is packing density. In membrane literature, two different definitions for packing density are commonly used. First one is membrane area divided by the volume of the module (Shimizu et al. 1996). The other common definition is the ratio between the cross sectional area of the membrane divided by the total cross sectional area, where the unit of packing density is percent. While high packing density is important for obtaining high effective surface area per process volume demand, it has been shown that increasing packing density too much can have a negative effect on the filtration process efficiency mainly due to increased fouling. (Günther et al. 2010).

There has been little research about how different areas of these type of modules or individual fibers perform during hollow fiber filtration. In study by Yeo and Fane (2005), it was shown that even in bundles of just 9 fibers, the permeate flux of the middle fiber can be 50 % smaller than

the average flux in the bundle. Yeo and Fane (2005) presented two possible explanations for this: uneven hydrodynamic conditions and merging cake layers. Uneven hydrodynamic conditions refers to stagnant areas inside the bundle, where the cross flow is especially low. This decreases shear stress on the membrane surface and increases fouling of all sorts. The other explanation refers to a phenomenon, where cake layers around individual membranes merge creating areas between the membranes that are inactive during the filtration (Shimizu et al. 1996). The stagnant zones and merged cake layers are very likely made more frequent by high packing density. Thus, lowering packing density can improve the filtration performance of middle part of the module. Other methods for achieving this include aeration, increasing cross flow in the module and frequent cleaning. (Yeo and Fane, 2005)

As stated above, the performance of an individual fiber in a bundle is depended on its location, for example fibers in the middle of the module can have lower permeate flux than fibers in the outer areas under certain conditions. In addition to this, the permeate flux at each point of the same fiber is rarely uniform. As seen from equations (2) and (7), the permeate flux is affected by the transmembrane pressure. The pressure inside the fiber has an axial gradient due to the the suction pressure located at the open-end. If the pressure outside the fiber is constant, this means that the permeate flux is the highest near the open-end, where the pressure inside the fiber is the lowest. This effect has been demonstrated by Carroll & Booker (2000) in experiments with hollow fiber membranes of different lengths. Increasing the fiber length yielded diminishing results on the total flux until increasing the fiber length had no noticeable results in total permeate flux. When the filtration was kept going for longer time, the fluxes of membranes of different lengths started to decrease until reaching a constant state.

The study done by Carroll & Booker (2000) considered cases with constant pressure outside the membrane. However, in most real-life modules this is not the case. Günther et al. (2010) applied computational fluid dynamics (CFD) to model submerged hollow fiber filtration. In the case, where the pressure at the bottom of the module is higher than at the top, there will most likely be some amount of vertical flow outside the fiber. This is most relevant for open-bottom modules, where the pressure at the bottom of the module is close to the surrounding tank pressure but can apply to other module types as well. The bottom to top flux around the membranes will cause pressure drop, which decreases transmembrane pressure towards the open-end of the fibers. High packing density reduces the space the vertical flux has and

increases the pressure drop outside the fiber. The model that was developed by Günther et al. (2010) predicted that with high enough packing density (at least > 0.6) the permeate flux would be higher near the bottom of the membrane. It should be noted that the model makes some big assumptions like uniform filtration conditions and doesn't account for critical effects like cake layer formation, which most likely would have large effect with high packing density.

Because the permeate flux is different in different areas of the fiber, these areas also foul at different rates. The basic idea behind this it that areas with high local permeate flux will have foul faster than areas with lower local permeate flux. Thus, at the start of the filtration fouling will occur mainly in areas with high permeate flux, but as the fouling evolves in these areas, the local permeate flux will drop, and fouling will start to increase in other areas of the module. (Carroll & Booker, 2000). If the filtration is kept going long enough, the module will reach a state of uniform permeate flux distribution, where $\Delta p/R$t is constant at each location, as stated in equation (7).

Lee & Kim (2012) have studied to local fouling in pilot plant using a PVDF hollow fiber membrane (nominal pore size of 0.1 µm) for filtrating river water. The pilot process used coagulation (not in-line) as pretreatment for separating particulate matter and operated for 3 months. After the pilot process had ended, Lee & Kim (2012) tested the degree of fouling of different fiber samples by conducting individual filtration experiments, where the fouling resistance terms (R_r and R_{ir}) were calculated for each sample. The results did not show correlation between reversible fouling and the distance of the fiber sample from the open-end, but irreversible fouling did correlate with this distance, when the SS loading was low (average 12.6 mg/L). Possible explanation for this, according to Lee & Kim (2012), was that areas with high permeate flux initially developed high amounts of irreversible fouling, which in turn decrease the reversible fouling developed after chemical cleanings, resulting in close to uniform permeate flux distribution along the fiber. This explanation appears logical, and for example Zhuang et al. (2015) have also presented the idea that by manipulating the membrane resistance, the cake layer distribution and permeate flux could reach a uniform state along the fiber.

4. Methods used for monitoring and identification of fouling

Monitoring of membrane fouling is important for predicting treatment results and for following the membrane condition. Monitoring can be conducted on-line (real time) or offline. On-line monitoring present many challenges as suitable analysis method has to be accurate, fast and it shouldn't disturb the filtration or damage the membrane. A major benefit to online monitoring is that the data is real-time and more suitable for reacting to variating conditions. The membrane filtration also doesn't have to stopped in order to conduct the measurements. Currently, online monitoring of fouling is non-direct, but rather the permeate flux and TMP are monitored instead. Combined permeate flux and TMP data can be processed with an equation relating permeate flux and filtration resistance, for example equation (9), and the results can be used for monitoring the change in fouling resistances (Kimura & Oki. 2017). Moreover, initial flux after cleaning can be used to calculate recovered flux for each segment, which may give information about the development of irreversible fouling (Lohwacharin et al. 2010).

Analysing the permeate flux by itself doesn't necessarily give accurate information about the occurring fouling type or membrane condition. Thus, multiple online measurement techniques, which can be used for monitoring membrane condition directly, have been developed to accommodate the permeate flux/TMP data. These techniques include e.g. optical laser sensor for monitoring cake layer thickness and electrical impedance spectroscopy. (Hamachi & Mietton-Peuchot 2001, Cen et al. 2015)

Online monitoring is quite clearly more difficult for complex module designs, such as hollow fiber modules, where the fouling is not uniform. Another factor to consider is that online monitoring tools have to be set-up and operated *in-situ* and the resources for installing equipment are limited. Careful offline and off-site analysis can be the only method capably of discovering the more intricate details considering fouling and membrane condition. Once such offline analysis has been conducted, it can be fitted with the online data in order to be able to predict factors which couldn't be otherwise determined based on just online monitoring. This section presents different offline analysis methods for identification of fouling in published studies and it prefaces the chosen methods used in experimental part of this work. Analysis methods from studies concerning MF/UF membrane fouling in surface water treatment are presented in Table III. The results of some of the studies have already been presented in earlier sections of this work so they won't all be covered in this section as it focuses on the

methodology. The analysis methods and experiment conditions are presented in Table III include AFM (atomic force microscope), contract angle -analysis, FTIR, SEM, desorption of foulant from fouled membranes, FTIR, analysis of flux and backwash concentrations, fluorescence analysis, and CLSM. The purpose and main results of the analyses are presented in text below.

Table III Different analysis methods used for identification of NOM-based fouling.

Source	**Feed water source:**	**Membranes material and size**	**Main analysis methods**
Lee et al. (2004)	Four French surface waters: • Marve River • Yffniac river • Cazau lake • Reservoir	• PES (100 kDa) • Cellulose (100 kDa) • PVDF (0.22 µm) • Mixed cellulose ester (0.22 µm)	• AFM • Contact Angle • FTIR • SEM
Lohwacharin et al. 2010)	• River water (Tama) • River water+ PAC • River water+CB	• Cellulose (100 kDa)	• BET analysis • FTIR • SEM
Kimura et al. 2004	• River water (Chitose)	• PES (750 kDa)	• Desorption • FTIR
Huang et al. 2007	Four different raw waters: • River (White) • Canal (Twente) • Bay (Tampa) • Secondary effluent	• PVDF (0.02 µm) • PVDF (0.1 um) • PES (150-200 kDa) • PES (100 kDa)	• Flux concentration
Peiris et al. 2011	• Grand river water	• PS (20 kDa) • PES (60 kDa)	• Fluorescence analysis
Sun et al. 2011	• Simulated surface water	• PVDF (0.04 µm)	• CLSM

Atomic force microscope (AFM) can be used for section analysis of the membrane. This includes detecting changes in roughness caused by fouling and detecting fouling mechanisms present. Fouling known as surface coverage should make the surface of the spend membranes appear smoother, while pore blocking can appear as the valleys from the side section analysis are being filled (Lee et al. 2004).

Scanning electron microscope (SEM) is a common instrument used for detecting changes in the membrane and fouling. Pore blocking and changes in porosity can be detected from SEM images (Lee et al. 2004) SEM combined with image analysis can also be used to determine the pore size distribution of the membrane. (Zhao et al. 2000) SEM combined with energy-dispersive X-ray spectroscopy (SEM-EDS) can be used to detect changes in the membrane surfaces elemental composition (You et al. 2007)

Fourier-transform infrared spectroscopy (FTIR) measures the infrared spectrum of the measured substance. The spectra can be used for identifying bonds between elements and have also been used to identify foulants by comparing the spectra from clean and fouled membrane (Lee et al. 2004). For example, in the study conducted by Lohwacharin et al. (2010) the spectra of virgin membrane and fouled membrane after CB/UF filtration had similar peaks and intensities while in spectra of fouled membranes without preatreament or PAC treatment the peaks of the virgin membrane had diminished in intensity showing that the CB pretreament was effective at maintaining membrane condition.

SEM images can be used to compare cake layer porosity as well as membrane porosity. (Yu et al. 2013). Cake layer porosity has been also been analysed by Brunauer-Emmett-Teller (BET) analysis, which can be used to measure specific surface area and pore volume through nitrogen (or other inert gas) adsorption/desorption data. (Lohwacharin et al. 2010).

Contact angle can be used as measurement for the hydrophobicity of measured surface. The hydrophobicity of membranes can change as fouling progresses and measuring the contact angle of spent membrane can give information about the type of foulants present at the membrane surface. In the study by Lee et al. (2004), the contact angle of hydrophobic membranes (contact angle > 50 °) decreased during membrane filtration while the contact angle of hydrophilic membranes (contact angle < 20 °) increased. These types of measurements give an idea about how hydrophobic the foulants present in membrane surface could be. However, as Lee et al. (2004) noticed, the change in contact angle is not necessarily correlated with other changes fouling causes for example in permeate flux.

Membrane fouling, especially irreversible fouling, can also be analysed by extracting foulants from its surfaces. The study by Kimura et al. (2004) included a section, where foulants were extracted from spent membranes, which had been used in pilot plant for treating river water. The FTIR spectra of fouled membranes before and after the extraction combined with flux concentration analysis indicated that polysaccharide-like organic matter has caused most of the irreversible fouling during the filtration.

The analysis of backwashing solution can be used for detection of reversible foulants. In study by Huang et al. 2007, high-MW macromolecules and colloidal particles were identified as main source of fouling in surface waters for both UF and MF membranes. Backwashing experiment was conducted with membranes used for NOM filtration and high concentrations of high-MW macromolecules were detected in the backwash flow using SEC-DOC method. This reinforces the theory that the mechanism of fouling caused by the HMW factor was suspected to be a combination of membrane pore blocking and cake layer formation. (Huang et al. 2007) In addition to concentration analysis, other measurements like fluorescence spectroscopy, which measures the excitation emissions matrixes of the samples, can be used to analyse permeate, feed and retentate fluxes. This analysis combined with PCA gives specific information about the type of components present in the water. (Peiris et al. 2011) Fluorescence spectroscopy have also been used for analysing backwashing and extraction solutions (Peiris et al. 2013).

Confocal laser scanning microscopy (CLSM) combines microscopy with laser excitation and emission analysis. While its more common in other fields, it is relatively rare for analysing membrane fouling, but it has been utilized in studies by Sun et al. (2011) and Peter-Varbanets et al. (2010) to analyse foulants attached to membranes. In these studies, the sample membranes are prepared by staining them with fluorophoric staining agents that are specific to certain foulants such as polysaccharides, proteins or bacteria. In the study by Sun et al. (2011), CLSM was combined with image analysis to calculate biomass volumes on the membrane surface. The study revealed that, while the biomass volume of polysaccharides was lower than proteins, the polysaccharide content correlated better with flux decline.

For membrane studies, pore size distribution and average pore size are useful parameters that can give information about the functionality of the membrane. These values are commonly analysed and published in studies that cover membrane modification or synthesis but have been rarely applied in membrane fouling studies. Lohwacharin et al. 2010 compared the average pore size of combined membrane and cake layer sample after filtration with either

CB/PAC pretreatment or without pretreatments. The results were obtained by Brunauer-Emmet-Teller (BET) analysis, which is a measurement technique based on inert gas adsorption/desorption. When no adsorbents were used, the pore diameter of the membrane decreased during the filtration (from 16.3 nm to 8.4 nm). On the contrary, when adsorbents were present during the filtration, the average pore size of the combined layers increased due to porous cake layer (32.8 nm with CB and 17.7 nm with PAC). They however didn't either measure or publish the full pore distributions or analyse separately the change in average pore size that had occurred purely in the membrane. Recently, Virtanen et al. 2020 published pore area and volume distributions (also obtained by BET analysis) of membranes fouled by different solutions used in biorefineries.

5. Materials and methods

An UF pilot plant designed for drinking water production from surface water (obtained from Lake Päijänne) was set-up by Helsinki Region Environmental Services Authority (HSY) in Helsinki. The plant's purpose was to determine the viability of the UF process for drinking water production as well as to test treatment results with different coagulants and doses. After the pilot plant had been operational for three months, the used membrane modules and filtration data from the plant were send to the Lappeenranta-Lahti University of Technology LUT for further analyses. The goal of these experimental studies was to analyse the change in the membrane condition and to obtain information about the prevailing fouling mechanisms and foulants of the pilot filtration.

5.1 Membrane modules

The pilot process used four submerged hollow-fiber modules (S10N, Memcor) The hollow fiber membranes were made of PVDF. The modules were all submerged in the same water tank with each module being place towards a different corner from the centre. The configuration of the flow was outside-in. The relevant module parameters are presented in Table IV.

Table IV Hollow fiber module (S10N, Memcor) parameters according to the manufacturer.

Parameter	**Memcor S10N**
Membrane material	PVDF
Membrane pore size, µm	0.04
Membrane area per module, m^2	23
Overall module length, m	1.195
Overall module diameter, m	0.131
Packing density, $m^2\ m^{-3}$	1429

5.2 Pilot process parameters and operation

The raw water used in the pilot plant came from Lake Päijänne. The average water quality during the experiment is presented in table V.

Table V Average quality of raw water used in the pilot experiment (number of measurements=7).

Parameter	Average value	Range (min–max)
Alkalinity, mmol	0.32	0.31–0.32
pH	7.1	6.9–7.3
Turbidity, FNU	0.29	0.23–0.44
Conductivity, µS/cm	70.8	69.8–71.2
Total organic carbon, mg/l	6.6	6.5–6.7

The pretreatment for membrane filtration consisted of in-line coagulation, pH adjustment and flocculation. The used coagulant and dosage were changed during the experiment. Only one coagulant was used at a time: either ferric sulfate (PIX-322) or polyaluminum chloride (PAX XL-100). The dosage of both coagulants was changed several times. The dosage for PIX varied between 1.5–6.0 ppm of Fe and the dosage of PAX varied between 3.0–4.8 ppm of Al. The pH adjustment was only used during a brief period in the middle of the pilot experiment at a time when the coagulation dosage was 1.5 ppm of Fe.

During the filtration the permeate flux was kept around 43–46 LMH by adjusting the suction pressure. The operation temperature was 8–12 °C. The membranes were backflushed every 20 mins for 60 seconds first 45 s with air (30 nm^3/h) and then 15 s with mixture of air and water (15 m^3/h) Due to adjustments to the suction pressure, the transmembrane pressure also altered at the range of 40–100 kPa.

Due to fouling, the suction pressure, that was required to maintain the flux, had to be increased as the filtration was proceeding. After the suction pressure reached around 80 kPa, the filtration was stopped and the membrane modules were chemically cleaned with first with acid and then with alkaline solutions. The acid solution consisted of 0.2 % of HCl and 0.5 % of citric acid and

the alkaline consisted of 0.2 % of NaOCl. During the chemical cleaning the membranes were washed with both solutions separately following slightly modified cleaning procedures. Both cleaning procedures started with the regular backflushing procedure described earlier. Then the filtration tank was emptied and filled with permeate water. When the tank was full, the chemicals needed for forming the cleaning solution (acid or alkaline) were added. While the chemicals were being added, the solution was recirculated through the membrane module by backflushing. When all of the chemicals had been added, and the cleaning solution was complete, the backflushing was stopped, and the tank was heated to 25 °C. After the this temperature was reached, the modules were left to soak in the cleaning solution for appointed time, which was 30 mins for the alkaline solution and 10 mins for the acid solution. The alkaline treatment was followed with an automated flushing series, which was repeated three time. The series consisted of:

- Emptying and filling the tank with raw water
- Flushing with air for 15 seconds
- Emptying and filling the tank with raw water for the 2nd time
- Flushing with air for 60 seconds with simultaneous backflushing with permeate for last 15 seconds
- Emptying and filling the tank with raw water for the 3rd time
- Filtration for 60 seconds.

After the acid solution had soaked for 10 mins, the solution was aerated for 5 mins. This pattern was repeated three times, which was followed by the same automated flushing series used in the alkaline treatment.

As mentioned, the process used a total of 4 modules, which were assumed to function mostly identically to each other. After the filtration experiment had ended, one of the modules was taken off the filtration unit and the other three modules were washed one last time using the same cleaning procedures described earlier. This way the effectiveness of the chemical cleaning could be analysed by comparing the modules. The fouled module, which was not chemically washed after the pilot experiment ended, is referred in this work as M_f and the three chemically washed modules are referred as M_{c1}, M_{c2} and M_{c3}.

5.3 Sampling

The modules' large size and high number of fibers present challenges for effective sampling. Based on the literature presented in section 3.10, it was hypothesized that the degree of fouling would vary vertically and horizontally around the centreline of the module. For the sampling, it was also assumed that the filtration tank was well mixed with constant bulk concentration, which would cause the horizontal fouling gradient to be symmetrical around the centre line. Sampling of the fouled membrane was conducted by collecting 10 cm long fiber samples from different areas of the used modules. All the samples from one particular module were collected from the same side, or in other words from the same angle relative to the centre. By placing the module on a coordinate system on its side with the centre line at x-axel and the open-end at y-axel (graph presented in Fig. 3, the location of each sample can be expressed by two coordinates:

- *d*=distance from the open-end of the module (cm)
- *r*=distance from the centre line of the module (cm).

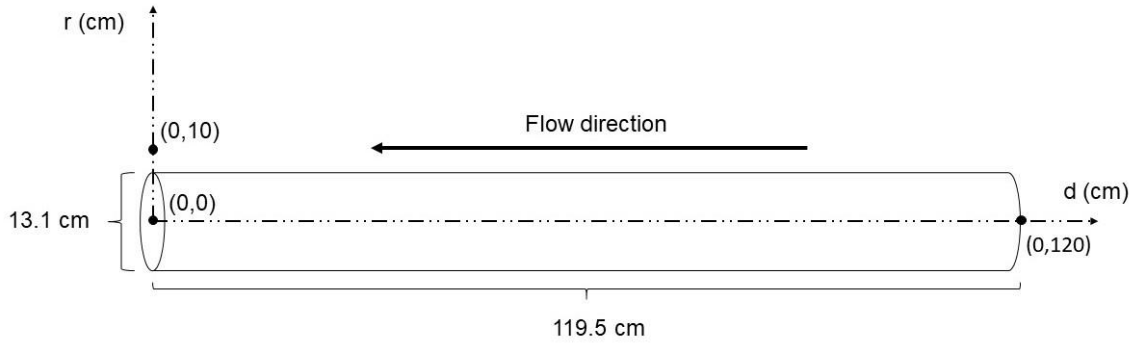

Figure 3 Picture of a membrane module no its side and the sampling coordinates in a 2-D coordinate system. In the filtration unit the modules were placed upwards with the open-end towards top.

Membrane samples were stored in two distinctive ways. Some samples were collected straight into plastic bags in order to leave the cake layer intact as much as possible. Other samples were put into plastic containers filled with deionized water, which were stirred slightly by hand

in order to separate most of the cake layer from the fibers. The samples washed with water are referred as washed samples and the unwashed samples stored in plastic bags as dirty or fouled samples.

Separate cake samples were also collected from the badly fouled areas. The cake samples were collected by scraping the cake layer off from the membrane surface with a box-cutter knife. Clean fiber samples were also collected from an unused module. All clean samples were soaked in deionized water for 30 mins and then rinsed under running deionized water. After washing, the samples were then kept in fresh deionised water at least 10 hours before using them for analyses.

5.4 Chemicals used in analyses

Two staining agents were used for staining samples for the CLSM analysis: basic fuchsin manufactured by Merck and Concanavalin A with fluorescein (FITC) conjugate (Sigma-Aldrich, 3–6 mol FITC per mol protein, 5–15 % biuret). The phosphate buffered saline (PBS) solution used for washing samples in conjunction with CLSM was prepared from PBS tablets (Amiresco) designed for creating 10 mM solution, which was done by diluting one tablet into 100 ml of deionized water.

Oxalic acid (Aldrich, 98 %) and sodium hydroxide (0.1 M, analytical volumetric solution, Reagecon) were used in the desorption experiment. Hydrochloric acid (ROMIL, super purity) and nitric acid (ROMIL, super purity) were used in preparation of ICP samples. The ultra pure water used for diluting ICP samples was prepared with PURELAB flex (Elga).

5.5 Methods for fouling analysis

5.51 Analysis of permeate flux and transmembrane pressure data

Data analysis was conducted in order to monitor the amounts of irreversible and reversible fouling, which had occurred during the pilot plant filtration. For processing the data, the pilot filtration was divided into filtration periods, which were determined by starting a new period after each chemical cleaning. Due to irreversible fouling, the initial normalised permeate increased

between two filtration periods after a chemical cleaning, in most cases. The initial normalised permeate flux ($J_{n,i}$) can be defined as:

$$J_{n,i} = J_i/\Delta p_i \quad (10)$$

, where:

J_i is initial volumetric flux after a chemical cleaning (m/s or $L^3\ m^{-2}\ h^{-1}$)

Δp_i is transmembrane pressure corresponding to q_i (Pa).

Fouling during the filtration periods was monitored by calculating the fouling resistance terms at the start and end of each period. $R_{t,i}$ could be calculated from $J_{n,i}$ based on equation (7):

$$R_{t,i} = \mu/J_{n.i} \quad (11).$$

R_m and R_{ir} at the start of each filtration period were calculated from equation (9) by assuming that R_m was constant during the filtration and R_r was 0 after each chemical cleaning. R_t at the end of each filtration period ($R_{t,e}$) was similarly calculated by using the measured volumetric flux, pressure and viscosity.

The total fouling rate ($\Delta R_t/\Delta t$) was also calculated based on filtration time (t) for each filtration period, in order to present how fast the fouling occurred during the periods. The total fouling rate was defined as:

$$\frac{\Delta R_t}{\Delta t} = \frac{R_{t,e} - R_{t,i}}{t} \quad (12).$$

5.52 Analysis of the foulant composition with infrared spectroscopy

Attenuated total reflectance Fourier transform infrared spectroscopy (ATR-FTIR) was used to study the chemical composition of the fouled membranes. All samples were dried before the measurements. The clean reference sample was dried overnight in a desiccator. Fouled membrane and cake samples were either dried overnight in oven at 65 or 105 °C or freeze-dried using ALPHA 2-4 LD plus (Christ). After drying the samples were kept in desiccator for at least 1 hour before the measurements.

For the ATR-FTIR measurement of fouled membranes, 2–3 fibers from each sample group were measured and the measurement was repeated for 3 times for each fiber making the total amount of measurement for each sample group 6 or 9. For cake samples, ATR-FTIR measurement was repeated 3–6 times. For the clean membrane sample the measurement was repeated 3 times. The resolution, data interval and spectral range were set to 4 cm^{-1}, 1 cm^{-1} and 400–4000 cm^{-1} respectively. The data was processed with ATR correction, normalization and baseline correction. Normalization was conducted based on the main peak of the clean membrane spectrum found around 1185–1165 cm^{-1}. The procedure ensures that the intensities of the fouled membrane spectra are comparable.

5.53 Elemental analysis of filtration cake layer composition

CHN (carbon-hydrogen-nitrogen) analysis was done to cake samples with CHN628 (LECO) analyzer. The metal content of cake samples was analyzed with 7900 ICP-MS (Agilent Technologies). Cake samples were freeze-dried before both analyses. For the ICP-MS analysis, freeze-dried cake samples were weighted and dissolved into 3 ml of HCl and 1ml of HNO_3.

5.54 Determination of the pore size distribution and specific surface area of fouled membranes by Brunauer-Emmet-Teller (BET) analysis

The pore size distribution and specific surface area were studied using Brunauer-Emmet-Teller (BET) analysis. Before the analysis, the samples were freeze-dried and allowed to warm to room temperature in a desiccator. The sample fibers were cut to about 2 mm pieces and degassed at 30 °C for 600 min using a VacPrep 067 degassing unit. The BET analysis was conducted with Micromeritics 3Flex surface characterization analyser with nitrogen gas. The Barrett, Joyner and Halenda method combined with the reference curve Harkins-Jura was used to obtain the pore area and pore volume distribution. All calculations were conducted using MicroActive software.

5.55 Morphological analysis and comparison of the elemental composition of fouled surfaces with Energy-dispersive X-ray spectroscopy (EDS)

The structure of the membrane samples was analysed by SEM imaging using Hitachi SU3500 scanning electron microscope. For the cross-sectional images, samples were freeze-dried and then fractionated while immersed into liquid nitrogen. This is a well-known sample preparation procedure for hollow fiber membranes meant to ensure getting clean surfaces for cross-sectional images (Zhao et al. 2000). Some of the samples were also coated with Au and Pd coating using Scancoat Six (Edwards). The samples were fixed to the aluminium holder for the SEM with 2-sided carbon tape. Energy-dispersive X-ray spectroscopy (EDS) was conducted in conjunction with SEM.

5.56 Examination of the chemical composition of cake layer with confocal laser scanning microscopy (CLSM)

Three fiber samples were prepared for CLSM imaging: reference sample from the unused module, wet fiber sample and oven-dried sample. The fouled membrane samples were taken from the same module and location but the one sample was stored in water and the other was dried in oven at 65 °C in order to get cake layer to attach stronger on the membrane surface.

All samples were washed with fresh deionized water for 5 mins and cut to small, roughly 1 cm, pieces. Before the CLSM, each sample was stained with two staining solutions: first with 0.1 mg/ml basic fuchsine solution and then with 0.1 mg/ml ConA-FITC solution. ConA paired with different conjugates has been widely used for staining polysaccharides due to its attachment to *α*-mannopyranosyl and *α -D*-glucopyranosyl. (Sun et al. 2011, Peter-Varbanets et al. 2010). Basic fuchsine was used for staining the membrane surface. Staining was done by placing the samples into the staining solution at room temperature in an unlighted fume cabin. The samples were protected from light with aluminium foil during the staining, which lasted 30-45 min per each staining. After both stainings, the samples were immersed three times into 10 mM phosphate-buffered saline (PBS) solution for 5 minutes each time.

After the final washing with PBS, the samples immediately taken for the CLSM imaging and fixed on a glass holder with two-sided tape. The images were taken with LSM 710 (ZEISS). Objective used was EC Epiplan-Neofluar 20x/0.50 HD DIC M27. Two excitation lasers were

used simultaneously: 488 nm and 543 nm (both set to 0.2 % power). Two channels, with emissions ranges of 492–520 nm and 601–698 nm, were used for ConA and fuchsine respectively. The ranges and lasers were chosen based on fluorescence measurements after preparing samples that had been stained separately with fuchsine and ConA but not both. The setting for imaging were the following:

- Channel 1 (492–520 nm): master gain 791, digital gain 1.1, pinhole 1 airy unit (AU)
- Channel 2 (601–698 nm): master gain 1200, digital gain 1.0, pinhole 1 AU

The 3d-images were composed of stacks of pictures of same area (x- and y-coordinates) at different height (z-levels). Dimensions of each image are announced in caption. The stack intervals were set to approximately 1 µm.

5.57 Experimenting on the desorption properties of the fouled membranes

To study the composition and reversibility of fouling of the membranes, an extraction experiment was conducted. Three samples (s1, s2, s3) weighting roughly 10 grams wet were collected from module M_{c2}. First step of the extraction experiment was to remove and weight the possible cake layer of the samples. The samples were placed into glass contrainers, which contained 500 ml of deionized water, for 2 hours. The fibers were then individually picked up from the water with tweezers, and slightly stirred under water to separate most of the cake layer, before washing them with fresh deionized water. After washing the samples, three fibers were collected as FTIR samples, and the rest of the fibers were placed into another batch of fresh deionized water and left to soak there overnight before further treatments. The 500 ml batch of water now containing most of the cake layer was filtrated using Büchner funnel and Whatman filtration paper (CAT No. 1442-070, 2.5 µm size cut-off). The filter paper was weighted before the filtration. After the filtration, the filter paper was dried at 65 °C in oven and weighted again. By comparing the weight of the filtration paper before and after filtration, the mass of the cake layer could be determined. The filtrate was saved, and its contents were analyzed with ICP-MS and TOC analysis at a later time.

The fibers that had been washed with water were then treated with three individual ultrasound (US) treatments in series. In each treatment the samples were placed into a different solution (each roughly 120 ml) and treated with ultrasound using W181 USF (FinnSonic) ultrasound

cleaning machine at room temperature. Each US treatment lasted 24 hours and the used solutions were in order:

- Deionized water
- Oxalic acid solution at pH 4
- NaOH solution at pH 9.

These treatments were named as: US treatment, US/Acid treatment and US/Alk. treatment. The solutions were chosen, because in desorption experiments by Kimura et al. (2004), oxalic acid and NaOH were found to be effective solutions at extraction of metals and organic matter, respectively. The solutions were prepared by diluting stronger solution while monitoring the pH using pH paper.

After each US treatment, the fibers were washed by placing them into a large fresh batch of deionized water, and then into another batch of deionized water where they were kept overnight. Three fibers were collected as samples for ATR-FTIR analysis after each US treatment. The treatment suspensions were filtrated using Büchner filtration with glass sinter, which had been dried overnight at 65 °C in oven. The ceramic filters and the fiber samples were dried in oven at 65 °C. After the final treatment, the fibers were dried at 105 °C to ensure no moisture was left inside the samples. After drying samples and filters were kept in desiccator for at least 1 hour and weighted. The mass of the residue fibers (m_r, dried at 105 °C) were added to the masses of the ATR-FTIR samples (collected after each treatment, $m_{s,w}$, $m_{s,us}$, $m_{s,us/acid}$, $m_{s,us/alk}$) to calculate the total dry weight of the three fiber samples (s1, s2 ,s3) used in the exraction experiment. The dry masses were used for calculating the extracted amounts per sample mass (mg/g) as well as the cake layer weight fraction. When calculating the extracted amounts (mg/g), the dry masses had to be adjusted due to the collected samples. For example, during the US/Acid treatment the actual dry mass of the fouled fibers was the residue mass (m_r) of that particular sample added to the mass of the FTIR samples collected after the US/Alk. treatment ($m_{s,us/alk}$).

The cake filtrate and US treatments suspensions were analysed for total carbon and metal concentrations using TOC-L (Shimadzu) and 7900 ICP-MS (Agilent technologies) respectively. The extracted amounts of metals were compared to the cake layer composition in order to study the fouling characteristics of each detected metal. This was done by comparing the

concentration of the metal among other extracted metals (C_e) to the concentration of the metal among the other metals of the cake layer (C_c). For each metal, this was expressed as a C_e/C_c -value, which was calculated as:

$$\frac{C_{e,j}(i)}{C_c(i)} = \frac{m_{e,j}(i) \div m_{e,j}(tot.)}{m_c(i) \div m_c(tot.)} \quad (13)$$

, where:

$C_{e,j}(i)$	is ratio between the extracted amount of metal *i* and total amount of extracted metals in extraction *j*
$C_c(j)$	is ratio between the amount of metal *i* that was found in the cake layer and the total amount of metals
$m_{e,j}(i)$	is mass of extracted metal *i* in extraction *j*
$m_{e,j}$(tot.)	is sum of all metals extracted in extraction *j*
$m_c(i)$	is mass of metal *i* measured in the cake layer
$m_c(tot.)$	is total mass of all metals measured in the cake layer.

6. Results and discussion

6.1 Evolution of irreversible fouling during the pilot filtration

The evolution of fouling in the modules was tracked by calculating the individual fouling resistances at the start of each filtration period, which were divided by chemical cleanings. The total fouling resistance at the end of each filtration period was also calculated. The rate at which the total fouling resistance increased was calculated for each period as well. The results are presented in Fig. 4.

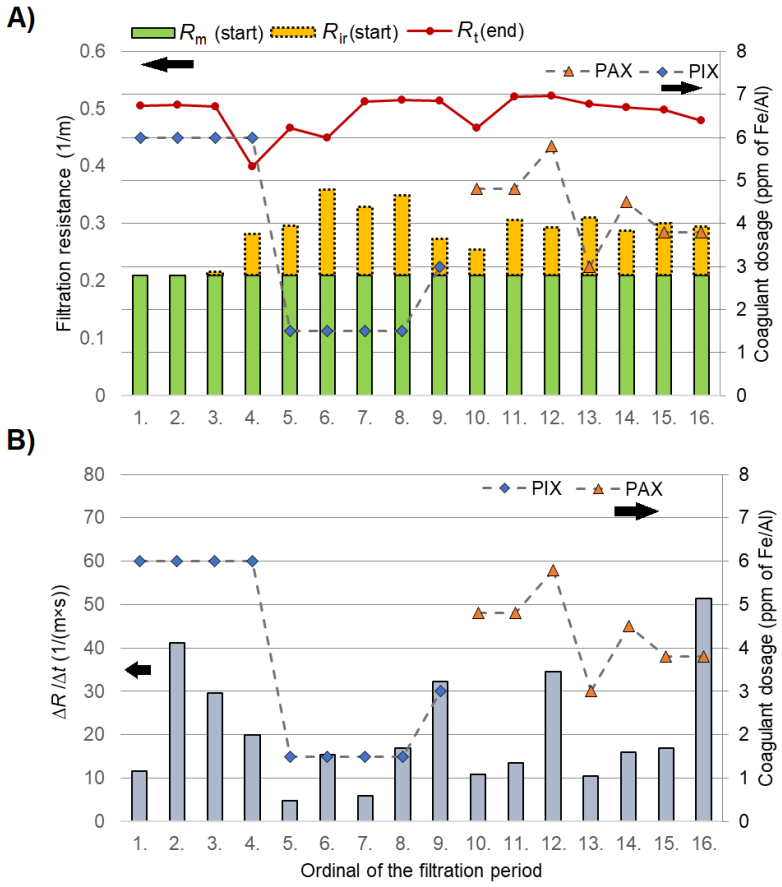

Figure 4 A) The individual fouling resistances at the start of each filtration period and the total fouling resistance at the end of each period presented with the corresponding coagulant dosage, B) The average increase rate of the total fouling resistance during each period (from start to end) presented with the corresponding coagulant dosage.

As Fig. 4 shows, there occurred little irreversible fouling during the first two periods. The irreversible fouling suddenly increases by 969 % during the 3rd period without a change in the coagulant dosage. This hints that irreversible fouling is not necessary dependant on the coagulant dosage but rather on the filtration sequence. The irreversible fouling increased constantly in the modules until it decreased slightly during the 6th period. R_{ir} also decreased more during the 8th and 9th periods. Although R_{ir} is theoretically not supposed to decrease, during a long filtration with varying coagulant dosage, there are multiple possible explanations for this. Based on other analyses conducted for this work, most of the irreversible fouling has likely been caused by cake layer formation, which has not been successfully removed from the modules during the chemical cleanings. Changes in the cake layer structure, location and porosity during the long pilot filtration may very well have caused the fluctuation in R_{ir}.

There was some variation in the downtime between filtrations, which could affect the fouling evolution. Most of the filtrations had relatively little downtime after them (< 48 hours) but there were some exceptions. After the 1st period there was downtime for 19 days, which could explain why the R_{ir} only started to increase during the 2nd filtration. There was also significant downtime after the 8th and 9th filtrations (13 days and 5 days). As seen from Fig. 4, the downtime matches well with the decrease in R_{ir} after these two periods. Soaking the fouled membranes in water for long time can be expected to cause dissolving and dispersion of foulants in the modules, and thus the downtime is a reasonable explanation for the increase in R_{ir}.

Based on Fig. 4, irreversible fouling in the modules seems to have reached a constant state two time during the pilot filtration. First during the 1.5 ppm PIX filtrations (periods 6–8, pH adjusted to 7), and then during the PAX filtrations (periods 11–16). As stated earlier, it was confirmed during the analyses, that there was cake layer inside the modules after the pilot filtration, and it's very likely that there was cake layer inside the modules already during the PIX filtrations. Based on this and Fig. 4, the results suggest that the residue cake layer formed by PIX (at 7 pH) caused a more severe fouling (drop in initial flux) than the residue cake layer formed during the PAX filtrations. This agrees with results by Yu et al. (2013a), where fouling caused by flocs formed from either iron chloride or aluminium sulfate were compared, and the iron-based in-line coagulation caused a bigger decrease in TMP.

In Fig. 4 B, the average rate that the total fouling resistance (R_t) increased during the filtrations is presented for each filtration period. Based on comparison of Fig. 4 A and B, the rate of fouling doesn't seem to correlate with the amount of irreversible fouling. Although the filtration times varied from 13 to 126 hours (16th and 5th period, respectively), this did not seem to affect the reversibility of fouling, which occurred during the filtrations. However, there could be some degree of correlation found between the coagulant dosage and filtration time, with some exceptions. During the first four filtrations (6 ppm PIX), the fouling was likely still be evolving, which could explain the variations in the fouling rates. During the last filtration, the filtration temperature was clearly below average and also decreased during the filtration from 8.8 to 8.2 °C, which could perhaps explain the fast fouling rate. With those exceptions, increasing coagulant dosage seems to generally increase the fouling rate, which could result simply from directly increasing the particle matter in the feed water or from improving the removal rates of compounds, thus decreasing the amount of compounds passing through the membrane. Correlation found between TSS in the feed and total fouling rate also indicates that cake formation was the main cause of flux decline during the pilot filtration. However, it should be noted that analysing this correlation is difficult, because the total fouling rate is likely not only affected by new cake layer being formed but also by the amount of residue cake layer left in the module by the previous chemical cleaning.

6.2 Elemental composition of the cake layer

All modules, even those that had been chemically cleaned after the end of the pilot filtration, were found to contain cake layer with a gel-like appearance during module autopsy. In other words, the chemical cleaning was ineffective at removing the cake layer from the modules. The elemental composition of dry cake layer from a chemically cleaned module (M_{c1}) is presented in Table VI. As stated in section 2.2, typical composition for humic substances is 40–60 % carbon, 30–50 % oxygen, 4–5 % hydrogen and 1–4 % of nitrogen with small amounts of sulfur and phosphorus (Sutzkover-Gutman et al. 2010). Based on the low carbon content (21 %) of the cake sample presented in Table VI, it can be roughly estimated that 35–50 % of the cake layer might have consisted of NOM-based organic content.

Table VI Elemental composition of freeze-dried cake layer sample taken from module M_{w1} (*d*=10–50 cm, *n*=number of measurements).

Analysis method	**Element**	**Content, w-%**
CHN (n=3)	C	21.17 (± 0.049)
	H	3.97 (± 0.038)
	N	0.58 (± 0.024)
ICP-MS (n=2)	Fe	8.24 (± 3.09)
	Al	5.12 (± 0.064)
	Ca	0.26 (± 0.0084)
	K	0.25 (± 0.20)
	Mg	0.019 (± 0.0011)
	Other	60.38

The metal content in the cake layer was around 10–15 %. Both aluminium and iron were found in the cake layer, which was unexpected because only aluminium-based coagulant was used during the last 7 filtration periods. This means that even after 8 chemicals cleanings, iron-based cake layer was not removed from the module. The iron content showed high deviation between the two ICP-MS measurements, which may suggest that the iron-based cake layer had been removed or moved from some of areas of the modules.

The large unidentified fraction in Table IV probably consists mostly of oxygen and small amounts of ash. Typical ash content for different fractions of NOM is > 1 % although the hydrophobic neutral fraction has been measured to have as high as 37.2 % ash content (Krasner et al. 1996). Because the oxygen content in the sample is assumingly high compared to the oxygen content normally found in NOM (30–50 %), it is most likely that some oxygen is bonded with the metal ions due formation of metal oxides or hydroxides. The EDS measurements (presented in section 6.6) did detect some silicon in the cake layer surface as well (1–3 %), but silicon content was not measured in the ICP-MS.

The H/C and C/N ratios for the cake layer presented in Table VI were 2.23 and 42.9, respectively. The H/C ratio is much higher than the typical values for humic substances (average 1.1 for fulvic acid and 0.9 for humic acid, details presented in section 2.2) and the C/N

ratio is somewhat low but not untypical (average 93.1 for fulvic acid and 32.5 for humic acid) (Rodriguez & Nunez, 2011). Likely explanation for the high H/C ratio could be due to metal hydroxides present in the cake layer. As mentioned earlier, there are multiple floc formation mechanisms for metal-based coagulants, but what could be considered successful coagulation is often depended on the presence of metal hydroxides or metal hydrolysis species. (Jarvis et al. 2004, Adusei-Gyamfi et al. 2019).

6.3 Identification of foulants on the membrane surface

Identification of foulants is important for being able to improve fouling control. Elemental analysis doesn't give precise information about the compounds present in the cake layer, so other tools, such as ATR-FTIR, must be used for their identification. The ATR-FTIR spectra of freeze-dried cake layer, fouled membrane and clean membrane are presented in Fig. 5. Peaks in the spectra represent different chemical bounds between the compounds, and thus can be used for identification of chemical compounds. While ATR-FTIR mainly analyses foulants on the membrane surface, the analysis method does penetrate the membrane to some extent, which is reflected in the results.

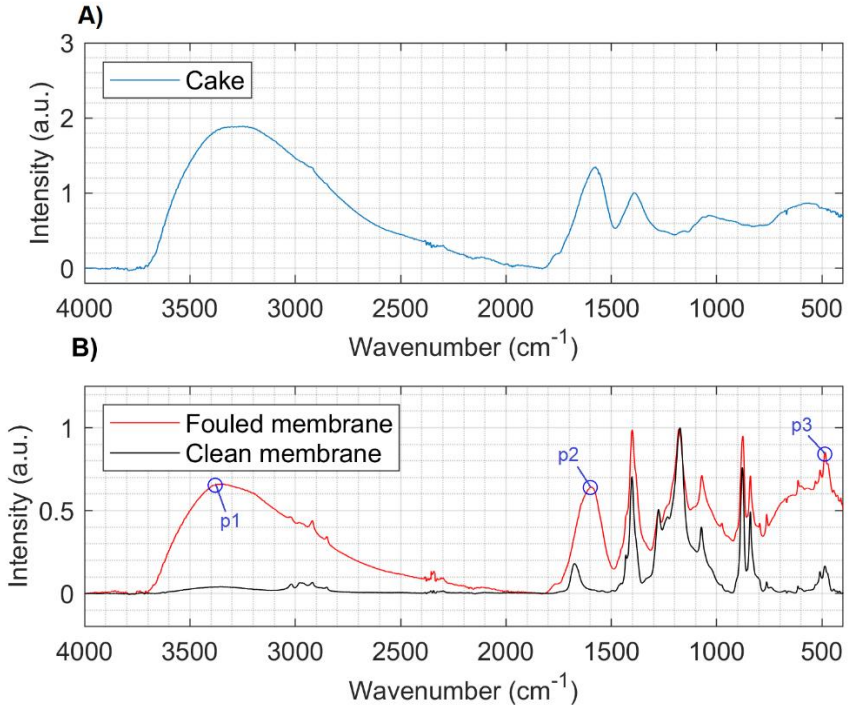

Figure 5 A) ATR-FTIR spectra of a freeze-dried cake layer, B) ATR-FTIR spectra of a fouled membrane (M_{c1}, *d*=15 cm, *r*=5.6 cm, dried at 65 °C) and clean reference membrane, peaks at certain wavelengths (p1 at 3380 cm^{-1}, p2 at 1600 cm^{-1} and p3 at 487 cm^{-1}) are marked on the fouled membrane spectrum.

As shown in Fig. 5, the cake layer spectrum has very wide, merging peaks, which made interpreting them challenging. Due to the high variety in NOM, it is likely that each peak corresponds to multiple different compounds. To ease processing the data, fouled membrane spectra were divided to three areas (3720–1820 cm^{-1}, 1800–1150 cm^{-1} and 1150–400 cm^{-1}) each represented by different peak (also shown in Fig. 5 B) located at at 3380 cm^{-1} (p1), 1600 cm^{-1} (p2) and 487 cm^{-1} (p3). The biggest problem with the accuracy of the ATR-FTIR measurements was that the cake layer attachment on the fibers was uneven, which was highlighted when the cake layer had dried. This was counteracted with large amounts of individual measurements (9) for badly fouled samples.

The large wide peak ranging from 3720–1820 cm^{-1} with maximum intensity approximately at 3380 cm^{-1} is most likely caused by the O-H stretch from organic groups (alcohols, phenols and carboxyl groups) (Rodriguez & Nunez. 2011). Similar bending can be found in FTIR spectrum of humic acid (SDBSWeb). Similar peak is commonly found in spectra of other organic compounds as well.

Some but not all membrane samples also had varied amounts of C-H stretching at 3000–2850 cm^{-1}, which could indicate presence of lipids (Kenne & Merwe. 2013). However, this stretch could also be caused by plastic contamination from either the plastic bags used for storing the samples or from nitrate gloves, which is more likely to be the case here, because similar stretches were only found in some of the spectra.

Both aluminium hydroxide and iron hydroxide have series of uniquely shaped peaks with high intensity at roughly the range of 2950–2850 cm^{-1} (SDBSWeb). These peaks weren't detected in any spectra of fouled membranes or cake samples. This and elemental composition of the cake layer made it seem plausible that the ATR-spectra were more representative of the organic compounds in the cake layer rather than the inorganic ones. Because metals, especially iron, are heavy compared to other elements, even if the weight fraction of a metal is high its mole fraction (and number of bounds formed) is much lower. Another factor supporting this interpretation is that there was little variation in the intensities of the larger peaks relatively each other, which indicates that the composition of the foulants on the membranes was uniform. This is contradicted by especially the iron concentration, which varied remarkably, as shown by the EDS results where iron concentration of same fiber could increase over 500 % between areas close to each other. Thus if iron concentration had large impact on the ATR-spectra, more variation could be expected in them.

The clean membrane ATR-FTIR spectrum has a peak at 1680 cm^{-1}, which is not found in the spectrum of pure PVDF and may be caused by some additive such as polyvinylpyrrolidone (PVP). This peak is covered in the badly fouled membranes by the wide peak at 1575 cm^{-1}, but the peak at 1680 cm^{-1} can be seen in spectra of few cleaner fouled samples.

In the cake spectrum in Fig. 5 A, there are multiple distinctive peaks at 1800–1150 cm^{-1}. The two main peaks at this range are at 1575 cm^{-1} and at 1386 cm^{-1}. Similar peaks have been found to be caused by symmetric and asymmetric COO^- -stretching, respectively, in a study by Guan et al. (2006) analysing ATR-FTIR spectra of dihydroxybenzoic acids. Thus, it is possible that the peaks at 1575 cm^{-1} and 1386 cm^{-1} have both been caused by carboxylic groups, which are common in humic substances.

As stated above, both major peaks from the band at 1800–1150 cm^{-1} might be caused by mainly by humic substances. Yamamura et al. (2008) found similar peaks as found in this study from ATR-FTIR spectra of NOM, which had been desorbed from membranes. In their study, the three main peaks in the band at 2000–800 cm^{-1} were found at 1660–1600 cm^{-1}, 1400 cm^{-1} and

1080 cm^{-1}. They also identified the peak at 1660–1600 cm^{-1} to be caused by humic substances although it was linked to C=C stretching. In the spectra studied by Yamamura et al. (2008), a shoulder at 1550 cm^{-1} was found, which was interpreted to correspond to protein content. This shoulder couldn't be detected in the cake spectrum of the present study, but it could be that it was masked by the broad peak at 1600 cm^{-1}.

The peaks found in Fig. 5 A in the band between 1150–400 cm^{-1} are harder to distinguish than the peaks in other areas. The main peaks appear around 1050 cm^{-1} and 560 cm^{-1}. Alcohols and aliphatic ethers can cause C-O stretch at 1095 and 1030 cm^{-1} (Rodriguez & Nunez. 2011). In other membrane fouling studies, stretching around 1080 cm^{-1} has been specifically linked to polysaccharide content, which is likely the right interpretation in this case as well (Yamamura et al. 2008, Kimura et al. 2004).

Kimura et al. (2004) suggested stretching below 1000 cm^{-1} in spectrum of a fouled membrane to be caused by metals. Spectra of iron hydroxide, aluminium hydroxide and aluminium oxide all have stretching at 800–400 cm^{-1} so metal content may be a reasonable interpretation (SDBSWeb). The intensity of FTIR spectrum of fly ash has been detected to overall increase towards smaller wavelengths with peaks at ca. 1060 cm^{-1}, 846 cm^{-1} and 533 cm^{-1} caused by Si-O-Al stretching (Naveed et al. 2019). However, out of plane C-H stretching, caused by organic compouds, can also occur at around 625 cm^{-1} (Lohwacharin et al. 2010). Thus, it is impossible to conclude the precise compounds that cause the stretching at < 1000 cm^{-1} in Fig. 5 A, but it is possible that it is caused partly by both metal and organic compounds.

The ATR-FTIR spectrum of water also has intense stretching at low wavelengths (< 1000 cm^{-1}). Thus, water content in the sample—leftover from drying or absorbed from air—may increase the intensity of stretching < 1000 cm^{-1}. Hydrophilicity of the sample may affect the intensity at this area as well.

To summarize, the ATR-FTIR spectrum of the cake samples indicate presence of alchohol, carboxyl, and phenolic groups. The presence of those groups is mostly likely caused by mainly humic substances. The stretch at 1100–1080 cm^{-1} is most likely caused by polysaccharides. On the other hand, the overall high intensity at 1150–400 cm^{-1} could be caused by multiple different substances. It could imply presence of iron and aluminium hydroxides or oxides. The stretching could also be caused partly by aluminium/silicate-based mineral-like compounds. This might be plausible as aluminium based coagulants have been suspected of forming

aluminium silicate hydroxides during filtration when silicate is present (Kimura et al. 2015). This is also supported by the EDS measurements, which indicate correlation between silica and aluminium content in the cake layer. Another just as likely explanation is that the stretch is caused by organic matter, because multiple common organic macromolecules have stretching in this area, for example humic acid, starch and cellulose acetate (SDBSWeb). Hydrophilic fouling may increase this intensity of this stretch.

6.4 Distribution of foulants in fouled and chemically cleaned modules

Based on the literature presented in section 3.10, the amount of fouling was expected to vary vertically and horizontally in the module. The fouling on the membranes was analysed based on the ATR-FTIR spectra. Because the spectra were normalized, the amount of fouling can be expected to correlate with the intensities of the peaks. This is demonstrated by Fig. 6, where spectra of three samples with different cake contents (in w-%) are presented. The cake contents of the samples were determined in conjunction with the extraction experiment.

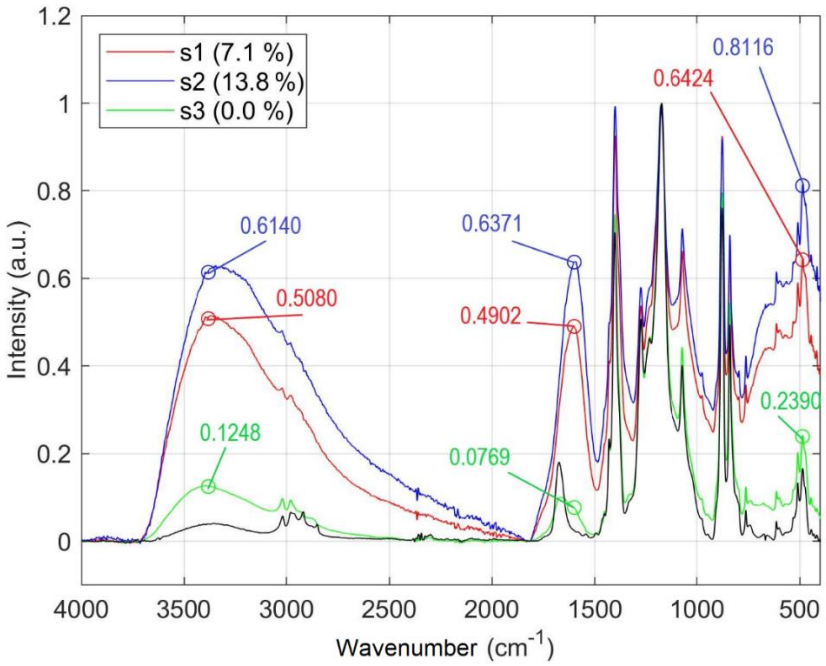

Figure 6 FTIR spectra of three samples with different cake contents. The cake contents and sample names are shown in the legend in parentheses. Samples were dried in oven at 65 °C. Reference sample is represented by the black line.

As seen from the spectra in Fig. 6, the intensities of the three distinctive peaks p1, p2 and p3 correlated with the cake mass fraction of the fiber samples. Thus, while the intensities can't be directly translated to foulant concentration, they can be used to estimate foulant amounts on the samples. Based on the previous section, the three peaks have been linked to different chemicals compounds:

- Intensity of p1(at 3380 cm^{-1}) caused by O-H stretching indicating organic fouling
- Intensity of p2 (at 1600 cm^{-1}) caused by COO^- or C=C stretching indicating humic substances
- Intensity of p3 (at 487 cm^{-1}) indicating possibly metal and/or organic fouling.

Comparison of these peak intensities has been applied in Fig. 7 and Fig. 8, which compare the horizontal (variation in the distance to the center line, *r*) and vertical (variation in distance to the open-end, *d*) fouling gradients in the fouled module and a chemically cleaned module. The intensities presented in Fig. 7 and Fig. 8 were calculated by extracting the intensity of the clean membrane spectrum from the fouled membrane spectra at specific wavelengths of p1, p2 and p3.

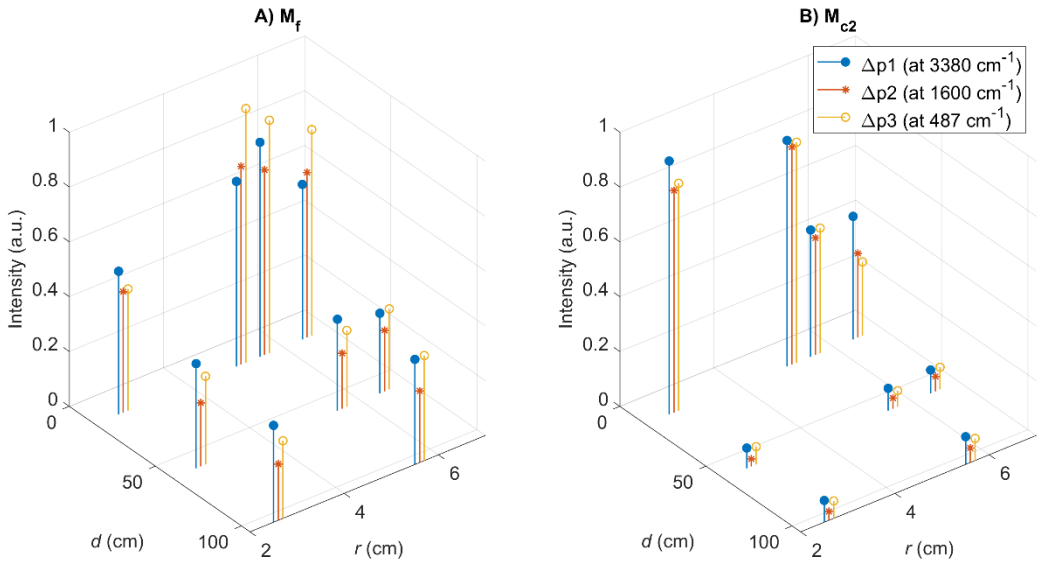

Figure 7 Surface fouling distribution in A) fouled membrane module (M_f) and B) chemically cleaned membrane module (M_{c2}) based on the intensity difference of ATR-FTIR spectra between the fouled samples and the clean sample at three specific wavelengths.

The foulant concentrations and placement (presented in Fig. 7) varied remarkably between the two modules. Near the open-end of the module (*d*=15 cm), the fouled module (M_f) was the most fouled at middle ranges of *r* (estimated 4–5 cm), while the chemically cleaned module (M_{c2}) was more fouled near the center (*r* < 2.6 cm). In other area, either at the middle of the module (*d*=60 cm) or near the closed-end (*d*=15 cm), module M_f had clearly more surface fouling than Mc_2 indicating that the chemical cleaning was effective at these areas. In general, the chemically cleaned module did not have any visible cake layer in these areas, while the M_f had some. Fig. 8 presents the vertical fouling gradient at fixed distance away from the center (*r*=5.6 cm).

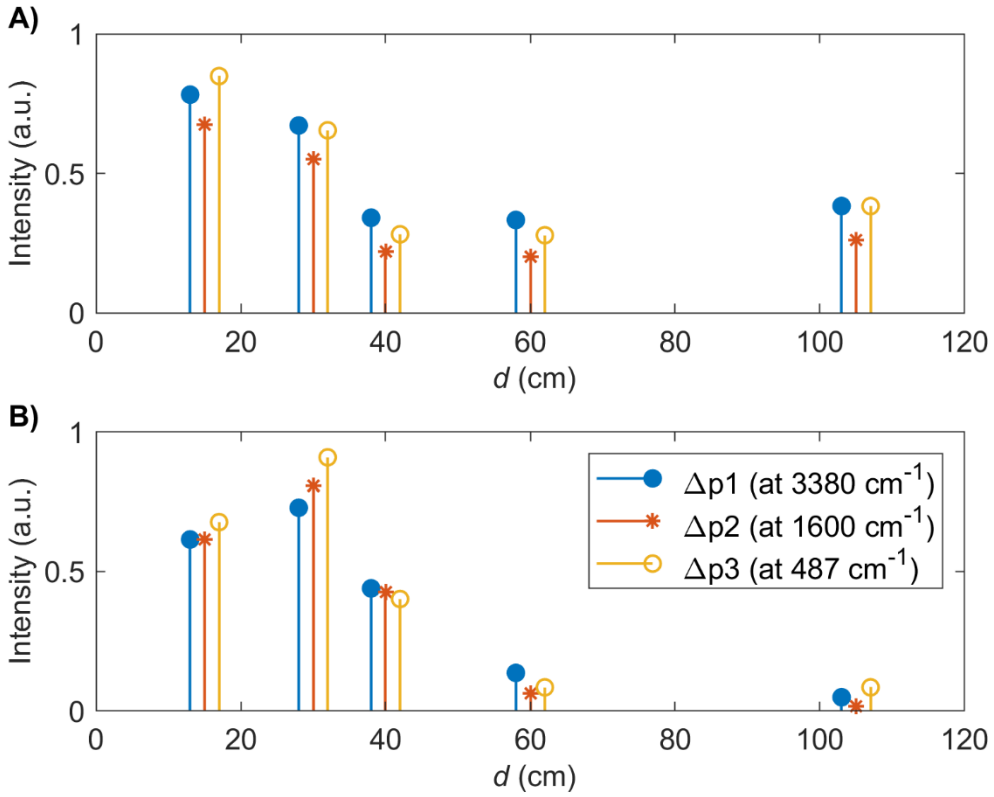

Figure 8 Vertical fouling gradient at in two modules at *r*=5.6 cm: A) M_f, and B) M_{c1}. Based on the intensity difference of ATR-FTIR spectra between the fouled samples and the clean sample at three specific wavelengths.

The vertical fouling gradients (presented in Fig. 8) varied between the two modules. In the fouled module (M_f), surface fouling increased while approaching the open-end from the middle. However, in the chemically cleaned module (M_{c2}), the fibers were most fouled at an area between the open-end and the middle of the module (*d*=15–30 cm). Another difference was that M_f was slightly more fouled near the closed-end than at the middle (also seen in Fig. 7).

Overall, the chemical cleaning procedure was ineffective at removing cake layer from the modules but rather it seems likely that the cleaning process pushed foulants towards the center of the modules, both horizontally and vertically. The results also indicate, that when the filtration was restarted after a chemical cleaning, foulants may have started to move away from the clogged center towards areas, where the permeate flux was the highest. This might be the best explanation for why the areas, which were badly fouled in the chemically cleaned modules, had less fouling in M_f. Thus, the fouling profiles of M_f can be used as some indication about where

the permeate flux has been the highest during filtration, because areas were permeate flux is high can be expected to foul more rapidly than areas with low permeate flux (as mentioned in section 3.10). However, it should also be noted that there are other factors to fouling besides the permeate flux, such as hydrodynamic conditions. The areas near the outer border of the modules most likely had increased crossflow velocity and were mixed better, which could be why they were generally a bit cleaner in M_f than areas couple centimetres towards the center. The increased fouling of areas near the closed-end compared to middle parts of the module in M_f could also be explained by uneven hydrodynamic conditions, due to the bottom of module restricting water flow. Overall, it appears likely that areas at the outer border near the open-end had the highest local permeate flux of all areas. It should be noted that while the chemically cleaned modules and M_f both contained high amounts of cake layer, the total fouling resistance (R_t) still recovered a lot during the chemical cleanings, as seen in Fig. 4. It could be that by pushing the cake layer away from the most active filtration areas, the chemical cleanings were still somewhat effective at recovering permeate flux. It appears that the fibers in the center of the module might have been ineffective at filtrating the feed water at all points of the filtration periods, because they were either clogged by the cake layer (start of filtration) or surrounded by it (end of filtration).

As stated in the section 5.3 concerning sampling, the horizontal fouling gradient was assumed be symmetrical around the centreline. The three chemically cleaned modules were also assumed to be mostly identical regarding fouling. If these assumptions were not correct, the reliability of the produced results would suffer and the sampling could not be considered comprehensive. To test this assumption, samples with same coordinates (*r,d*) were selected from different modules and from different sides of the same module, and ATR-FTIR analysis was conducted for these samples. The results are presented in Fig. 9. Overall, the compared samples had similar spectra, which suggests that the assumptions made for the sampling were correct. There is still some deviation in the badly fouled samples, most likely due to the non-uniform distribution of the dried cake layer. Also because the long fibers in the modules were only attached to both ends of the module in a loose manner, there might have existed some variation to local packing density, due to fibers being able to move past each other.

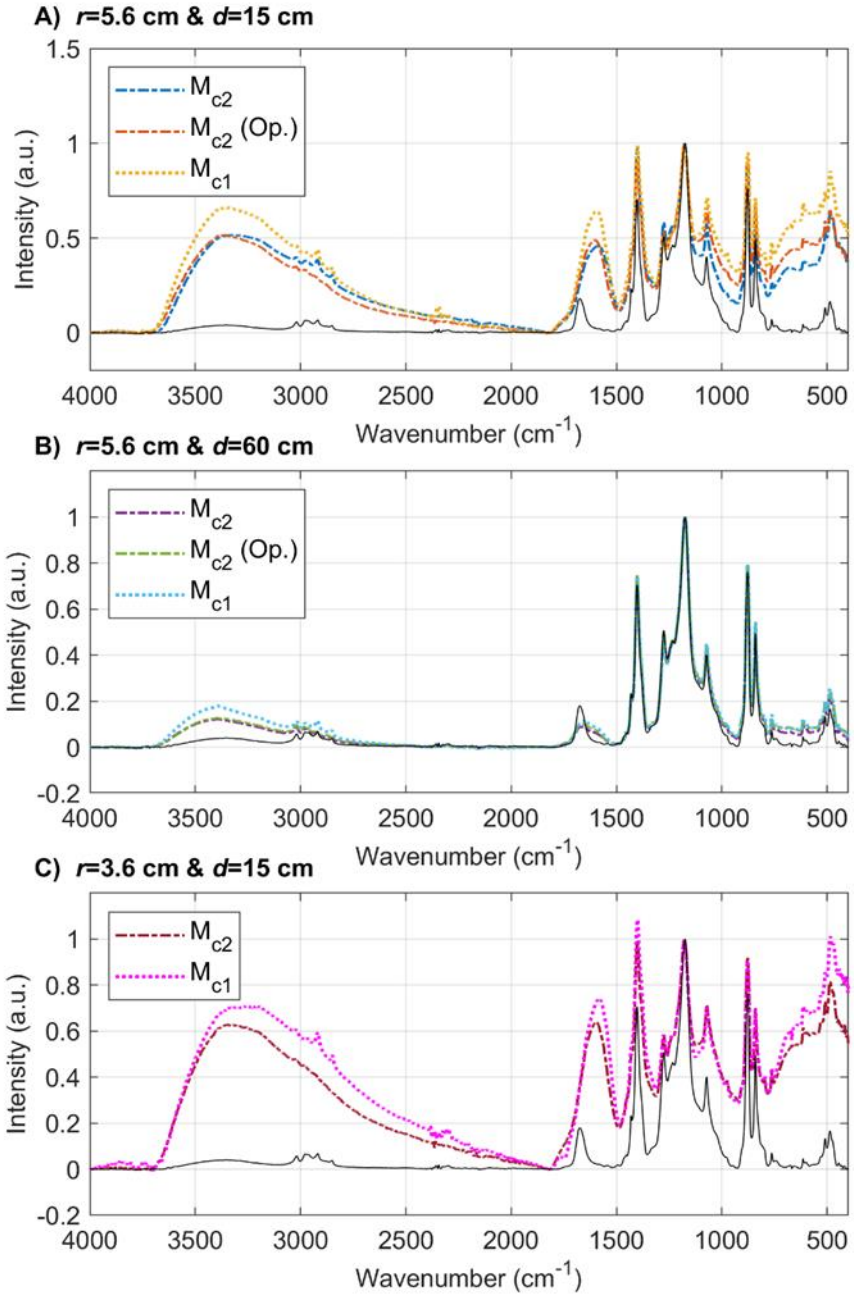

Figure 9 Comparison of ATR-spectra of fouled membrane samples from different modules at same coordinates: A) *r*=5.6 cm, *d*=15 cm, B) *r*=5.6 cm, *d*=60 cm and C) *r*=3.6 cm, *d*=15 cm (Op. indicates that the sample was taken from the opposite side to the other sample from the same module).

6.5 Morphological analysis of fouled membrane surfaces

SEM analysis was used to study the structure of the cake layer attached to the fouled membranes. SEM images of a fouled membrane sample (M_{c1}, *d*=15 cm, *r*=5.6 cm) with the cake layer attached to it are presented in Fig. 10. The sample was not washed after collecting it and it was freeze-dried for the SEM imaging.

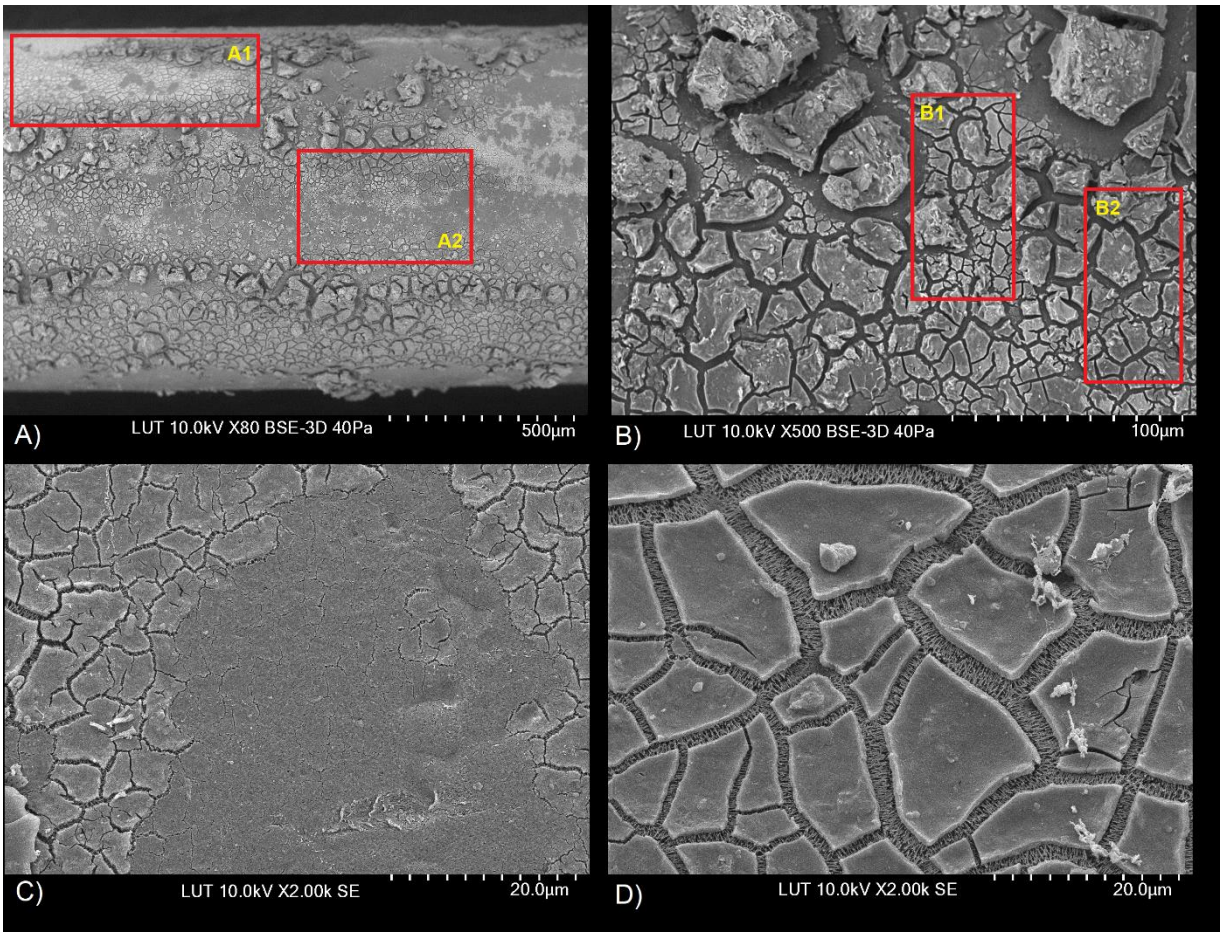

Figure 10 SEM images of the surface of a fouled membrane sample (M_{c1}, *d*=15 cm, *r*=5.6 cm), A) and B) BSE images with uncoated sample and C) and D) are close-ups of the coated sample.

The images presented in Fig. 10 (A and B) are back-scattered electron (BSE) images, in which the areas with high concentrations of heavier elements appear brighter. In this case, the lighter coloured surfaces (for example A1 and B1 in Fig. 10) represent areas, which may have higher

average iron concentrations than darkly coloured areas (A2 and B2). Although the BSE images cannot be used for precise determination of element concentrations, when used together with EDS measurements, they can be used as some indication of local differences in the elemental composition.

As seen from Fig. 10, the iron concentration appears to variate between different areas. Iron-based coagulants were not used during the last seven filtration periods in the pilot, thus the cake layer containing high iron concentration must have formed during the early or middle parts of the pilot filtration. It's possible that this iron-rich cake layer has been partly removed during the chemical cleanings between the PAX filtrations and replaced with cake layer with less iron content. Thus, based on the results, it appears that the chemical cleanings applied at the pilot plant have been only partly effective. When collecting the fiber samples, it was noticed, that some of the badly fouled fibers were bound together by merged cake layer. Merging cake layers might explain why the chemical cleanings have been ineffective at some areas but not others, as merging cake layer can restrict water flow heavily in specific areas (Shimizu et al. 1996).

Fig. 10 (C and D) are close-up images of a coated surface. They are no longer BSE images. From the figures, it can be observed that the whole membrane surface is coated by a thin layer of cake. For some reason the freeze-drying couldn't preserve the cake layer structure as it is was supposed to, but rather the cake layer has been cracked during either the freezing, drying or storage (Fig. 10 D). It should also be noted, that during the freeze-drying large amounts of cake layer was detached from the membrane surface, perhaps due to being pulled apart from the membrane by its own weight.

Fig. 11 compares the surface pores of a clean membrane samples (Fig. 11 A and B) and a fouled membrane sample (Fig. 11 C and D). The fouled membrane sample was stored in water after collecting it in order to remove most of the cake layer. Both membrane samples were freeze-dried before the imaging. The surface of the fouled membrane seems to be covered by a foulants. These images indicate that the outer areas of the pores have not been cleaned completely by simply water treatment, which removed most of the cake layer. The images also indicate pore blocking as potentially relevant fouling mechanism as some of the pore openings appear completely blocked.

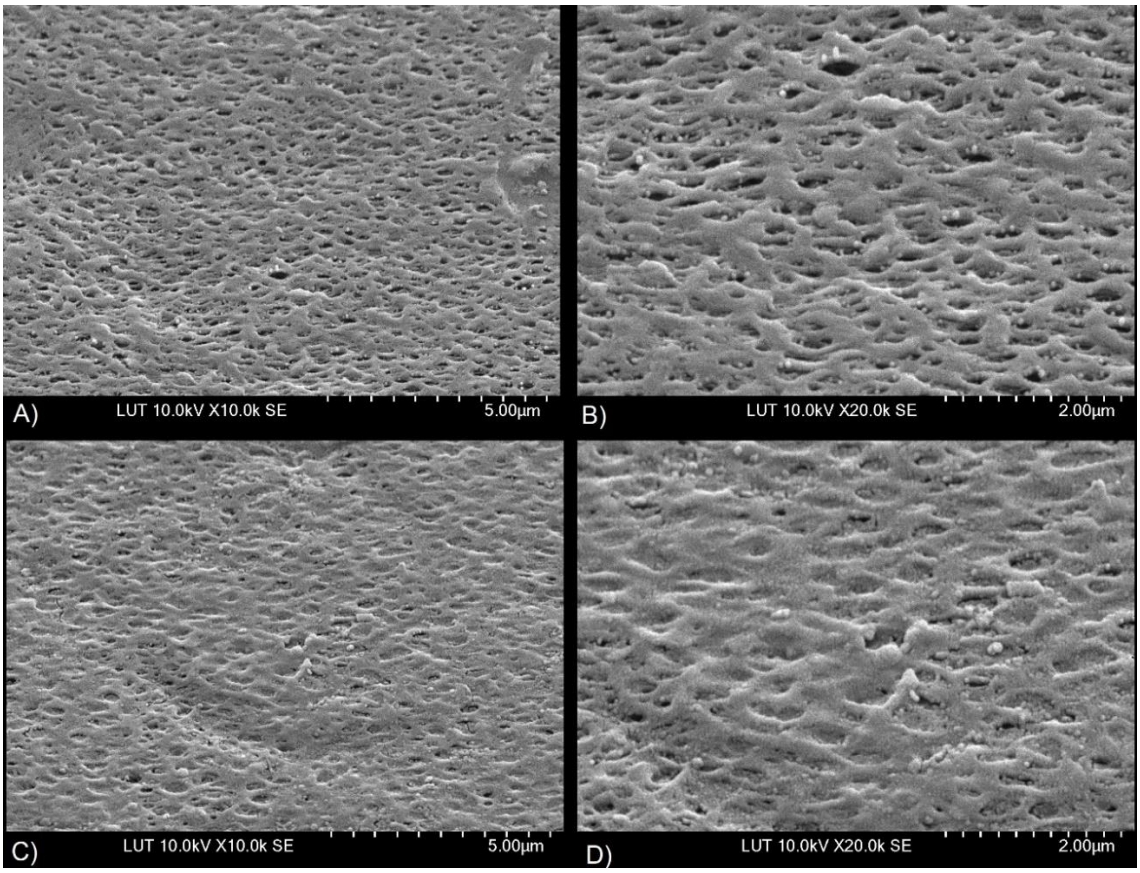

Figure 11 SEM images of the surface of a clean membrane sample, (A and B), and a fouled membrane sample, which had been washed with water (M_{c1}, *d*=15 cm, *r*=5.6 cm), (C and D).

6.6 Comparison of the elemental compositions of different membrane surfaces

The elemental compositions of different membrane and cake layer surfaces were compared with SEM-EDS and the results are presented in Table IX. Both membrane cross-sections and inner surfaces were analysed with SEM-EDS to identify fouling inside the membranes. At membrane surfaces fouled with organic matter, the C/F and O/C ratios could be expected to increase, due to the foulants containing oxygen but not fluoride. The coated and uncoated measurement results of the inner and cross-sectional surfaces were contrary regarding the C/F and O/C ratios. It should also be noted, the SEM-EDS measurements are not very accurate and small differences (< 1 %) can't be considered to be reliable. Overall, the EDS measurements of the cross-sections or the inner surfaces of the membrane samples were not able to detect internal fouling.

Some aluminium was detected in the cross-sectional area and the inner surfaces of the clean membrane. This was most likely caused by scattering rather than foulants as the used equipment contained aluminium surfaces. This means that the aluminium amounts found in all cross-sectional or inner surface measurements are not reliable. Scattering may correlate with the roughness of the analysed surface, which explains why the measured aluminium amounts were higher in the cross-sections rather than in the inner or outer surfaces. No aluminium was found in the outer surface of the clean membrane, so the aluminium measurements of the outer surfaces are most likely reliable. Coating of the samples also decreased the detected aluminium amounts.

EDS analysis was also conducted on the outer surfaces of several fouled membrane samples. These measurements had several goals. EDS could be used to measure elements that were not detected in CHN or ICP-MS analysis such as silicon, sulfur and chlorine. EDS was also used for determining local differences in the cake layer.

The EDS measurement results of the outer surfaces of different samples had more significant differences. Iron content was confirmed to correlate with lighting of the BSE images in the measured areas and as high as 19 % iron content was measured in a lightly coloured area, while the iron content in darker area of the same membrane was only 2.9 %. Even a surface without visible cake layer was shown to include metals ions. In the EDS results, silicon and aluminium contents were found to correlate with each other, which indicates that the formation of silica-aluminium hydroxide complexes on the membrane surface is indeed a possible option. However, it should be noted, that the measurement numbers are low so the correlations found can’t be considered very strong. Sulfur and chloride were also detected in the badly fouled membrane in small amounts. It should be noted that because NOM can contain sulfur, the sulfur does not necessary origin from the ferric sulfate coagulant.

Table VII Elemental composition measured with SEM-EDS from different areas of samples, that include: clean membrane sample and two freeze-dried fouled membrane samples (one washed with water and another with cake layer still intact) collected from the same area (M_{c1}, *d*=15 cm, *r*=5.6 cm). Cake layer samples were attached to oven-dried (65 °C) membrane (M_{c1}, *d*=15 cm, *r*=3.1 cm).

Area of measurement	**Sample**	**C (w-%)**	**O (w-%)**	**F (w-%)**	**Al (w-%)**	**Fe (w-%)**	**Si (w-%)**	**S (w-%)**	**Cl (w-%)**	**Ca (w-%)**	**C/F (g/g)**	**O/F (g/g)**	**O/C (g/g)**
Cross-section	Clean membrane	39.9 (49.4)	1.0 (4.5)	56.8 (45.1)	2.3 (1.0)	-	-	-	-	-	0.7 (1.10)	0.017 (1.10)	0.024 (0.091)
	Washed membrane	37.8 (45.3)	1.5 (3.5)	57.8 (49.9)	2.8 (1.3)	-	-	-	-	-	0.65 (0.91)	0.026 (0.070)	0.04 (0.077)
	Dirty membrane	38.2 (45.5)	1.8 (3.1)	56.9 (50.3)	3.0 (1.0)	-	-	-	-	-	0.67 (0.90)	0.032 (0.062)	0.047 (0.062)
Inner surface	Clean membrane	43.4	2.0	54.5	0.3	-	-	-	-	-	0.8	0.037	0.046
	Washed membrane	43.2	2.4	54.2	0.3	-	-	-	-	-	0.8	0.044	0.056
Surface	Clean membrane	39.0	1.0	59.7	-	-	-	-	-	-	0.65	0.016	0.024
	Dirty membrane (+ visible cake)	32.6	23.7	29	4.2	8.6	0.7	-	0.9	0.3	1.12	0.82	0.73
	Dirty membrane (no visible cake)	39	6	53.1	0.6	1.3	-	-	-	-	0.73	0.1135	0.15
Cake layer	Dark area in BSE	29.2	51.3	-	11.4	2.9	3	0.4	1.3	0.4	-	-	1.76
	Lighter area in BSE	35.5	37.3	-	5.5	19	1	-	1.1	0.6	-	-	1.05

6.7 Analysis of foulants and reversibility of fouling in different fouled membrane samples

An extraction experiment was conducted to assess how much cake layer was attached to each sample and how well the fouling could be reversed by different treatments. Three samples (s1, s2, s3) with varying degrees of fouling were selected for the experiment. The s3 sample was the only sample with no visible cake layer attached to it. The ATR-FTIR spectra of the used samples are presented in Fig. 6. The extraction experiment involved four treatments for each sample. First the cake layer was washed away with water, then the samples went through three ultrasound (US) extraction treatments with different solvents: deionized water, oxalic acid solution (pH 4) and NaOH solution (pH 9).

The amounts of solids extracted by each treatment was measured for each sample in order to calculate the total amount of cake layer (or solid foulants) in each sample. However, almost no solids were detached during the US treatments after the samples were initially washed with water. In some specific cases, small amounts of solid matter could be visually detected in the extraction solutions, but the amounts were too small to be measured by the used methods with two exceptions: during the US treatment of sample s1 (1.1 mg of solids) and the alkaline treatment of s2 (6.3 mg of solids). The cake and moisture contents of the samples are presented in Table VIII. The moisture content of the cake itself was estimated to be 88 % matching the gel-like appearance of the cake.

Table VIII Cake and moisture contents in the three fouled membrane samples from a chemically cleaned module (M_{c2}). The cake content is based on the dry weight of the detached cake layer and the dry weight of the clean fiber samples obtained after all three US treatments. Moisture content is based on the wet weight of the fiber sample and moisture mass calculated by extraction.

Sample name and location	**Cake content, w-%**	**Moisture content, w-%**
Sample s1 (*d*=15 cm, *r*=5.6 cm)	7.1	76.7
Sample s2 (*d*=15 cm, *r*=3.6 cm)	13.8	78.4
Sample s3 (*d*=60 cm, *r*=5.6 cm)	0.00	75.2

Fig. 12 presents the metal ion (excluding magnesium due to small concentrations) and total dissolved carbon (TC) concentrations extracted in each treatment. It should be noted that the extracted amounts presented only consider dissolved compounds. For example, most humic substances are insoluble to water at the used pH ranges, which makes the measured amounts of extracted organic foulants only indicative of the real organic foulant concentrations. While the amount of extracted solid substances was also monitored by filtrating the extraction solution and weighting the used sinters, masses smaller than 1 mg would most likely not be noticed due to measurement errors.

.

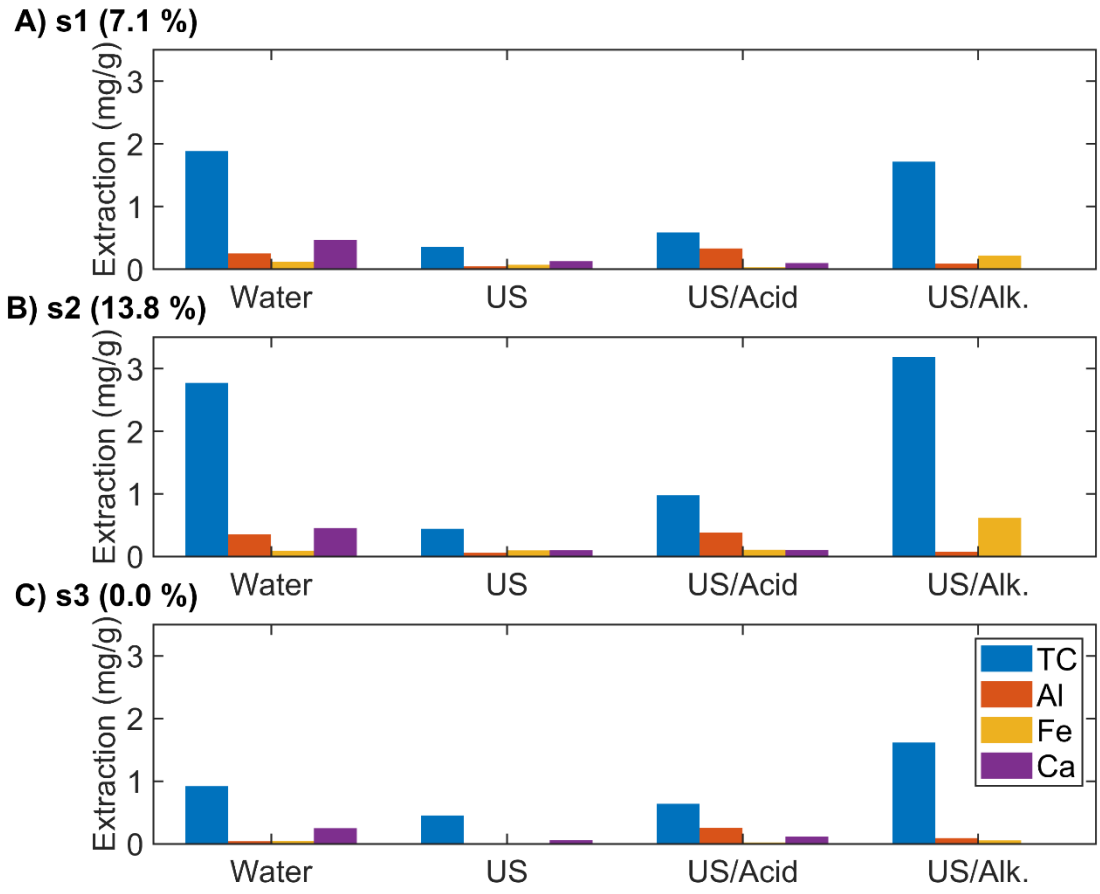

Figure 12 Extracted amounts of dissolved substances in each treatment proportional to the dry weight of the fouled fiber samples: A) S1 (cake content 7.1 %), B) S2 (13.8 %) and C) S3 (0.0 %).

As shown in Fig. 12, carbon was by far the most detected element in most of the extraction solutions. Because the measured carbon was total dissolved carbon (TC) and not dissolved organic carbon (DOC), all of the detected carbon might not have been actually extracted from the fibers, but rather dissolved into the solution from air. TC concentration of 1.3 mg/L was measured for a deionized water sample, which went through similar filtrations and storage time as the other samples but did not contain any extraction products. For reference, the TC concentration measured in the filtrate of S3 after water treatment was 3.6 mg/L, which was the lowest concentration measured during the whole filtration experiment (other samples had at least twice this amount). This shows that probably most the carbon detected in all samples was extracted carbon, but the extracted amounts by the water treatment and the US treatment might have a significant error marginal. DOC determination, rather than TC determination, might have been a better option for this particular experiment in hindsight.

The water treatment removed almost all of the cake layer from the samples. It also removed second most TC overall and most of the calcium from the samples. The US treatment was ineffective compared to the other extractions as only small concentrations of TC and metals were extracted from the samples. The US/Acid extraction was by far the most effective at removing aluminium. This was expected as acid treatment is commonly used specifically for removal of metals oxides and hydroxides from UF membrane (Shi et al. 2014). However, only small amounts of iron were removed during the US/Acid treatment compared to the extracted amounts of the US/Alk. treatment. This contradicts the results obtained by Kimura et al. (2004), where acids treatments were much more effective than alkaline treatments (NaOH at 12 pH) at extracting iron from a fouled PS MF membrane (for example, 4.1 mg/L extracted by 2 pH oxalic acid compared to 0.1 by NaOH at 12 pH). It could be that the used pH of 4 for the US/Acid treatment was too low. It could also be that in this study the iron was strongly attached to the large amounts of organic foulants, which were detached during the US/Alk treatment. US/Alk treatment was the most effective treatment at extracting carbon, which was expected as alkaline treatments are generally efficient at removal of organic foulants (Kimura et al. 2004, Shi et al. 2014). In other words, perhaps the complexation of iron with NOM affected the reaction it had to the treatments.

Because s3 did not contain cake layer, the total extracted amounts from it can be used to estimate how the elemental composition of the foulants found on the membrane differs from foulants in the cake layer. This comparison has been made by comparing the ratios of different

metals and carbon in both s3 and the cake layer (composition can be found in Table VI). Results are presented in Table IX.

Table IX Molar ratios between different metals and carbon presented for the cake layer and for the extraction products of s3, a fouled membrane sample without cake layer. The molar ratio of overall metal and carbon content is also presented.

Molar ratio	**Cake layer**	**Fouled membrane (s3)**
Al/C	0.11	0.049
Fe/C	0.084	0.0077
Ca/C	0.0037	0.035
Mg/C	0.0004	0.005
Metal/C	0.196	0.096

As seen in Table IX, the extraction products of the fouled membrane sample contained significantly less of the two main metals (Al and Fe) than the cake layer. This is influenced by the fouled membrane having overall much lower metal to carbon ratio. The aluminium content of s3 was much higher than the iron content, while in the cake layer the iron and and aluminium contents were close to even. The calcium and magnesium rations are 10 times higher for s3 than for the cake layer. Overall, the foulants found from s3 contain more organic matter than the cake layer. The s3 foulants also contain less iron and more calcium and magnesium than the cake layer.

The results of the extraction treatments on the membrane condition were followed by collecting fiber samples after each treatment and measuring the ATR-spectra of these samples. The results are presented in Fig. 13. Because the cake layer was detached from the s1 and s2 samples only partly, even after all the treatments, the ATR-FTIR results of these samples suffer from some variation due to the non-uniform cake layer. The results of the s3 sample has less variation and can be considered the most reliable.

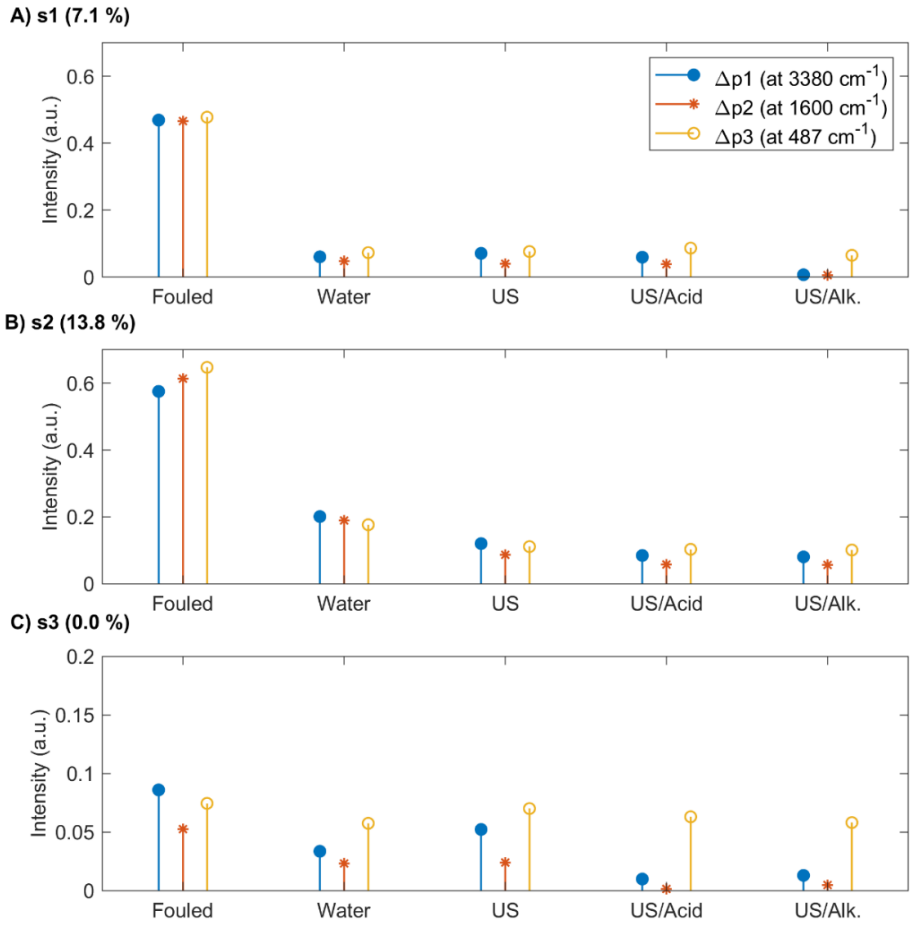

Figure 13 Intensity differences in the ATR-spectra at various wavelengths between the fouled samples before and after different treatments and the clean membrane sample

Fig. 13 tracks the membrane condition during the extraction treatments. It can also be used for assessing how different foulants, which are represented by p1, p2 and p3, behave during the treatments. As determined earlier, p1 and p2 represent organic compounds (OH and carboxylic groups, respectively) and p3 likely a mixture of organic and metallic compounds. From Fig. 13 it should be noted, that the y-axis is scaled differently in Fig. 13 C compared to Fig. 13 A and B. Overall, the samples were cleaned well during the extractions, as the peaks indicating fouling diminished significantly, especially for s1 and s2.

As seen from Fig. 13, the water treatment caused the biggest difference in the intensities. Although the samples had already been chemically cleaned at the pilot plant, soaking them in the water removed large amounts of foulants even from s3. The US treatment had little to no effect on the membrane conditions, as could be expected based on the extracted amounts.

By observing Fig. 13 C, it appears the US/Acid treatment was efficient at removing organic foulants from the s3 sample, while the US/Alk treatment had a lesser effect. For s1, this effect was completely opposite and US/Alk had the bigger impact on the membrane condition. Possible explanation for this is that because s3 had no visible cake layer and less iron content than the other samples, most of the organic foulants in s3 after the US treatment resided in aluminium-NOM complexes, which were removed during the US/Acid treatment. On the other hand, s1 might have had more organic foulants attached to the iron-based complexes, which were affected more by the alkaline treatment. Of all the peaks, p3 was the least affected by the treatments overall, indicating that p3 represents foulants which were resistant to the US treatments.

There are a few extraction studies on fouled membranes, where the FTIR spectra of the extraction products are analysed (Kimura et al. 2004, Yamamura et al. 2007). For some reason, the residue foulants still left on the membranes are rarely analysed, although it could also be that there were none in the mentioned studies. For this work, the ATR-FTIR spectra of residue foulants of different samples have been analysed and presented in Fig. 14. This figure was obtained by extracting the spectra of the clean membrane from the spectra of the samples after the US/Alk. treatment. It showcases, which foulants resided in the membrane samples after all of the treatments thus representing highly irreversible fouling.

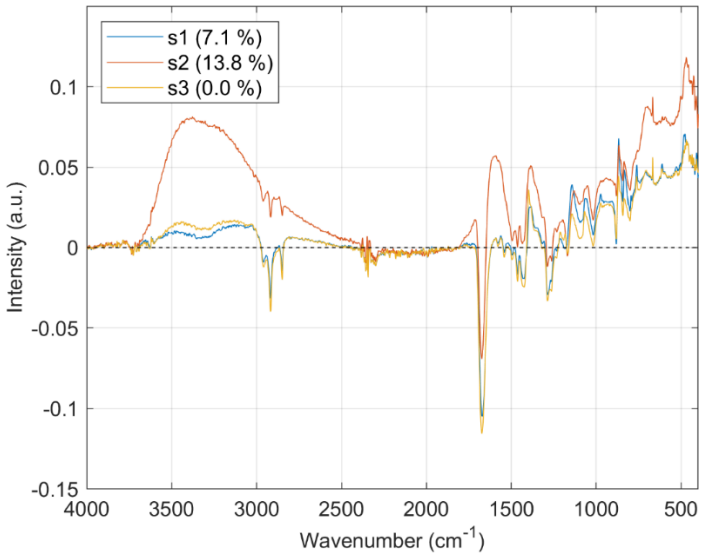

Figure 14 Residue foulants in the membrane samples after US/Alk. treatment.

The s2 still had some cake layer attached to it after all treatments, so the main peaks of the cake layer (presented in Fig. 5 A) can be found from its spectrum in Fig. 14. The s1 and s3 samples did not have noticeable cake layer at this point (in the measured areas), so their spectra differ from the cake spectrum. The p2 peak at 1600 cm^{-1} (carboxylic groups or C=C streching) has completely disappeared indicating absence of these compounds. On the other hand, some organic fouling can still be detected from p1 (at 3300 cm^{-1}, O-H streching) and at 1400 cm^{-1}. Although the peaks at 1600 and 1400 cm^{-1} were both linked to humic substances (COO^-) in section 6.3, it appears there might be some differences in the compounds they represent, since the stretching at 1600 cm^{-1} is greatly decreased in Fig. 14 but stretching at 1400 cm^{-1} is still present. Nevertheless, due to the lack of carboxylic groups, it appears that the residue organic foulants represented in Fig. 14 (s1 and s3) differ from the foulants found in the cake layer. It is possible that these organic compounds were not attached to the flocs, which is part of the reason why they did not get detached from the membranes during the treatments. These type of organic foulants could be a significant source of irreversible fouling, because if they are not affected by coagulation mitigating this type of organic fouling could be difficult.

In Fig. 14, there does not appear to be strong stretching at around 1080 cm^{-1} in the s1 or s3 spectra, which indicates the absence of polysaccharides. This type of stretching has been found in ATR-FTIR spectra of extracted matter in other membrane studies, thus it is likely that

the polysaccharides present on the membrane surface were extracted during this experiment as well. (Yamamura et al. 2008, Kimura et al. 2004)

The intensity of p3 diminished a lot less than intensities of p1 or p2, as seen in Fig. 14. Thus, p3 represents highly irreversible fouling. Based on the results, the composition of the residue foulants represented by p3 can't be determined with complete accuracy but some estimates can be made. Based on the interpretation of the cake layer spectrum, p3 could either represent metallic compounds or some set of simple, perhaps hydrophilic, organic compounds. Because, the p3 stretch is much stronger than stretching in other areas, it's most likely not caused purely by organic foulants. The best suggestion for the residue composition, with current knowledge, might be some sort of aluminium compounds possibly aluminium-silicate complex. In the extraction experiment by Kimura et al. (2004), some extraction products had similar stretching as the spectra of this study at low wavelengths >1000 cm^{-1}. The stretching was explained to be caused by desorbed metals, especially aluminium. Al-O-Si bonding has been found to cause similar stretching in a spectrum of fly ash to what can be observed in Fig. 14 at <1000 cm^{-1}. (Naveed et al. 2019). To further support the interpretation, aluminium silicate hydroxides have also been found to cause irreversible fouling by Kimura et al. (2015) and the SEM-EDS measurements conducted for this study found correlation between aluminium and silicon contents.

Fig. 15 presents the individual ATR-FTIR spectra measurements of alkaline treated s1, s2 and s3 samples, which have been used to calculate the average values presented in Fig. 14. The figure shows, that even while s2 sample seemed more fouled than s1 or s3 based on Fig. 14, actually only small parts of s2 still have cake layer attached to them and otherwise s2 might be as clean or even cleaner than s3. This shows that while s2 had more cake layer attached to it than s3, it might not have suffered more irreversible surface. There are also some explanations, why some areas in s2 might be even cleaner than s3 regarding irreversible fouling. For example, the cake layer around s2 might have protected it from foulants causing irreversible fouling. Another thing to consider is that in areas with large amounts of cake, merging cake layers may form no-filtration zones, which reduce permeate flux to almost zero (Shimizu et al. 1996). These areas might be almost completely unaffected by irreversible fouling due to the low permeate flux.

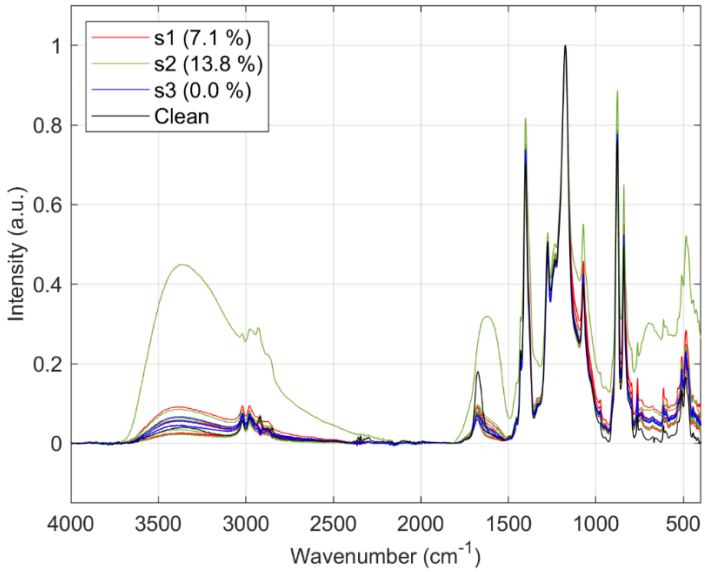

Figure 15 Comparison of individual ATR-FTIR measurements of samples taken after the US/Alk. treatment.

6.8 Comparison of fouling characteristics of different foulants

All of the extracted metals and TC are presented in Table X. In the table, the content of different metals among all of the extracted metals is compared to the cake composition, which is represented by the C_e/C_c -value (calculated from equation 13). This value was calculated based only on the three US treatments thus excluding the water treatment to exclude metals originating from the cake layer. In practice, high C_e/C_c -value suggests that the metal is over-represented among the extraction products, meaning that this metal might have higher concentration on the membrane surface or inside the membrane compared to its concentration in the cake layer. Obviously, this cannot be used to draw any strong conclusions, but it is indicative about what kind of fouling the metal may cause. Based on the C_e/C_c -values given in Table X, iron is the only metal under-represented among the extraction products, meaning that the concentration of iron is higher in the cake layer than among the extraction products. Calcium and magnesium both have larger concentration among the extraction products, which might indicate that they are more easily adsorbed inside or on the outer surface of the membranes than iron. Results for aluminium are between those of iron and calcium/magnesium. Of course, it is possible that not all metals have dissolved from the samples, in which case solubility of the metals would have large effect on the results.

Table X Extracted metal and carbon amounts for each treatment and sample, sum of the total extracted amount for each compound and the average C_e/C_c between all US treatments for metals.

Treat. and sample		**TC, mg/g**	**Al, mg/g**	**Fe, mg/g**	**Ca, mg/g**	**Mg, mg/g × 10**
W.	s1	1.89	0.25	0.12	0.47	0.35
	s2	2.77	0.37	0.091	0.46	0.39
	s3	0.92	0.043	0.045	0.25	0.16
Us	s1	0.36	0.047	0.071	0.13	0.081
	s2	0.44	0.061	0.097	0.10	0.09
	s3	0.45	0.011	0.006	0.059	0.051
US/Acid	s1	0.59	0.33	0.03	0.099	0.065
	s2	0.98	0.38	0.11	0.10	0.047
	s3	0.64	0.26	0.022	0.11	0.15
US/Alk.	s1	1.72	0.089	0.22	-	-
	s2	3.19	0.076	0.62	-	-
	s3	1.62	0.092	0.056	-	-
Sum	s1	4.55	0.72	0.44	0.69	0.50
	s2	7.38	0.88	0.91	0.66	0.52
	s3	3.63	0.4	0.13	0.42	0.36
		TC	**Al**	**Fe**	**Ca**	**Mg**
C_e/C_c	s1	-	0.98	0.58	11.93	10.54
	s2	-	0.87	0.8	9.5	9.89
	s3	-	1.23	0.28	17.07	23.46
	Average	-	1.0	0.55	12.8	14.6

The visual presentation in Fig. 16 has been composed based on the extraction values given in Table X. In Fig. 16, the total extracted amount of each metal is presented as a function of the cake content of the sample. By comparing the shapes of the trendlines fitted to the date, information can be obtained how much the cake amount found in the sample affects the amount of extracted foulants. Relatively high intercept-point with low slope means that the extracted metal amount is less affected by the cake amounts that metals with low intercept-point with high slope. Correlation of the metals with the cake content is probably based on the fact that s1 and s2 samples still contained some residue cake after the water treatment, which is why some compounds found in the cake layer correlate with the initial cake content strongly. The obtained results are similar to those obtained by comparing the C_e/C_c -values. As seen from Fig. 16, samples with low cake amounts have more aluminium, magnesium and calcium

compared to iron, because the iron content residues mainly in the cake layer. It seems that iron is less likely to have adsorbed on the membrane than aluminium, for example. Of course, it's possible than all iron, which is not strongly attached to the cake layer, has been washed away during the chemical cleanings, which occurred after iron-based coagulation was stopped at the pilot filtration.

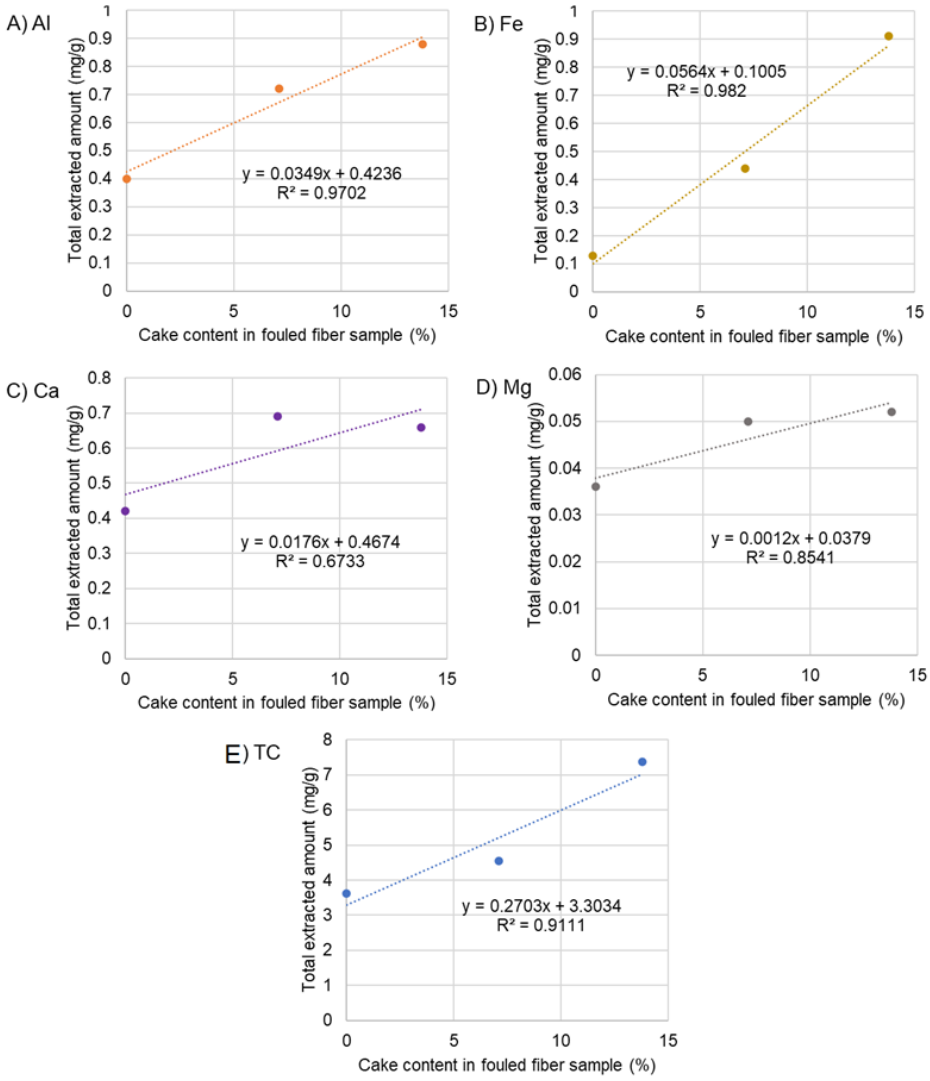

Figure 16 Extracted metal amounts and TC from fouled membrane samples as a function of the total cake amount (w-%) in the samples

6.9 Identification of changes to the pore structure of fouled membrane

BET analysis was conducted to identify changes in the pore structures of the fouled membranes. Theoretically fouling can cause multiple different type of changes to the pore structure of the membrane, depending on the fouling mechanism:

- Cake formation: increases number of pores
- Pore blocking: decreases number of pores
- Pore adsorption: decreases the average diameter of pores.

Samples for BET analysis were taken from a chemically cleaned module (M_{c1}). Samples from the same location were prepared in two different ways for the BET analysis; some fiber samples were collected with the cake layer still attached to them and some were washed with water to detach most of the cake layer (these are marked at “washed” samples). Theoretically, by comparing results of these samples, changes to the pore structure could be differentiated between those caused by cake layer and those caused by changes in the membrane pores. The ATR-FTIR spectra of the samples used for the BET analysis are presented in Fig. 16. As shown in Fig 17, the order of samples from most fouled to least fouled was B1>B2>B3 with B1 and B2 very close to each other. As expected, the samples washed with water were less fouled than unwashed samples. B3 sample had no visible cake layer before or after washing. Oddly, B1(*r*=5.6 cm) was more fouled than B2 (*r*=3.6 cm), although the B2 was collected from closer to the center, which went against the principle presented in Fig. 7. In Table XI, samples specifications and total pore volume and area are presented according to the BET analysis. In Fig. 18 the pore area and volume distributions of the samples are presented.

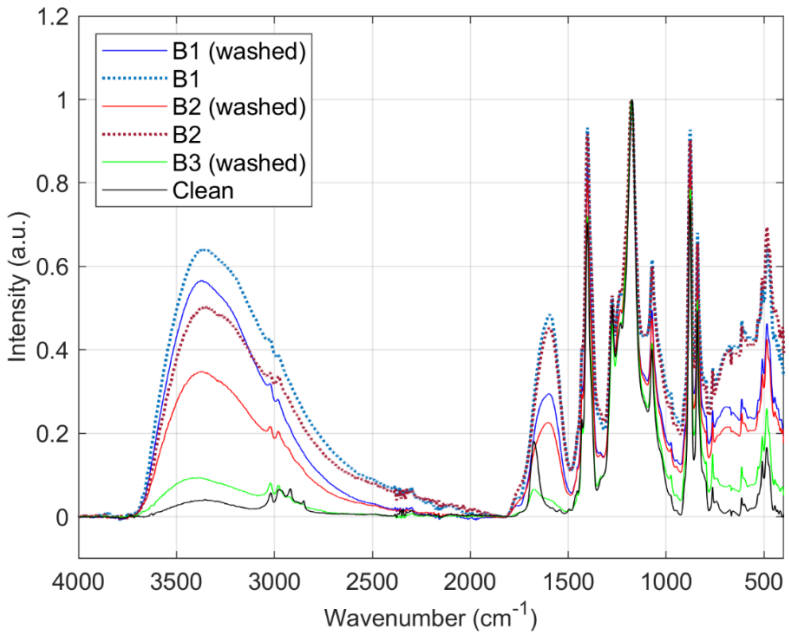

Figure 17 ATR-FTIR spectra of samples used for BET analysis.

Table XI BET analysis samples as well as pore area and volume for each sample according to the BET analysis. All fouled samples were from M_{c1} and were freeze-dried before the analysis.

Sample name	**Location (*d*,*r*) cm**	**Pore area, m^2/g**	**Pore volume, cm^3/g**
Washed B1	(15, 5.6)	32.9	0.106
Dirty B1	(15, 5.6)	36.0	0.110
Washed B2	(15, 3.1)	38.7	0.114
Dirty B2	(15, 3.1)	35.9	0.108
Washed B3	(60, 3.1)	41.1	0.124
Clean	-	33.3	0.102

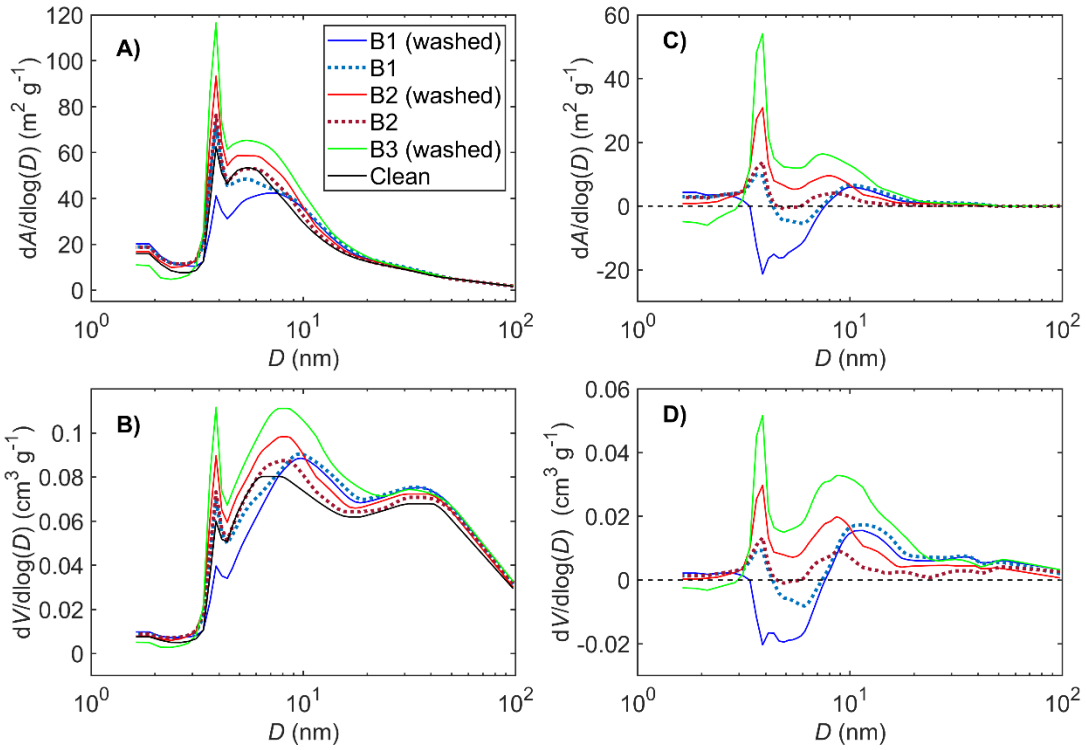

Figure 18 BET results: A and B show the BET logarithmic pore area and volume distributions, while C and D show the difference in pore area and volume distributions between the fouled membrane samples and the reference sample.

As seen from Fig. 18, sample with the most pores in most size ranges was B3. This was unexpected, as B3 was the cleanest of the fouled samples and didn't have visible cake layer, which was expected to increase the number of pores. Possible explanation for this is that the extended filtration and multiple chemical cleanings broke the structure of the used membranes causing an increase to porosity. It is even possible than some of the smaller pores expanded due to stress, as B3 has lower number of small pores (D < 2 nm) than the reference membrane. As seen from the change in the ATR-FTIR peak at 1680 cm^{-1} (which represents most likely some additive) between the clean membrane and B3 (Fig. 17), such structural changes during the pilot filtration are not completely out of question. Increased pore density could also be explained by a decrease in the density of the membrane during the filtration.

Assuming that all membrane samples were affected by the same changes as B3 compared to the clean membrane, it appears that fouling has decreased the number of pores in both B1 and B2 compared to B3. As seen from Fig. 17, these samples appear more affected by fouling than

B3. The decrease in porosity could be explained by pore clogging or pore adsorption. Both methods are possible, because B1 and B2 have a higher number of small pores (D < 2 nm) but a lower number of large pores (2 nm <D < 30 nm), which could indicate pore adsorption. The changes in the pore structure seen in Fig. 18 are quite noticeable but fouling inside the membranes could not be detected in SEM-EDS of the inner surfaces, which makes pore blocking more likely fouling mechanism than pore adsorption in this case with the current information. While the cake layer attached to B1 and B2 was expected to cause an increase to the number of pores, it is also possible that the cake layer might not have a high number of pores at this size range. It is also possible that the cake layer contains only small pores (<2 nm), which would fit the results as both B1 and B2 have higher number of pores in this size group. The hypothesis that cake layer would increase the number of pores per sample mass assumes that the pore density (per mass) of the cake layer is higher than of the used membrane, but this has not been confirmed.

With this explanation, the order of the samples in terms of number of pores, B3>B2>B1, seems logical and consistent with the ATR-FTIR results. However, lot of assumptions and quesswork had to made to explain the results in this manner. The most puzzling results presented in Fig. 18, is that washing the membrane with water seems to have caused opposite effects to B1 and B2. Analysing this effect would require more measurements, although the difference in pore distributions could be explained by different fouling mechanisms. As indicated in the earlier sections, cake layer might have been pushed to the location of B2 during the chemical cleanings, but based on Fig. 7 it can be assumed that the permeate flux was higher in the area of B1 compared to the area of B2. Thus, there would have occurred more pore adsorption/blocking in the area of B1, which would affect especially the pore size distributions of the washed samples. Of course, this does not completely explain the different reactions the samples had to washing with water, but rather explains why there might be large differences in pore blocking/adsorption between the two areas.

Overall, while the BET results were unexpected, they could be explained to indicate pore adsorption or blocking in the badly fouled membranes. The results do confirm that the pilot filtration did affect the pore structures of the fouled membranes. However, before further measurements, the precise mechanisms, which were causing those effects, cannot be defined in conclusive manner.

6.10 Identification of polysaccharides and morphological analysis by CLSM

Sample staining and CLSM imaging was used for identification of polysaccharides and for studying the foulant dispersion on the membrane surface. CLSM images for clean and washed membrane samples are presented in Fig. 18.

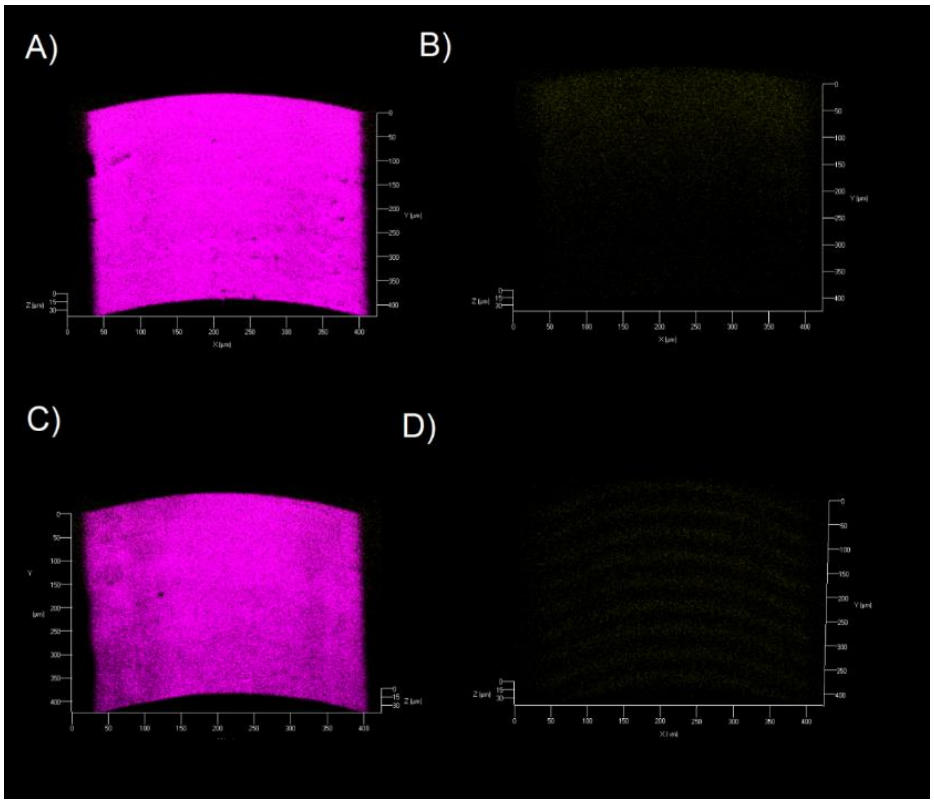

Figure 19 CLSM 3-d images of clean sample (A & B) and a fouled membrane sample (C & D: M_{c1}, d=15 cm, r=3.1 cm). A & C show fluorescence emissions from both used channels (Channel 1: yellow, channel 2: magenta) and C & D only show emissions from channel 1. Image dimensions, (*x,y,z*) µm, are: (424.27,424.27,42.00) for A & B and (424.27,424.27,44.00) for C & D.

The fouled membrane samples in Fig. 19 were washed before and stored in water before drying. Both samples were successfully stained with fuchsine, but fluorescence from ConA-Fitch was not detected from either of the samples. However, even the clean membrane surface was stained with ConA when fuchsine was not used. Seems like fuchsine worked as a blocking agent for the ConA by blocking the unspecific binding sites and only leaving specific binding sites for ConA to bind to. Fuchsine seems to have bounded stronger to the clean membrane

(Fig. 19 A) than to the fouled membrane (Fig. 19 C), perhaps due to higher hydrophobicity of the clean membrane as the fouling was suspected to be mostly hydrophilic. Thin cake layer could be visually observed on the fouled membrane sample, but it did not have noticeable effect on the binding of fuchsine or ConA.

In Fig. 19, there are presented CLSM images of four areas of a fouled membrane sample, which was dried in oven with the cake layer still intact. As shown in Fig.19, the cake layer was generally not stained with fuchsine most likely due to its hydrophilic nature. The exception is very thin layers of cake, for example seen in the left side of Fig. 19 C, which were seemingly partly stained with fuchsine. It is also possible that the thin cake layer wasn't stained itself at all, but rather the fluorescence emissions detected in the area may have come from the membrane surface below it. As seen in Fig. 19, some concentrated areas of the cake layer were clearly stained with ConA, which indicates the presence of polysaccharides.

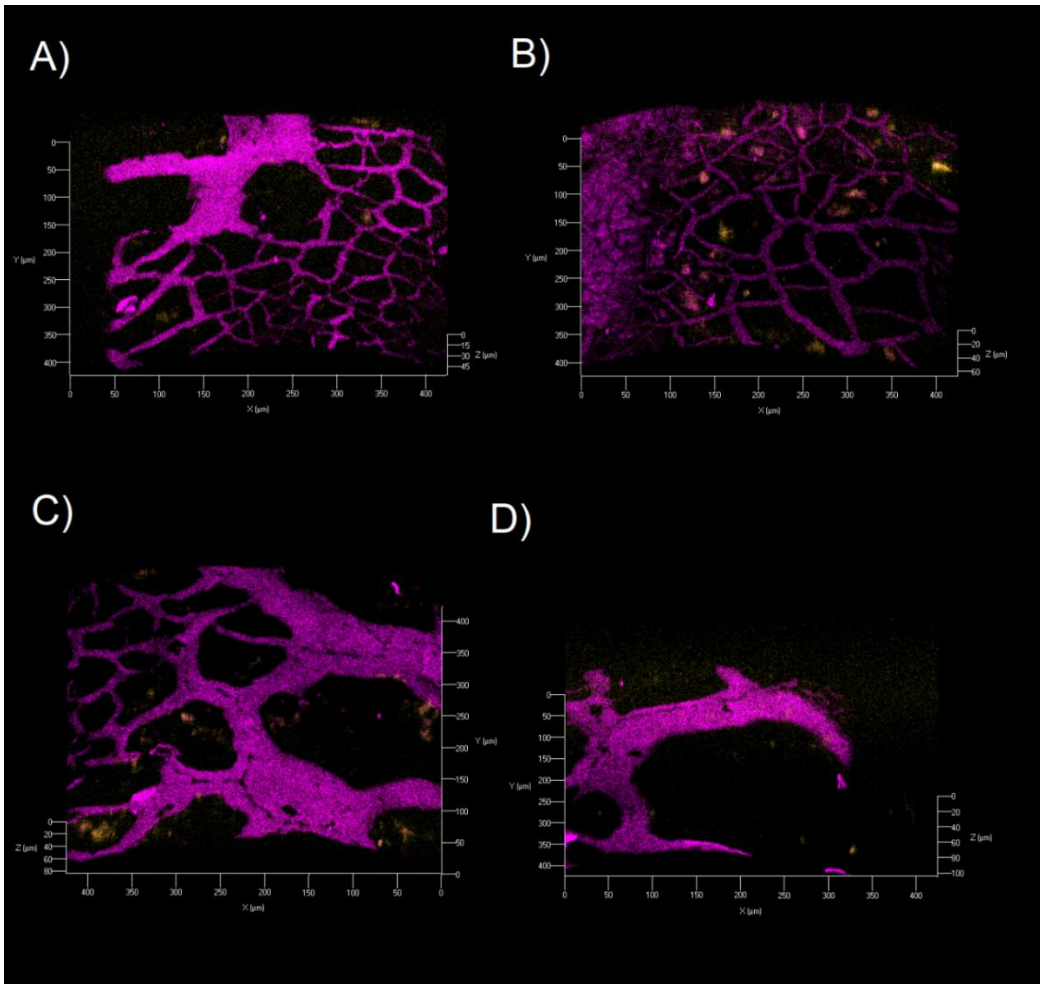

Figure 20 CLSM 3-d images of different areas of fouled membrane sample (M_{c1}, d=15 cm, r=3.1 cm). Emissions in channel 1 (primary ConA) shown in yellow, while emissions in channel 2 (primary fuchsine) shown in magenta. Image dimensions, (*x,y,z*) µm, are: A: (424.27,424.27,57.00), B:(424.27,424.27,67.00), C:(424.27,424.27,83.00) and D:(424.27,424.27,105.00).

As seen from the Fig. 20, the areas stained with ConA are placed irregularly in small areas. By rotating the 3-D images, which Fig. 20 is based on, it was apparent that in most places, the ConA was placed inside/on the cake layer rather than on the membrane, which indicates that the detected polysaccharides were not attached to the membrane but rather to the cake layer.

It is important to assess, how the cake layer structure has been altered by the drying process. For one, water-soluble compounds might have been moved and attached to specific spots (such as irregular surface shapes) during the drying. If the compounds that ConA attached to were initially dispersed in the water phase surrounding the membrane, it might explain why

they weren’t detected in the fouled membrane sample that was washed with water (CLSM image presented in Fig 19 C). It might also explain the odd irregular concentration seen in Fig. 20, as the polysaccharide fouling may be assumed to be more regular around the fibers, naturally. Another option is that the cake layer involved some polysaccharide specific adsorptive sites although there is not much prove of such phenomenon.

7. Conclusions

In this work fouling of hollow fiber modules used in a pilot experiment by HSY was examined. The aim was to identify the prevailing foulants and fouling mechanisms as well as to find how the fouling control of the process could be improved. In general, fouling of hollow fiber modules is more complex than fouling of flat-sheet membranes. The shape of hollow fiber modules also complicates monitoring of fouling, which makes off-site analysis the only viable option before more advanced models are developed. The main results of this study can be concluded as followed:

- The membrane modules were affected by irreversible fouling, which started to affect the permeate flux significantly during the 3rd filtration period. This fouling was likely caused primarily by cake formation.
- In general, the amount of irreversible fouling did not seem affected by the coagulant dosage, but it might have been affected by the type of coagulant. It appears cake formation caused more irreversible fouling resistance when PIX was used rather than PAX. Filtration sequence and specifically downtime after filtrations also seem to have affected formation of irreversible fouling.
- Increasing coagulant dosage could have increased the fouling rates during filtrations due directly or indirectly (by decreasing the amount of dissolved matter) increasing the feed TSS.
- The chemical cleaning procedure was ineffective as the cake layer contained significant amounts of iron (ca. 8.2 w-%) even after 8 chemical cleanings since the use of iron-based coagulation was stopped.
- Elemental analysis results indicate that the cake layer was composed of about 35–50 % of organic matter, which contained both humic substances and polysaccharides based on the ATR-FTIR and CLSM analyses. Several metals, mainly iron (8.2 w-%) and aluminium (5.1 w-%), were also identified in the cake layer. Large fractions of the metals most likely existed in hydroxide forms.
- Chemical cleaning was not effective at removing the cake layer from the areas near the open-end of the module, where the filtration was the most active. In those areas, cake layer was pushed towards the center of the module. The chemical cleanings were more

effective in the areas with less fouling, where the foulant concentrations were clearly reduced. Movement of the cake layer inside the module may have had a large part in the decrease of the permeate flux during filtration, although the exact significance remains undefined.

- SEM-EDS analysis found that the cake layer fully covered the membrane surfaces in areas where visible cake layer could be found. Pores openings on the surface of the membrane would not be cleaned after removing the cake layer with water and the SEM images indicated that pore blocking may be a relevant fouling mechanism.
- SEM-EDS analysis did not find signs internal fouling (internal pore blocking or pore adsorption).
- Even membranes with no visible cake layer were affected by fouling. Significant amounts of organic foulants (TC of 3.64 mg/g), aluminium (0.4 mg/g), and calcium (0.42 mg/g) were extracted from such sample. The same sample was less affected by iron-induced fouling than samples with visible cake layer. However, the reason for this could simply be that the chemical cleanings were more successful at cleaning the iron from areas without cake layer.
- Foulants had been left into all tested membrane samples by the chemical cleaning. Large portions of the remaining foulants could however be easily removed by simply washing with deionized water.
- Extraction results indicate that the areas with no visible cake layer were mostly affected by fouling caused by some type of Al-NOM complexes, while the cake layer contained a higher fraction of Fe-NOM complexes. Acid treatment might be better at removal of Al-NOM complexes while Fe-NOM complexes were more affected by alkaline treatment. Calcium, and possible Ca-NOM complexes, were removed from the fouled membranes by flushing the samples with water.
- The applied mix of US treatments appears to have removed humic substances and polysaccharides from the samples. After the US treatments, the surfaces of the fouled membranes still contained some type of organic foulants, and most likely some other on identified foulants, such as Al-O-Si complexes.
- The residue organic foulants contain O-H groups. The composition of the residue foulants likely differs from the composition of the foulants found in the cake layer, and it is possible that the residue foulants were not absorbed on the flocs.

- Overall based on both the experimental results and the literature review, it appear that under conditions of the pilot filtration cake layer formed by iron-based flocs reduced the permeate flux more (at least when pH was adjusted), but aluminium-based flocs were more likely to accumulate on the membrane surface even in areas with no cake layer. The aluminium compounds found on the membrane also appear resistant to chemical cleaning.
- BET analysis showed that filtration or fouling affects the pore structure of the used membranes although the results are inconclusive about the precise effects and mechanisms. It's possible that the pilot filtration increased the number of large pores (D>2 nm) in all samples compared to the reference membrane, while pore blocking or adsorption decreased the number of pores in that size range in badly fouled membranes.

Cake formation has been identified as a major source of fouling in the modules. To improve the process, several actions can be suggested. Changing to a different membrane module with lower packing density might be helpful. This might help to reduce the formation of the merging cake layers, which were noticed during sampling, and increase the efficiency of the chemical cleaning procedure. Also, changing the membrane material could be considered, because PVDF has been found to be more prone to fouling than other similar membrane materials in multiple studies. If the current modules are kept unchanged, the chemical cleaning procedure should be improved. It appears that downtime reduced fouling from the modules, so perhaps soaking the modules in the cleaning solutions for longer could help to achieve better results. Results of the extraction experiment indicate that starting the chemical cleaning with the alkaline treatment could be beneficial when using PIX and starting with the acid treatment would be better with PAX. However, these results are only indicative and need more testing.

While the cleaning procedure contained multiple backwashing sequences, if the module is fouled badly enough, this will not alone be enough to push all of the cake layer outside the module. Introducing constant mixing or aeration to the module tank might help to increase crossflow and mixing and reduce cake formation. Introducing new pretreatments to the process could most likely improve the fouling control. Calcium has been shown to increase fouling caused by NOM and other colloidal particles, such as flocs, thus removing calcium from the

feed water before the filtration might show good results. Similarly, using pretreatments to reduce the foulant loading overall should reduce fouling

To improve the fouling properties of the cake layer, the cake porosity can be attempted to increase by changing the used coagulant or by controlling the flocculation parameters i.e. pH, flocculation time and coagulant dosage. In theory, lowering pH and increasing flocculation time could lead to increased floc size and higher porosity in the cake layer. In practice, this might require a series of laboratory tests as changing these parameters might also have ill-advised effects due to neutralization of NOM or formation of nanoflocs. Another approach could be optimizing the coagulation in terms of DOC removal as this has shown to have good results on fouling in other studies.

Sources

Adusei-Gyamfi, J., Ouddane, B., Rietveld, L., Cornard, J. & Criquet, J. 2019. Natural organic matter-cations complexation and its impact on water treatment: A critical review. Water Research, 160, pp. 130-147

Alresheedi, M. T., Barbeau, B. & Basu, O. D. 2019. Comparisons of NOM Fouling and Cleaning of Ceramic and Polymeric Membranes during Water Treatment. Separation and Purification Technology 209, pp. 452-460

Bhatnagar, A. & Sillanpää, M. 2017. Removal of natural organic matter (NOM) and its constituents from water by adsorption – A review. Chemosphere, 166, pp. 497-510

Bolto, B., Dixon, D., Eldridge, R., King, S. & Linge, K. 2002. Removal of natural organic matter by ion exchange. Water Research, 36(20), pp. 5057-5065

Bottino, A., Capannelli, C., Del Borghi, A., Colombino, M. & Conio, O. 2001. Water treatment for drinking purpose: Ceramic microfiltration application. Desalination, 141(1), pp. 75-79

Braghetta, A., Digiano, F. & Ball, W. 1998. NOM Accumulation at NF Membrane Surface: Impact of Chemistry and Shear. Journal of Environmental Engineering, 124(11), pp. 1087-1098

Brant, J. A. & Childress, A. E. 2002. Assessing short-range membrane–colloid interactions using surface energetics. Journal of Membrane Science, 203(1-2), pp. 257-273

Carroll, T. & Booker, N. 2000. Axial features in the fouling of hollow-fibre membranes. Journal of Membrane Science, 168(1), pp. 203-212

Cen, J., Vukas, M., Barton, G., Kavanagh, J. & Coster, H. 2015. Real time fouling monitoring with Electrical Impedance Spectroscopy. Journal of Membrane Science, 484, pp. 133-139.

Chellam, S. & Zander, A. 2016. 'Membrane science and theory', in Christensen, M.(ed.) Microfiltration and ultrafiltration membranes for drinking water. Second edition. Denver, CO: American Water Works Association, pp. 35 - 50

Cheng, Y., Lee, D. & Lai, J. 2011. Filtration blocking laws: Revisited. Journal of the Taiwan Institute of Chemical Engineers, 42(3), pp. 506-508

Crozes, G., Jacangelo, J., Anselme, C. & Laîné, J. 1997. Impact of ultrafiltration operating conditions on membrane irreversible fouling. Journal of Membrane Science, 124(1), pp. 63-76

Dong, H., Gao, B., Yue, Q., Rong, H., Sun, S. & Zhao, S. 2014. Effect of Fe (III) species in polyferric chloride on floc properties and membrane fouling in coagulation–ultrafiltration process. Desalination, 335(1), pp. 102-107

Fiksdal, L. & Leiknes, T. 2006. The effect of coagulation with MF/UF membrane filtration for the removal of virus in drinking water. Journal of Membrane Science, 279(1), pp. 364-371

G. Kenne and D. Merwe. 2013. Classification of Toxic Cyanobacterial Blooms by Fourier-Transform Infrared Technology (FTIR). Advances in Microbiology, Vol. 3(6A), 2013, pp. 1-8

Gao, W., Liang, H., Ma, J., Han, M., Chen, Z., Han, Z. & Li, G. 2011. Membrane fouling control in ultrafiltration technology for drinking water production: A review. Desalination, 272(1), pp. 1-8

Guan, X., Shang, C. & Chen, G. 2006. ATR-FTIR investigation of the role of phenolic groups in the interaction of some NOM model compounds with aluminum hydroxide. Chemosphere, 65(11), pp. 2074-2081

Günther, J., Schmitz, P., Albasi, C. & Lafforgue, C. 2010. A numerical approach to study the impact of packing density on fluid flow distribution in hollow fiber module. Journal of Membrane Science, 348(1), pp. 277-286

Hamachi, M. & Mietton-Peuchot, M. 2001.Cake Thickness Measurement with an Optical Laser Sensor. Chemical Engineering Research and Design, 79(2), pp. 151-155

Hao, Y., Moriya, A., Maruyama, T., Ohmukai, Y. & Matsuyama, H. 2011. Effect of metal ions on humic acid fouling of hollow fiber ultrafiltration membrane. Journal of Membrane Science, 376(1-2), pp. 247-253

Harman, B., Koseoglu, H., Yigit, N., Beyhan, M. & Kitis, M. 2010. The use of iron oxide-coated ceramic membranes in removing natural organic matter and phenol from waters. Desalination, 261(1), pp. 27-33

Hermia, J. 1982. Constant pressure blocking filtration laws-application to power-law non-Newtonian fluids. Transactions of the Institution of Chemical Engineers, 60, pp. 183-187

Howe, K. J. & Clark, M. M. 2006. Effect of coagulation pretreatment on membrane filtration performance. Journal - American Water Works Association, 98(4), pp. 133-146

Huang, H., Lee, N., Young, T., Gary, A., Lozier, J. C. & Jacangelo, J. G. 2007. Natural organic matter fouling of low-pressure, hollow-fiber membranes: Effects of NOM source and hydrodynamic conditions. Water Research, 41(17), pp. 3823-3832.

Jarvis, P., Jefferson, B., & Parsons, S. A. 2004. Characterising natural organic matter flocs. Water Science & Technology, 4(4), 79-87

Jonsson, G., Prádanos, P. & Hernández, A. 1996. Fouling phenomena in microporous membranes. Flux decline kinetics and structural modifications. Journal of Membrane Science, 112(2), pp. 171-183

Kakihana, Y., Cheng, L., Fang, L., Wang, S., Jeon, S., Saeki, D., Rajabzadeh, S., Matsuyama, H. 2017. Preparation of positively charged PVDF membranes with improved antibacterial activity by blending modification: Effect of change in membrane surface material properties. Colloids and Surfaces A: Physicochemical and Engineering Aspects, 533, pp. 133-139

Kim, S., Chu, K. H., Al-Hamadani, Y. A., Park, C. M., Jang, M., Kim, D., Yu, M., Heo, J., Yoon, Y. 2018. Removal of contaminants of emerging concern by membranes in water and wastewater: A review. Chemical Engineering Journal, 335, pp. 896-914

Kimura, K. & Oki, Y. 2017. Efficient control of membrane fouling in MF by removal of biopolymers: Comparison of various pretreatments. Water Research, 115, pp. 172-179.

Kimura, K., Hane, Y., Watanabe, Y., Amy, G. & Ohkuma, N. 2004. Irreversible membrane fouling during ultrafiltration of surface water. Water Research, 38(14-15), pp. 3431-3441

Kimura, K., Maeda, T., Yamamura, H. & Watanabe, Y. 2008. Irreversible membrane fouling in microfiltration membranes filtering coagulated surface water. Journal of Membrane Science, 320(1-2), pp. 356-362

Kimura, M., Matsui, Y., Saito, S., Takahashi, T., Nakagawa, M., Shirasaki, N. & Matsushita, T. 2015. Hydraulically irreversible membrane fouling during coagulation–microfiltration and its control by using high-basicity polyaluminum chloride. Journal of Membrane Science, 477(C), pp. 115-122

Krasner, S. W., Croué, J., Buffle, J. & Perdue, E. M. 1996. Three approaches for characterizing NOM. Journal - American Water Works Association, 88(6), pp. 66-79

Lebeau, T., Lelièvre, C., Buisson, H., Cléret, D., Van de Venter, L. W. & Côté, P. 1998. Immersed membrane filtration for the production of drinking water: Combination with PAC for NOM and SOCs removal. Desalination, 117(1-3), pp. 219-231

Lee M., Kim, J. 2012. Analysis of local fouling in a pilot-scale submerged hollow-fiber membrane system for drinking water treatment by membrane autopsy. Separation and Purification Technology, 95, pp. 227-234

Lee, N., Amy, G., Croué, J. & Buisson, H. 2004. Identification and understanding of fouling in low-pressure membrane (MF/UF) filtration by natural organic matter (NOM). Water Research, 38(20), pp. 4511-4523

Lee, S. & Cho, J. 2004. Comparison of ceramic and polymeric membranes for natural organic matter (NOM) removal. Desalination, 160(3), pp. 223-232

Lee, S., Kim, S., Cho, J. & Hoek, E. M. 2007. Natural organic matter fouling due to foulant–membrane physicochemical interactions. Desalination, 202(1), pp. 377-384

Lohwacharin, J., Oguma, K. & Takizawa, S. 2010. Use of carbon black nanoparticles to mitigate membrane fouling in ultrafiltration of river water. Separation and Purification Technology, 72(1), pp. 61-69.

Ma, B., Xue, W., Hu, C., Liu, H., Qu, J. & Li, L. 2019. Characteristics of microplastic removal via coagulation and ultrafiltration during drinking water treatment. Chemical Engineering Journal, 359, pp. 159-167

Matilainen, A., Gjessing, E. T., Lahtinen, T., Hed, L., Bhatnagar, A. & Sillanpää, M. 2011. An overview of the methods used in the characterisation of natural organic matter (NOM) in relation to drinking water treatment. Chemosphere, 83(11), pp. 1431-1442

Nakatsuka, S., Nakate, I. & Miyano, T. 1996. Drinking water treatment by using ultrafiltration hollow fiber membranes. Desalination, 106(1-3), pp. 55-61

Naveed, A., Noor-Ul-Amin, F., Saeed, M., Khraisheh, M., Al Bakri, S. & Gul, S. 2019. Synthesis and characterization of fly ash based geopolymeric membrane for produced water treatment. Desalination and Water Treatment, 161, pp. 126-131

Parsegian, V. & Zemb, T. 2011. Hydration forces: Observations, explanations, expectations, questions. Current Opinion in Colloid & Interface Science, 16(6), pp. 618-624

Peiris, R., Budman, H., Legge, R. & Moresoli, C. 2011. Assessing irreversible fouling behavior of membrane foulants in the ultrafiltration of natural water using principal component analysis

of fluorescence excitation-emission matrices. Water Science and Technology, 11(2), pp. 179-185

Peiris, R., Jaklewicz, M., Budman, H., Legge, R. & Moresoli, C. 2013. Assessing the role of feed water constituents in irreversible membrane fouling of pilot-scale ultrafiltration drinking water treatment systems. Water Research, 47(10), pp. 3364-3374.

Peter-Varbanets, M., Hammes, F., Vital, M. & Pronk, W. 2010. Stabilization of flux during dead-end ultra-low pressure ultrafiltration. Water Research, 44(12), pp. 3607-3616

Ratnaweera, H., Hiller, N. & Bunse, U. 1999. Comparison of the coagulation behavior of different Norwegian aquatic NOM sources. Environment International, 25(2), pp. 347-355

Rodriguez, F. & Nunez, L. 2011. Characterization of aquatic humic substances. Water And Environment Journal, 25(2), pp. 163-170

Sablani, S., Goosen, M., Al-Belushi, R. & Wilf, M. 2001. Concentration polarization in ultrafiltration and reverse osmosis: A critical review. Desalination, 141(3), pp. 269-289

SDBSWeb : https://sdbs.db.aist.go.jp (National Institute of Advanced Industrial Science and Technology,date of access: 18.3.2020)

Sharp, E., Jarvis, P., Parsons, S. & Jefferson, B. 2006. The Impact of Zeta Potential on the Physical Properties of Ferric-NOM Flocs. Environmental Science & Technology, 40(12), pp. 3934-3940

Sheng, C., Nnanna, A. A., Liu, Y. & Vargo, J. D. 2016. Removal of Trace Pharmaceuticals from Water using coagulation and powdered activated carbon as pretreatment to ultrafiltration membrane system. Science of the Total Environment, 550, pp. 1075-1083

Shi, X., Tal, G., Hankins, N. P. & Gitis, V. 2014. Fouling and cleaning of ultrafiltration membranes: A review. Journal of Water Process Engineering, 1, pp. 121-138.

Shimizu, Y., Okuno, Y., Uryu, K., Ohtsubo, S. & Watanabe, A. 1996. Filtration characteristics of hollow fiber microfiltration membranes used in membrane bioreactor for domestic wastewater treatment. Water Research, 30(10), pp. 2385-2392.

Speth, T.F. & Reiss, R.C. 2016. 'Water quality', in Christensen, M.(ed.) Microfiltration and ultrafiltration membranes for drinking water. Second edition. Denver, CO: American Water Works Association, pp. 7 - 34

Su-Hua, W., Bing-Zhi, D. & Yu, H. 2010. Adsorption of bisphenol A by polysulphone membrane. Desalination, 253(1), pp. 22-29.

Sun, C., Fiksdal, L., Hanssen-Bauer, A., Rye, M. B. & Leiknes, T. 2011. Characterization of membrane biofouling at different operating conditions (flux) in drinking water treatment using confocal laser scanning microscopy (CLSM) and image analysis. Journal of Membrane Science, 382(1), pp. 194-201

Sutzkover-Gutman, I., Hasson, D. & Semiat, R. 2010. Humic substances fouling in ultrafiltration processes. Desalination, 261(3), pp. 218-231

Tien, C. & Ramarao, B. V. 2011. Revisiting the laws of filtration: An assessment of their use in identifying particle retention mechanisms in filtration. Journal of Membrane Science, 383(1), pp. 17-25

Wang, S., Liu, C. & Li, Q. 2011. Fouling of microfiltration membranes by organic polymer coagulants and flocculants: Controlling factors and mechanisms. Water Research, 45(1), pp. 357-365

Vickers, J. C., Thompson, M. A. & Kelkar, U. G. 1995. The use of membrane filtration in conjunction with coagulation processes for improved NOM removal. Desalination, 102(1), pp. 57-61

Vickers, J.C. 2016. 'Introduction', in Christensen, M.(ed.) Microfiltration and ultrafiltration membranes for drinking water. Second edition. Denver, CO: American Water Works Association, pp. 1 - 6

Virtanen, T., Rudolph, G., Lopatina, A. Al-Rudainy, B., Schagerlöf, H., Puro, L., Kallioinen, M., Lipnizki, F. 2020. Analysis of membrane fouling by Brunauer-Emmet-Teller nitrogen adsorption/desorption technique. Scientific reports, 10

Yamamura, H., Chae, S., Kimura, K. & Watanabe, Y. 2007. Transition in fouling mechanism in microfiltration of a surface water. Water Research, 41(17), pp. 3812-3822.

Yamamura, H., Okimoto, K., Kimura, K. & Watanabe, Y. 2014. Hydrophilic fraction of natural organic matter causing irreversible fouling of microfiltration and ultrafiltration membranes. Water Research, 54, pp. 123-136

Yeo, A., & Fane, A. G. 2005. Performance of individual fibers in a submerged hollow fiber bundle. Water Science and Technology, 51(6-7), 165-172.

You, S., Tseng, D. & Hsu, W. 2007. Effect and mechanism of ultrafiltration membrane fouling removal by ozonation. Desalination, 202(1), pp. 224-230

Yu, W., Graham, N., Liu, H. & Qu, J. 2013(a). Comparison of FeCl3 and alum pre-treatment on UF membrane fouling. Chemical Engineering Journal, 234, pp. 158-165

Yu, W., Graham, N., Liu, H., Li, H. & Qu, J. 2013(b). Membrane fouling by Fe-Humic cake layers in nano-scale: Effect of in-situ formed Fe(III) coagulant. Journal of Membrane Science, 431, pp. 47-54

Zhang, M., Liao, B., Zhou, X., He, Y., Hong, H., Lin, H. & Chen, J. 2015. Effects of hydrophilicity/hydrophobicity of membrane on membrane fouling in a submerged membrane bioreactor. Bioresource technology, 175, p. 59

Zhao, C., Zhou, X. & Yue, Y. 2000. Determination of pore size and pore size distribution on the surface of hollow-fiber filtration membranes: A review of methods. Desalination, 129(2), pp. 107-123

Zhuang, L., Guo, H., Wang, P. & Dai, G. 2015. Study on the flux distribution in a dead-end outside-in hollow fiber membrane module. Journal of Membrane Science, 495, pp. 372-383